Programa de doctorado "Matemáticas"

PhD Dissertation

Optimization models in Solar Power Tower plants design.

Design of the heliostat field and the tower receivers

Author

Carmen-Ana Domínguez Bravo

Supervisors

Prof. Dr. *Emilio Carrizosa Priego*

Prof. Dr. *Enrique Fernández Cara*

Dr. *Manuel Quero García*

October 26, 2015

A mi hermana, mis padres y mi tita Mari,
por apoyarme en todo momento para alcanzar esta meta.
A mis abuelos y mi tía Victoria,
por haberme guiado con su cariño y sus sabios consejos.
A Edu por aportarme siempre alegría y optimismo.

"The world we have made, as a result of the level of thinking we have done thus far, creates problems we cannot solve at the same level of thinking at which we created them."

A. Einstein

Me gustaría empezar los agradecimientos mencionando a mis directores de tesis. Emilio, Enrique y Manuel gracias por haber confiado en mi desde un principio para llevar a cabo esta tarea. Ha sido para mi un placer y un privilegio trabajar con vosotros.

En especial a Emilio y Enrique agradecerles sus enseñanzas, su paciencia y cariño durante estos años de doctorado.

Agradecer a mi amiga Amaya, que me ha ido abriendo camino y ha hecho que estos años hayan sido una prolongación de la licenciatura. ¡Gracias por todo! A mi "familia trianera", María, Juanma y Soto, ¡gracias por hacer de Sevilla mi segunda casa! Mencionar también a mis niñas gaditanas, que han estado ahí en todo momento aunque las haya tenido tan abandonadas.

Y por último agradecer a todos y cada uno de mis compañeros del IMUS. En especial a mis "hermanas de doctorado" por su apoyo, a mi compi Marithania por nuestras charlas y a Vanesa por compartir su amor por los animales conmigo. ¡Gracias a todos! Me llevo muy buenos recuerdos y espero que coincidamos en el futuro de nuevo.

La investigación realizada para llevar a cabo esta tesis doctoral ha sido principalmente financiada por Abengoa Solar y se ha llevado a cabo en el Instituto de Matemáticas de la Universidad de Sevilla, mediante el contrato de investigación CapTorSol-0494.

This research has been mainly supported by Abengoa Solar and it has been carried out at the Institute of Mathematics of University of Seville, through the research contract CapTorSol-0494.

Resumen

El diseño de plantas solares con tecnología de torre (utilizaremos las siglas en inglés SPT) comenzó a ser estudiado en los años 70 y sigue siendo hoy en día un área de investigación muy activa. En esta tesis doctoral se estudia el diseño óptimo de la planta solar bajo distintos aspectos, enfocándose en el diseño del sistema torre-receptor y del campo de heliostatos.

El primer capítulo presenta una idea general sobre SPT, describiendo los componentes que intervienen en el problema y detallando el modelado matemático utilizado a lo largo de este documento. Un algoritmo para resolver el problema de base se propone en el Capítulo 2. Se trata de un algoritmo, basado en la heurística voraz, que introduce un enfoque innovador al resolver el problema de la localización de heliostatos sin preestablecer ningún patrón geométrico. Este algoritmo se extiende en el capítulo 3 para resolver el diseño del campo solar con heliostatos en bloques llamados "pod" (estructuras triangulares que albergan varios heliostatos).

Los capítulos 4 y 5 versan sobre los procedimientos heurísticos adaptados para dar solución a nuevos problemas que surgen en este tipo de tecnologías: diseño de sistemas con receptores múltiples y diseño de campos multi-talla. Ambos son problemas desafiantes debido a su alto grado de complejidad. El algoritmo heurístico presentado en el capítulo 2 ha sido modificado y combinado con distintos procedimientos de optimización para facilitar una solución, que aunque no óptima, sea competitiva y pueda ser considerada como una buena solución.

A lo largo de todos los capítulos, los resultados han sido comparados con los resultados disponibles en la literatura. Esto ha permitido validar los algoritmos propuestos. Las conclusiones generales y algunos comentarios sobre trabajos futuros se comentan en el último capítulo.

Abstract

The design of solar power tower (SPT) plants started to be studied in 1970s and is still being an active field of research nowadays. In this dissertation, the optimal design of an SPT plant under different considerations is addressed, focusing on the tower-receiver and heliostat field design.

The first chapter provides the general ideas on SPT plants, with a description of the components involved in the problem and a presentation of the mathematical modelling used in this document. An algorithm to solve the basic problem is proposed in Chapter 2. It is a greedy-based heuristic algorithm, which introduces an innovative approach solving the heliostat location problem without fixing geometrical patterns. This algorithm is extended in Chapter 3 to address the solar field design with heliostat pod systems (triangular structures having several heliostats on it).

Chapters 4 and 5 concern heuristic procedures adapted to the solution of innovative problems arising in this technology: multiple receivers system design and multi-size field design. Both are challenging problems due to their high complexity. The heuristic algorithm in Chapter 2 has been modified and combined with different optimization procedures in order to furnish a solution which, although not optimal, is competitive and can be considered as a good solution.

Along all the chapters, the results have been compared to the state-of-the-art results, when available. This has allowed to validate the proposed algorithms. The general conclusions and some comments on further work are commented in the last chapter.

Contents

List of Figures

List of Tables

Glossary

A heliostat area

a triangle height of the heliostat pod

$A_{\mathtt{e}}$ heliostat effective mirror area

AR heliostat aspect ratio

A_w area of heliostat size w

α receiver azimuth angle

α_1 empirical atmospheric coefficient in $(0, 1)$

α_2 empirical atmospheric coefficient in $(0, 1)$

α_3 empirical atmospheric coefficient in $(0, 1)$

$\alpha_{\mathtt{sun}}$ solar azimuth angle

β_1 empirical cost coefficient in $(0, 1)$

β_2 empirical cost coefficient in $(0, 1)$

$\beta_{\mathtt{sun}}$ solar height angle

C construction cost function

c cost per heliostat

$c_{\mathtt{e}}$ heliostat effective area coefficient

$c_{\mathtt{f}}$ land costs (purchasing an preparing)

$c_{\mathtt{r}}$ heliostat reflectivity coefficient

d heliostat diagonal

$d_{\mathtt{ap}}$ distance between the aperture and the coordinate origin

Δ set of heliostat coordinates on the heliostat pod

δ heliostat security distance function

$d_{\mathtt{s}}$ heliostat safe distance

$\mathcal{D}$ finite set of heliostat dimensions

E collected thermal annual energy function

$\tilde{E}$ thermal annual energy into the receiver

$\mathcal{E}$ systems efficiency

F objective function

γ heliostat pod tilt angle with respect the vertical axis

γ_1 constant thermal energy losses of the system

γ_2 constant thermal energy losses of the receiver aperture

h receiver height in the tower

$h_{\mathtt{max}}$ maximum receiver height in the tower

$h_{\mathtt{sun}}$ solar hours

I solar irradiance function

κ angle between w and p

K tower-receiver cost function

l triangle side length of the heliostat pod

$l_{\mathtt{min}}$ minimum triangle side length of the heliostat pod

Lh heliostat horizontal side

Lv heliostat vertical side

λ_1 cost positive constant

λ_2 cost positive constant

N number of heliostats

N_w number of heliostats of size w

Ω available free region for the field

Ω_i^w aiming regions for multiple receivers system

$\vec{p}$ output vector perpendicular to the aperture $\vec{p} := (-\cos\xi, 0, \sin\xi)$

φ product of efficiency factors

Π_0 minimal power at $T_{\mathtt{d}}$

Π^+ maximum power at $T_{\mathtt{d}}$

Π_t receiver outlet thermal power at time t

Π_t^* incident solar energy at time t

$\tilde{\Pi}_t$ solar power into the receiver at time t

Ψ heliostats cost function

$Q_{\mathtt{e}}$ center of the receiver aperture (target point) $Q_{\mathtt{e}} := (d_{\mathtt{ap}}, 0, h)$

r radius of the receiver aperture

$r_{\mathtt{max}}$ maximum receiver aperture radius

$r_{\mathtt{min}}$ minimum receiver aperture radius

$\mathcal{S}$ finite set of coordinates of the centers of the heliostats

$\mathscr{S}$ feasible set for $\mathcal{S}$

$|\mathcal{S}|$ cardinality of set $\mathcal{S}$ (number of heliostats in the field)

t time instant

T final time instant

$T_{\mathtt{d}}$ design point

Θ variables associated with the tower-receiver system

$\mathbf{\Theta}$ feasible compact set for Θ

ς_i aperture angles of multiple receivers

$\vec{v}_{\mathtt{sun}}$ solar vector

w heliostat size

$\vec{w}$ vector from the heliostat center to the target point $\vec{w} := (d_{\mathtt{ap}} - x, -y, h - z_0)$

$w_{\mathtt{sun}}$ sun angular position

ω weight parameter used with multiple receivers system

ξ receiver aperture tilt angle from the vertical

Z finite set of coordinates of the centers and sizes of the heliostats

z_0 heliostat height

(x, y) heliostat center coordinates

(x, y, z_0) heliostat center coordinates and height

(x, y, w) heliostat center coordinates and size

Acronyms

CSP Concentrated Solar Power

NSPOC Nevada Solar Power Optimization Code

LCOE Levelized Cost Of Energy

LEC Levelized Energy Cost

LCOC Levelized Cost Of Coating

IMUS Institute of Mathematics of University of Seville

SPT Solar Power Tower

TIA Technology Innovation Agency

Introduction

This dissertation deals with the optimization of the design of solar power tower (SPT) systems. The optimization problems under different assumptions have been modelled and solved. This has included the selection of the decision variables, the specification of the constraints (related to the geometry of the problem and the technological requirements) and the determination of a single objective function (the construction cost and the annual energy are essentially the two criteria involved). Heuristic procedures have been developed to solve these problems using novel algorithms.

In the first step of the Doctoral period, a purely numerical work was undertaken to determine without ambiguity the cost and energy functions. Also, a comprehensive literature search was performed in order to be aware of the state-of-the-art of similar approaches.

Then, the modelling of the optimization problem and the study of resolution algorithms were held. In this second step, the selection of an appropriate heuristic algorithm was made. At the same time, the implementation of the algorithm was performed using Matlab© and taking into account that an efficient programming was needed in order to obtain results in a reasonable computational time.

Finally, a validation and comparative analysis phase was realised. This third and last phase aimed to endorse the validity of the proposed procedure and show its competitiveness.

Once these three steps were achieved, the procedure has been used as starting point to design and implement optimization strategies to solve innovative approaches arising from this technology.

Background and motivation

The SPT system here considered comprises a tower with a receiver on the top and a field of mirrors (called heliostats). The mirrors are fixed in the ground through a pedestal with two-axis movement, and they are assumed to concentrate the sunlight into the receiver. They should not contact each other, which implies that a clear-out circle surrounding each mirror position has to be considered.

The problem under consideration consists of designing an SPT in a optimal way.

Two functions are involved, namely, the construction cost and the energy collected. This problem can be written as a multi-objective problem because of the two optimization criteria involved, see [4]. However, as it is usual in this framework, the two objective functions are aggregated into a single criteria: the cost per unit of energy collected over a year.

From the mathematical point of view, this dissertation deals with an optimization problem in which the decision variables are those describing the tower-receiver system (dimensions and position) and those related to the heliostat field (coordinates of the heliostat positions). In order to design the SPT system, it is essential to understand the performance of the subsystems formed by the receivers and the heliostat field. The field and the receivers are interdependent, as pointed out in [93], where it is shown that an increase of the height of a receiver reduces some optical losses (shading, blocking and cosine effects) in large heliostat fields. It is thus important to design both components simultaneously.

Regarding the optimization of the field layout, where the main difficulty of the optimization problem lies, the problem consists of finding the optimal location of an unknown number of points within a given feasible region in $\mathbb{R}^2$. The main challenges when solving this problem are detailed as follows:

- The dimensionality of the problem is unknown, but, at the same time, the expected number of variables is large (for instance, real projects could have up to $3,000$ heliostats [21], which implies $6,000$ decision variables in total.
- Non-convex constraints associated with each point have to be included, that is, each point has a clear-out circle surrounding due to safety constraints.
- The value of the objective function depends on the relative position of all the points. This means that the location problem cannot be reduced to packing circles in a feasible region [48, 71, 66]. Contrarily, depending on the distances between the points the objective value varies.
- In addition, the objective function does not have a closed formula and its evaluation is computationally very expensive. Hence, its mathematical structure cannot be exploited in the optimization algorithm, and the computational time has to be taken into account when selecting an appropriate algorithm.

Therefore, this dissertation deals with a large-scale optimization problem with non-convex constraints and a non-convex objective function with a computationally expensive evaluation. Due to the complexity of the problem, the exact solution is unknown and exact optimization approaches are not available. Therefore, new heuristic algorithms have been introduced and analysed.

Fixed geometrical patterns are traditionally used to solve the field optimization problem. That is, the heliostat positions are given by some parametrized curves. The fixed pattern is determined by a low number of parameters, which are regarded as decision variables. The parameters are optimized in order to obtain a field layout, following standard optimization procedures as genetic, descent [41] or Nelder-Mead algorithm [58, 73].

For instance, radially-staggered layouts are commonly assumed, originally proposed in [63], see also [27, 102, 111]. This pattern consists of concentric semi-circumferences where the parameters indicate the separation between the circumferences and the angular distances between the heliostats located at the same circumference, see Figure 1. The spiral pattern is also used, where two parameters are optimized, see [75, 82].

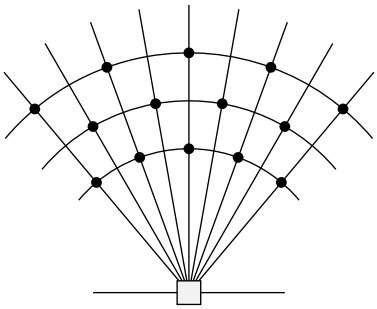

Figure 1: Radially-staggered layout

Since the cardinality of the problem is not fixed, traditionally the optimization of the problem is performed by assuming a number of points higher than actually required, obtaining an oversized first solution that will be reduced afterwards selecting the "best" heliostats in a greedy way.

Although these geometric patterns strongly simplify the heliostat field optimization, they may not reach good results if, for instance, time asymmetric climate conditions or terrain constraints are involved, as pointed out in [89]. The adaptability of the pattern is very limited and dependent on the chosen geometry, note that usually field symmetry is induced by the pattern itself.

The final aim of this dissertation, based on a connection with the engineering and construction company Abengoa Solar New Technologies S.A., was to introduce and make work new strategies, much more flexible and easily adaptable to solve future challenges as (for instance) multi-tower designs [35, 96] and designs in irregular regions [74].

Main contributions

A heuristic method for tower and pattern-free field optimization (Chapter 2)

This Chapter presents a heuristic method for simultaneously optimize the two subsystems, namely, the tower-receiver system (tower height and receiver size) and the heliostat field (heliostat locations and number). An alternating algorithm is proposed to sequentially optimize the field layout for a given tower-receiver configuration and then, the tower-receiver design is optimized for the previously obtained field layout. The optimization problem is decomposed in two sub-problems because of the different influences over the objective function of both subsystems.

Focusing on the heliostat location problem, the annual energy function is a non-convex and highly complex function which calculation involves interpolation and numerical integration. In particular, the effective calculation of the heliostat interactions, i.e. shading and blocking effects, introduces multi-modality and increases dramatically the computational time. Therefore, the analytical calculation of derivatives is non-viable, and the optimization techniques available cannot exploit the problem structure.

The methodology presented to solve the heliostat location problem is a greedy-based algorithm which does not impose geometric patterns for the heliostats locations and does not fix in advance the number of heliostats. In a greedy algorithm, solutions are iteratively built from scratch. The complete final solution is obtained progressively adding a new element at each iteration without destroying feasibility. The selection of this new element follows a greediness criterion, that is, the element with the higher incremental improvement is selected. Although optimization based on a pure greedy heuristic may not necessarily be optimal, e.g. [7, 87], it is frequently used in combinatorial optimization theory and practice. Its common use may be due to its simplicity, and, as stated in such paper, due to the fact that it is widely assumed that it often provides solutions that are significantly better than the worst ones. Also greedy solutions are combined with local search procedures or meta-heuristics, as for instance in randomized process such as GRASP [40]. The greedy algorithm has been successfully applied to other technological optimization problems in energy as for instance the location of wind-turbines, see [25, 77, 114]. See also [5, 32, 49, 109], for results of the greedy algorithm on a bunch of combinatorial optimization problems.

In the proposed greedy-based algorithm the points are located one by one at the best position within the feasible region. This way, at each step of the algorithm, an optimization problem in two variables is being solved, reducing and fixing the number of variables. A multi-start randomized process (in which different feasible initial solutions are considered) has been applied to avoid the local optima appearing while increasing the number of heliostats (because of the complex shading and blocking effects). The final position of each starting point is found as solution of local searches. The final number of points is obtained during the optimization process without using an oversized field

as starting point.

The proposed procedure follows a pattern-free method. The only constraints to be considered are: the shape of the field region and the non-convex constraints which force heliostats to not collide. The imposition of any pattern is avoided due to the difficulty to know the optimal one in advance and the high dependence on the test case studied.

The absence of a geometrical pattern to design the field and the simultaneous optimization of the field and the tower designs make this approach different from the existing ones.

Keywords: solar thermal power, heliostat field layout, thermo-economic optimization, non-convex optimization, greedy algorithm.

[23] E. Carrizosa, C. Domínguez-Bravo, E. Fernández-Cara, M. Quero.
A heuristic method for simultaneous tower and pattern-free field optimization on solar power systems,
Computers & Operations Research (2015), 57:109–122.

Field-design optimization with triangular heliostat pods (Chapter 3)

This Chapter deals with the optimal location of triangular heliostat pods. A heliostat pod consists of a structure with a particular shape in which several heliostats are positioned together. The particular case with a triangular structure in which six heliostats are installed is analysed.

One of the advantages of using pod systems is the possible reduction of the cost associated with the heliostats. In the pod system six heliostats are grouped reducing, among others, the number of foundations needed to install the heliostats in the field.

Regarding the optimization problem, the location of pods instead of individual heliostats introduces some benefits (the reduction of the number of decision variables) but also some drawbacks (the introduction of complex geometrical constraints and the increase of the complexity of the shadow and blockage effects).

A modified greedy-based algorithm has been developed, in which three optimization variables are considered to locate each pod. The proposed algorithm has been compared with a parabolic pattern model and an evolutionary genetic-based algorithm.

[38] C. Domínguez-Bravo, P. Richter, G. Heiming, S. Bode, E. Carrizosa, E. Fernández-Cara, M. Frank, P. Gauché.
Field-design optimization with triangular heliostat pods,
To appear in **Proceedings of SolarPaces** (2015).

Optimization of multiple receivers solar power tower systems (Chapter 4)

In this Chapter, multiple receivers on the top of the tower, instead of a single one, are considered. This innovative system allows one to reach a higher conversion efficiency of solar energy to electricity in large-scale plants (because higher temperatures are achieved). An algorithm is proposed in which the positions and dimensions of the receivers, together with the field boundaries, number of heliostats and locations, are sequentially optimized.

In this problem the additional difficulty lies in the calculation of the receivers aiming regions, that is, the determination of the receiver which corresponds to each heliostat. Some assumptions have to be made in order to obtain a realistic solution. Heliostats are assumed to focus always the same receiver and each receiver is assumed to have a separate aiming region where its heliostats are located.

The proposed method is based on an alternating greedy-based heuristic method, already presented in Chapter 2 with a single receiver, which simultaneously optimizes the receivers and the heliostat field. The proposed procedure allows one to determine the aiming region of each receiver, the heliostat locations and the overall number of heliostats.

Firstly, the selection of the aiming regions associated with each receiver has to be done in order to locate afterwards the heliostats. In the proposed approach the boundaries of these regions are directly obtained, taking into account the objective values calculated over the discretized feasible region. That is, the feasible region is discretized, and, for each point of the discretization, the receiver collecting the maximum objective value is selected as aiming receiver. Then, the boundary points where the receiver aiming changes are identified without imposing any particular shape. A polynomial fit is applied to each set of boundary points obtaining a separate aiming region for each receiver. Afterwards, the heliostats are located in each aiming region.

Finally, an alternating algorithm is applied, in which the receivers positions and field design are sequentially optimized, obtaining a reduction in the objective function value.

Assuming that each receiver could have its own technological requirements, the aiming regions obtained may not have the optimal shape. In order to explore different solutions, different weights are applied to the values obtained for the initial discretization, giving different priority to the receivers. The algorithm is then applied for each configuration, and the one giving the best solution is selected as final solution.

Keywords: solar thermal power, heliostat field layout, non-convex optimization, greedy algorithm, multiple receivers.

[24] E. Carrizosa, C. Domínguez-Bravo, E. Fernández-Cara, M. Quero.
Optimization of multiple receivers solar power tower systems,
Energy (2015), 90:2085–2093.

An optimization approach to the design of multi-size-heliostat fields (Chapter 5)

This Chapter studies the optimal design of a heliostat field when different sizes of heliostats are available. In this case, together with the coordinates of the heliostat center, the heliostat size is considered as an additional decision variable. Note that different heliostat sizes lead to different performance (different shading and blocking effects, greater or smaller clear-out circles, different associated costs, etc.).

An algorithm is proposed which starts from a single-size initial heliostat field (with a heliostat-size selected according with the receiver size) and allows one to study the performance of mixed or single-size fields considering two (or more) different sizes.

A two-phase algorithm is proposed, called Expansion-Contraction algorithm, which it is based on the heuristic greedy-based algorithm presented in Chapter 2. Firstly, an expansion phase is applied, expanding an initial single-size-heliostat field with small-size heliostats until a fixed upper-bound of the power is achieved. Secondly, during the contraction phase, heliostats having the worst objective values per unit area are sequentially deleted until a lower-bound of the power is achieved. Due to the interaction between heliostats (shading and blocking effects), it is essential to do it in a sequential way and update the ordered list every time a heliostat is removed. The algorithm continues applying both phases until the objective function value of the system does not increase.

This algorithm allows one to study the combination of different heliostats sizes in the same field, according to their corresponding costs per unit area. Of course, some combinations may lead to single-size fields, due to the better heliostat performance or cost of one of the sizes. To the best of the author knowledge, strategies to combine different sizes of heliostats have not been studied in the literature so far.

Keywords: solar thermal power, multi-size-heliostat field, greedy algorithm.

[22] E. Carrizosa, C. Domínguez-Bravo, E. Fernández-Cara, M. Quero.
An optimization approach to the design of multi-size-heliostat fields,
Technical Report IMUS (2014).
Available at: www.optimization-online.org/DB_HTML/2014/05/4372.html

Outline of contents

The dissertation has a total of six chapters. Chapter 1 gives a technical introduction, with a more detailed explanation about SPT systems, the functions involved, the technical and geometrical constraints, and the technological background of the problem.

Chapters 2, 3, 4 and 5 deal with the optimization problems addressed, where innovative results are presented. It is important to emphasize that Chapter 3 was achieved in collaboration with several researchers from various foreign universities. Finally, Chapter 6 is concerned with some problems in which the author is working on now or that she would like to address in the next future.

Chapter 1

Technological background

This chapter summarizes some basis concepts related to the optimization of solar tower power plants that will be the groundwork of this dissertation. It attempts to describe them in a clear manner, trying to facilitate reading comprehension and the understanding of the optimization problems this dissertation is dealing with.

Firstly, a brief introduction about concentrated solar plants and the most popular technologies at the moment is given. Secondly, the mathematical modelling of the general problem is presented, describing the decision variables, objective functions, constraints and the optimization problem definition itself. Finally, the analytical and computational model used to calculate the energy function are described.

1.1 What is an SPT system?

Solar power tower (SPT) systems are a particular type of concentrated solar plant (CSP). A CSP basically consists of a solar concentrator and a receiver, where the sunlight reflected by the solar concentrator is collected into the receiver. CSP technology can be classified in two groups depending on the concentrator shape (its implies different shapes of the focus where the sunlight is reflected): line concentrator (trough and linear fresnel) and point concentrator (tower and dish), see [51]. In particular, SPT plants are composed by point concentrators, and include the presence of a tower.

This dissertation deals with SPT plants where the solar concentrator is a field of rectangular mirrors, called heliostats, and the receiver is placed at the top of a tower, see Figure 1.2. Note that heliostats are mirrors having two-axis tracking movement (to reflect the rays correctly according the different sun positions) and with a fixed foundation, see Figure 1.1.

The heliostats reflect the direct light from the sun to a target point (the center of the receiver aperture) where energy is transferred to a working thermal fluid and produces electricity through a conventional thermodynamic cycle. As said in [69] "solar thermal

electricity may be defined as the result of a process by which directly collected solar energy is converted to electricity through the use of some sort of heat to electricity conversion device."

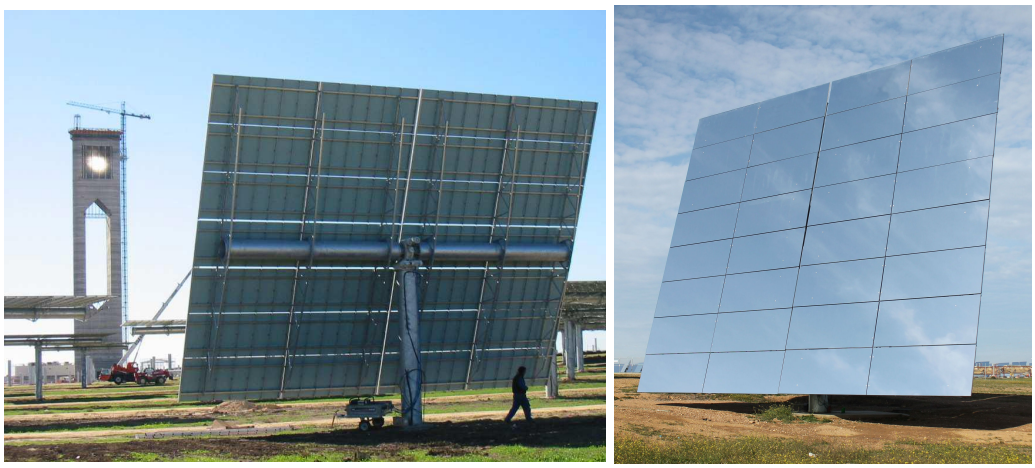

Figure 1.1: Heliostat (back and front). Source Abengoa

The optimal design of an SPT system consists basically of optimizing the *tower-receiver system* and the *heliostat field*. Regarding the tower-receiver system design, the variable characteristics are the tower height and the shape and dimensions of the receiver aperture. On the other hand, related to the heliostat field optimization, the location, number and type of heliostats have to be determined. The final aim is to design an SPT system which maximizes the annual thermal energy collected and minimizes the cost of the system.

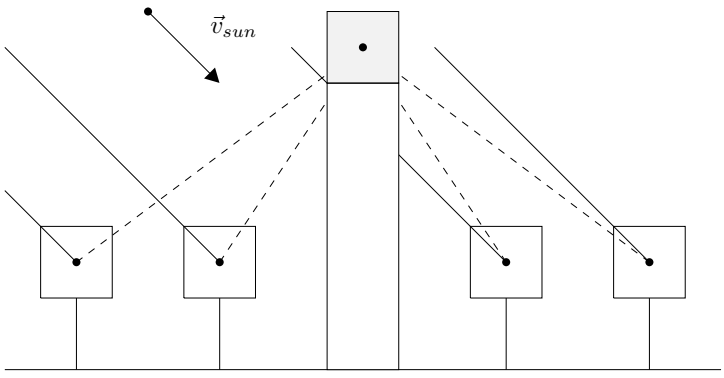

Figure 1.2: Sketch of an SPT system

This optimization problem has great interest in the renewable energy literature, having attracted researchers over the past thirty years. The design of SPT plants started to be studied in 1970s [62, 63, 64, 79, 108, 110] and the first plants were installed in

1980s. An exhaustive compilation of the existing SPT systems can be found in [57].

Much of this technology is recent and in the longer term, large low-cost plants will be necessary for large scale electricity and fuel production, see [69]. Some studies emphasize the use of CSP due to its ability to reach higher temperatures (resulting in high thermodynamic performances) [28], and SPT technology is known as one of the most promising applications [28, 69]. As said in [69]: "This is an exciting time for solar thermal system development."

The problem continues being a very active research field, as can be appreciated in some reviews and dissertations [4, 9, 69, 72, 85, 89, 104].

1.2 Mathematical modelling

As in the previous study [37], two sets of variables are differentiated, having different nature and influence over the objective function. The two sets of variables are those related to the tower-receiver system (*Tower Optimization*) and those related to the heliostat field (*Field Optimization*). Both sets of variables are interconnected, but they have a very different nature and effect in the problem. From now on Θ will denote the set of variables related to the tower-receiver system, and $\mathcal{S}$ will denote the set of coordinates of the centres of the heliostats that define the heliostat field.

In the following, both sets of optimization variables, the objective function, the constraints and the problem formulation will be detailed.

1.2.1 Heliostats field

In the chosen system of coordinates, the positive x axis is the North direction, the positive y axis is the West direction and the z axis is orthogonal to the ground. The heliostat position is given by its coordinate centre (x, y, z). It is assumed that all the heliostats have the same height, denoted by z_0, i.e. the heliostat centres are in the same plane $z = z_0$. In what concerns the heliostat field, the heliostats locations, given by the coordinates (x, y) of their centres, are the variables to be used. The tower is placed at the coordinate origin to remain the reference system valid regardless the location of the plant.

A heliostat is characterized by its geometry and its optical properties. For modelling the general problem, all heliostats are assumed to be rectangular, to be composed of rectangular facets and to have the same dimensions, see Figure 1.1. As pointed out in [10, 28, 67], the heliostat field is a key subsystem regarding the SPT design since it amounts to around 40% of the total cost and causes power losses of around 40% over the ideal collected solar power.

From now on $\mathcal{S} \subset \mathbb{R}^2$ will denote the set of coordinates of the centres of the heliostats that define the heliostat field, and several constraints have to be considered. Firstly the

heliostats must be located within a given region $\Omega \subset \mathbb{R}^2$, and secondly they have to rotate freely avoiding collisions between them. Therefore, the feasible region $\mathscr{S}$ can be written as follows:

$$\mathscr{S} = \left\{ \begin{array}{ll} \mathcal{S} \subset \Omega \subset \mathbb{R}^2 : & |\mathcal{S}| < +\infty \\ & ||(x,y) - (x',y')|| \geq \delta(x,y) + \delta(x',y') \\ & \forall\, (x,y),(x',y') \in \mathcal{S} \quad (x,y) \neq (x',y') \end{array} \right\}, \tag{1.1}$$

where the security distance function δ forces heliostats to not overlap.

In the following, some significant heliostat characteristics that influence the obtained solution, and are involved in the definition of the security distance function, are explained. Conventional heliostats are rectangular in shape, but their horizontal and vertical sides, denoted by Lh and Lv respectively, could vary along the different models, see Figure 1.3(b). The *aspect ratio*, denoted by AR, is usually defined as the quotient between the horizontal and vertical heliostat side,

$$AR(x,y) = Lh(x,y)/Lv(x,y)\,, \tag{1.2}$$

see [78] and Figure 1.3.

The *heliostat area*, denoted by $A(x,y)$, can be calculated directly as the area of the defined rectangle:

$$A(x,y) = Lh(x,y)\,Lv(x,y)\,. \tag{1.3}$$

Usually large heliostats are considered, in which the heliostat surface is composed by several mirror facets, see detail in Figure 1.1(b). Therefore, there exist gaps between these facets that will not reflect the sunlight. The *heliostat effective area* (the amount of area which reflects the sunlight), denoted by A_{e}, can be calculated as follows:

$$A_{\mathsf{e}}(x,y) = c_{\mathsf{e}}(x,y)A(x,y)\,, \tag{1.4}$$

where c_{e} is a fixed coefficient which takes into account the gaps between facets. This coefficient depends on the heliostat model used.

As it has been already mentioned, heliostats have two-axis movement (vertical and horizontal to the ground) which allows the sun rays reflection along the day, see Figure 1.1(a). As collisions between heliostats are avoided, all heliostats need a circular space around them to move freely at any time. This free space is translated into a circle on the ground, called *clear-out circle* see Figure 1.3(a), which centre is the heliostat coordinate centres and which radius can be considered as the *heliostat diagonal*, calculated as follows:

$$d(x,y) = \sqrt{Lh^2(x,y) + Lv^2(x,y)}\,. \tag{1.5}$$

Note that selecting the heliostat diagonal as clear-out radius includes all the possible positions, even the so-called stow position. The stow position (position in which heliostat mirror is parallel to the ground) is not used to reflect sunlight but to pause or protect the heliostat, since for instance it is the position of least vulnerability during high winds [105].

Of course, the heliostat diagonal vary with the heliostat aspect ratio. Hence, different aspect ratios will have different clear-out circles and therefore they will lead to different heliostat field layouts.

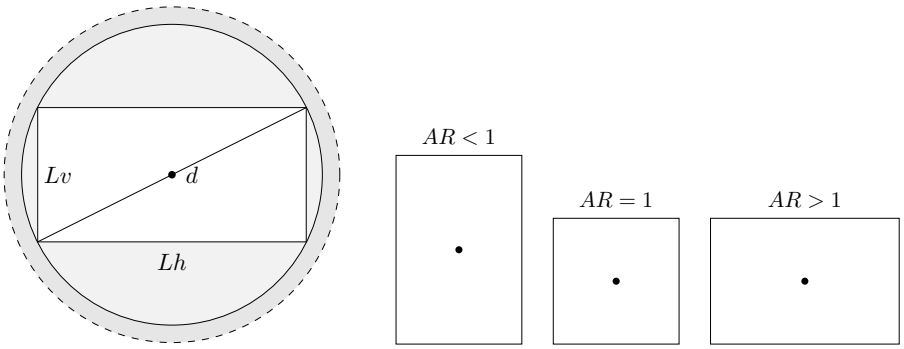

(a) Clear-out circle (b) Aspect ratio

Figure 1.3: Heliostat measurements

Some of the field layout methods found in the literature consider an extra distance, called *safe distance* (or safety distance) and denoted by d_s, see for instance [28, 29, 31, 91], where it is taken as around $0.30\,m$. This extra distance can be modified and plays an important role in the field layout method. It is introduced here in order to give a complete definition of the security distance function δ:

$$\delta(x, y) = d(x, y)/2 + d_s/2\,. \tag{1.6}$$

Note that if all the heliostats have the same dimensions, the distance between two adjacent heliostats centres must be greater than or equal to exactly the diagonal plus the safe distance. In general, heliostats cannot be placed closer than circles with radius $\delta(x, y)$.

1.2.2 Tower-receiver system

The front surface of the receiver, known as the receiver *aperture*, is especially important because it is here where strong radiative losses occur. For simplicity, this dissertation deals with cavity receivers with circular aperture, see Figure 1.4 and [9, 26, 104]. Although the proposed approach is valid for any receiver orientation, as general case it

is considered a North orientation (assuming that the coordinate origin is in the northern hemisphere).

In this approach the most relevant variables associated with the tower-receiver design are considered as detailed in Figure 1.4, namely the *height* h in the tower, the *aperture tilt angle* from the vertical ξ, the *azimuth angle* α which measures the aperture separation from the North axis, and the *aperture radius* r. Note that the fixed parameter $d_{\texttt{ap}}$ denotes the distance between the aperture center and the coordinate origin, and that the *aperture center* is denoted by $Q_{\texttt{e}}$. From now on Θ will denote the list of decision variables concerning the receiver,

$$\Theta = (h, \xi, \alpha, r) \in \mathbb{R}^4 \,. \tag{1.7}$$

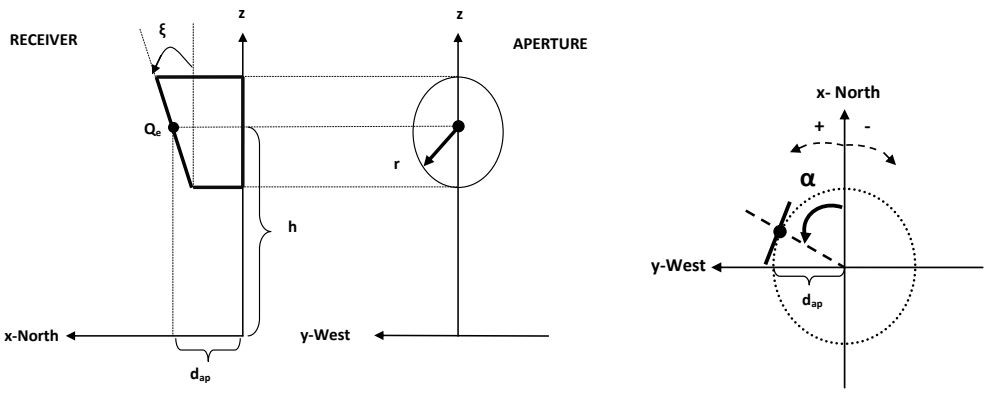

(a) Lateral-Front (b) Top

Figure 1.4: Receiver with circular aperture

Some constraints on these variables are determined by the operation scheme of the system, which is in turn influenced by technical and legal regulations, leading to a compact set $\boldsymbol{\Theta}$ as the feasible region for Θ. There exist minimum and maximum values, $r_{\texttt{min}}$ and $r_{\texttt{max}}$ respectively, for the aperture radius, a maximum value $h_{\texttt{max}}$ for the tower height and two different closed intervals for the two angles, ξ and α. The North axis corresponds to $\alpha = 0$, and this angle takes negative values to the East direction and positive values to the West. The feasible region $\boldsymbol{\Theta}$ can then be written as follows:

$$\boldsymbol{\Theta} = \left\{ \begin{array}{ll} \Theta \in \mathbb{R}^4 \,: & r_{\texttt{min}} \leq r \leq \min(h, r_{\texttt{max}}) \leq h_{\texttt{max}} \\ & \xi \in [0, \pi/2] \\ & \alpha \in [-\pi, \pi] \end{array} \right\} . \tag{1.8}$$

1.2.3 Optimization criteria

In the following the two criteria involved in the optimization (cost function and annual thermal energy function) and the objective function considered are described. A deep description of the analytical and computational model used to calculate the collected annual thermal energy is given in Section 1.3.

Cost function

The cost function considered, denoted by C, takes into account the investment in solar power plant equipment (tower-receiver and heliostat field), power electronics, purchasing of land, and civil engineering costs, see [103]. Hence, it depends on the receiver variable Θ, and the number of heliostats in the field $|\mathcal{S}|$, as follows:

$$C(\Theta, |\mathcal{S}|) = \beta_1 (h + \lambda_1)^{\lambda_2} + \beta_2 \pi r^2 + c_{\mathtt{f}} + c\,|\mathcal{S}|\,, \tag{1.9}$$

where β_1 and β_2 are empirical constants with values in $(0, 1)$, λ_1 and λ_2 are positive and given by appropriate physical considerations and c denotes the cost per heliostat. For simplicity, the cost associated with the land (purchasing and preparing) is considered fixed and denoted by $c_{\mathtt{f}}$. Note that, as the power block is not considered in the optimization problem modelling, the cost associated with the power block (electric power generation system and associated components) is not included.

Annual thermal energy function

The collected annual thermal energy function E takes the form:

$$E(\Theta, \mathcal{S}) = \int_0^T \Pi_t(\Theta, \mathcal{S})\, dt - \gamma_1\,, \tag{1.10}$$

where the function Π_t denotes the receiver outlet thermal power at time instant t and γ_1 is a constant which measures the fixed thermal energy losses related to the whole system.

In this work the collected annual thermal energy is computed using an algorithm detailed in section 1.3, which is based on NSPOC (Nevada Solar Power Optimization Code) procedure [33]. The reader is referred to [13, 30, 31, 104] for further details.

Objective function

Two criteria are taken into account for the optimization of the SPT system: the total construction cost and the collected annual thermal energy. As said in [36, 103], these objectives are in conflict to each other, since often a cheap system will collect a low amount of energy whereas a more efficient plant will be more expensive. Therefore,

the optimization problem is a non-linear bi-objective problem [42, 68]. No common optimum can be found for both criteria, and one common approach in the literature is to to deal with an aggregation function, as the minimization of cost per unit of collected annual thermal energy, denoted from now on by F and calculated as follows:

$$F(\Theta, \mathcal{S}) = C(\Theta, |\mathcal{S}|)/E(\Theta, \mathcal{S})\,. \tag{1.11}$$

This objective function is also known as the he levelized cost of electricity (LCOE) or levelized energy cost (LEC). It represents the cost per kilowatt-hour of building and operating a generating plant over an assumed financial life and duty cycle. Note that in this approach the thermal energy calculation is based on one year and that operations and maintenance costs (as for instance heliostat cleaning), taxes and uncertainty factors are neglected, see in [6, 44, 61] other approaches, where similar assumptions are considered.

As pointed out in [2], formulas for the levelized cost should be used with caution because they may include some important assumptions. New objective function definitions have been introduced recently in order to clarify theses issues. See for instance [106], where a new metric is developed, [15] where the levelized cost of coating (LCOC) is introduced and, [95], where the "concentration cost" objective function is defined. Note that the proposed optimization procedures are independent on the cost function used, so any of such new definitions can be used as optimization criteria.

1.2.4 Additional constraints

When designing an SPT system, usually a fixed instant of time is used to size the system, as explained in [26, 91, 93]. This time instant is known in the literature as the *design point*, $T_{\mathtt{d}}$. Two additional constrains should be imposed over the power absorbed by the receiver at $T_{\mathtt{d}}$. A minimal power Π_0 has to be achieved at this time. In real world designs, the receiver is also constrained by material properties, see [19, 83]. The maximum power absorbed by the receiver at $T_{\mathtt{d}}$ is limited by Π^+. This leads to the following constrains:

$$\Pi_0 \leq \Pi_{T_{\mathtt{d}}}(\Theta, \mathcal{S}) \leq \Pi^+\,. \tag{1.12}$$

A uniform distribution of heat flux on the receiver is required in order to avoid strong stresses. In the proposed approach this constraint it not considered, as the heliostat aiming strategy is fixed (all heliostats are aiming to the aperture centre). However, this is an important requirement that has to be studied together with the heliostat aiming strategy, see [12] and Chapter 6 for further remarks.

1.2.5 Optimization problem formulation

In general, this dissertation is addressing the following optimization problem:

$$(\mathcal{P}) \begin{cases} \min\limits_{\Theta,\mathcal{S}} & F(\Theta,\mathcal{S}) \\ \text{subject to} & \Theta \in \mathbf{\Theta} \\ & \mathcal{S} \in \mathscr{S} \\ & \Pi_0 \leq \Pi_{T_d}(\Theta,\mathcal{S}) \leq \Pi^+ \,. \end{cases} \tag{1.13}$$

Note that both sets of variables are highly interconnected, since the heliostat size has a significant impact in the receiver size and the operational constraints of the receiver and its size will also have a great influence the field layout, see [26, 34, 83]. Observe that the points of $\mathcal{S}$ belong to $\mathbb{R}^2$ and $\mathcal{S}$ can be viewed as a set of non-fixed cardinality. Consequently, the sequel relations can be written in the following form $\mathcal{S} \subset \mathbb{R}^2$.

Three challenging issues of the problem are the dimensionality of the heliostat field problem, with (a priori unknown) hundreds or thousands of variables, the non-convex constraints related to the location of heliostats (which prevent the heliostats from colliding), and the evaluation of the objective function. This evaluation is implicitly defined by the subroutine, and due to the nature of the process, is not smooth, multi-modal and has no apparent mathematical structure which can help to choose an appropriate optimization algorithm. As said in [28], one of the main problems of the full optimization of any heliostat field is the need of recalculate the shadows and blockages for all the heliostats at every step of the process due to the high computational time needed to calculate all the projections involved.

1.3 Analytical and computational model

In this section the model used to compute the thermal annual energy function is specified. The efficiency functions are described in detail, and the reader is referred to appropriate references for an in-depth study. The simplifications used in the computational model are also described.

As said in [43], master user-friendly modelling tools are needed to design, optimize and simulate the solar components of the system. Several codes have been developed for the design and optimization of the heliostat field layout since the 1970s. As said in [28], these codes are necessary because both the optimization process and the energy evaluation of a given field layout are rather complex problems.

In order to calculate the collected thermal annual energy, the different solar energy losses that appear during the sunlight reflection process need to be measured. In the next subsections the concepts involved in the calculation are introduced, namely, the solar irradiation data, the direction vectors, the efficiency functions and the annual

thermal energy. The following formulas were firstly introduced in [37] based on NSPOC Fortran code, see [33].

During this dissertation a prototype has been developed to solve the optimization problems involved implementing the proposed heuristic procedures. Matlab© software has been selected for the modelling of this prototype.

1.3.1 Solar irradiation data

The solar irradiation varies along the different time instants. $I(t)$ denoted the solar irradiation value at time t. These values will determine the solar power into the receiver at each time instant.

The selected approach considers for simplicity clear days, i.e. irradiation data if all the days were clear without clouds. Some authors include cloudy days in their computational experiences, see for instance [83], while others are against the use of clouds days during the optimization design process, see [20]. Note that in the daily life of the plant, the operational strategies (for instance the selection of active and inactive heliostats) will be calculated using the exact irradiation values (during cloudy or clear days).

The solar irradiation data can be approximately symmetrical with respect the central solar hour and with respect the months of the year, as can be appreciated in Figures 1.5. However, this property depends on the typical irradiation data of the selected site location, see for instance in Figure 1.5(b) an asymmetrical example with real world data.

1.3.2 Direction vectors

In order to determine the heliostat surface plane at each time t, the sun position has to be determined. The unit solar vector, denoted by $\vec{v}_{\mathtt{sun}}$, calculates the sun position (given the site latitude, solar hour and day of year). The selected approach makes use of the Spencer's formula to calculate the solar declination, see [1]. With these data, solar azimuth angle $\alpha_{\mathtt{sun}}$ and solar height angle $\beta_{\mathtt{sun}}$ can be obtained, and the solar vector can be calculated as follows:

$$\vec{v}_{\mathtt{sun}}(t) = (-\cos\beta_{\mathtt{sun}}(t)\cos\alpha_{\mathtt{sun}}(t), \cos\beta_{\mathtt{sun}}(t)\sin\alpha_{\mathtt{sun}}(t), \sin\beta_{\mathtt{sun}}(t))\,. \tag{1.14}$$

The heliostat mirror surface has to reflect the sunlight to the receiver aperture at each time instant. For simplicity, in the field optimization models is usual to consider the same aim point for all heliostats. In this approach, the aiming or target point is considered as the centre of the circular aperture, given by:

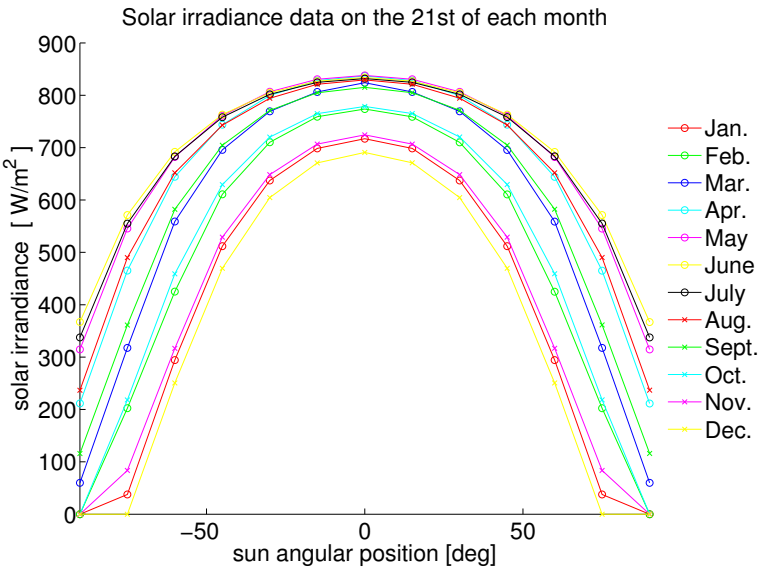

(a) Symmetrical

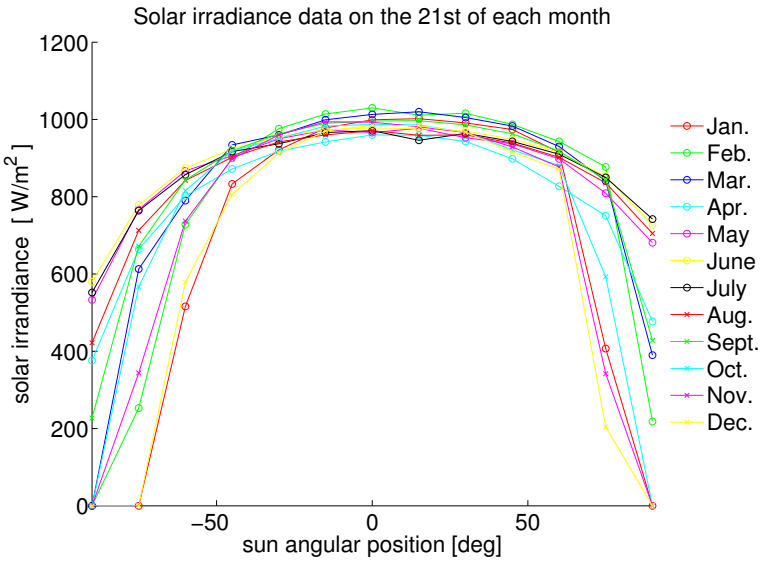

(b) Asymmetrical

Figure 1.5: Irradiation profiles

$$Q_{\mathtt{e}} = (d_{\mathtt{ap}}, 0, h)\,, \tag{1.15}$$

see also Figure 1.6. In Chapter 6, different strategies appearing in the literature to determine the aiming strategy are discussed.

Given the heliostat coordinate centre and once the target point is fixed, the reflected ray is defined by vector $\vec{w}$, from the heliostat centre to the target point $Q_{\mathtt{e}}$, that can be obtained as:

$$\vec{w}(x, y) = (d_{\mathtt{ap}} - x, -y, h - z_0)\,. \tag{1.16}$$

Analogously, the incident ray is defined by the vector which direction corresponds to the opposite direction to the sun vector, i.e. $-\vec{v}_{\mathtt{sun}}(t)$. Note that this vector is the same regardless of the heliostat position. Finally, the addition of the incident and reflected directions gives us the normal vector to the mirror plane η, as can be seen in Figure 1.6.

The normal vector to the receiver aperture within the output direction is introduced below. This vector is denoted by $\vec{p}$ and calculated as follows:

$$\vec{p} = (-\cos\xi, 0, \sin\xi)\,. \tag{1.17}$$

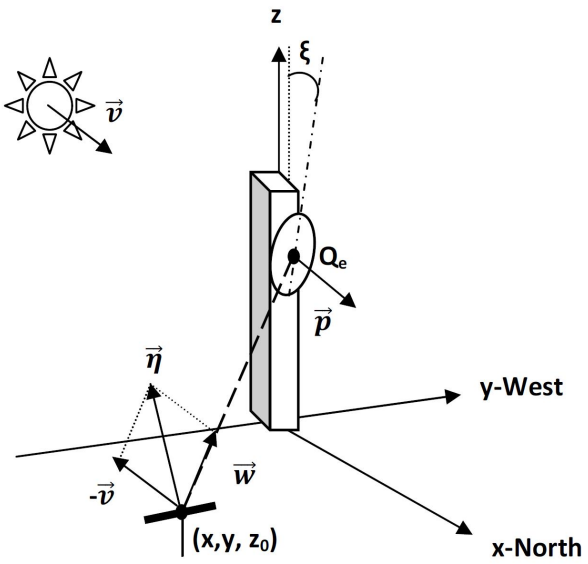

Figure 1.6: Direction vectors

1.3.3 Efficiency functions

As usual in this framework, five efficiency functions are considered to measure the energy losses that appear in the process. These functions give a coefficient in the range $[0, 1]$, which represents the proportion of the incident solar energy that will effectively reach the receiver aperture. In the following paragraphs their calculation, based on NSPOC [33], are going to be explained and appropriate references for a deeper study will also be detailed.

1. **Heliostat Reflectivity**

   The heliostat reflectivity, also known as mirror reflectance factor, is related to the mirror own properties and cleanliness, see [92]. That is, this factor measures the solar losses related to the mirror structure itself and has nothing to do with, for instance, the field configuration. This function can be expressed as the product of two coefficients, $c_{\mathtt{r}}$ (reflectance coefficient) and $c_{\mathtt{e}}$ (effective area), which is related to the mirror area, see (1.4); the heliostat reflectivity is expressed as follows:

   $$f_{ref}(x, y) = c_{\mathtt{r}}\, c_{\mathtt{e}}(x, y)\,, \tag{1.18}$$

   see [28, 92, 95, 112] for further details.

2. **Atmospheric efficiency**

   The atmospheric efficiency function decreases as the distance between the heliostat and the receiver increases. This efficiency, also known as atmospheric attenuation or atmospheric transmission efficiency, can be written as follows.

   $$f_{at}(x, y) = \alpha_1 - \alpha_2||\vec{w}(x, y)|| + \alpha_3||\vec{w}(x, y)||^2\,, \tag{1.19}$$

   where $||\cdot||$ denotes the Euclidean norm in $\mathbb{R}^3$, and α_i for $i = 1, 2, 3$ are fixed coefficients which values, in the interval $(0, 1)$, are determined empirically. See [13, 28, 31, 95, 112] for further details.

3. **Cosine efficiency**

   The effective sunlight depends on the relative position between the sun, the heliostat and the receiver aperture. The cosine efficiency, as its name suggests, measures the cosine of the angle between the incident ray $\vec{v}_{\mathtt{sun}}$ and the reflected ray $\vec{w}$. This efficiency can be calculated as follows:

$$f_{cos}(t,x,y,\Theta) = \sqrt{\frac{1}{2} + \frac{\vec{w}(x,y)\cdot\vec{v}_{\texttt{sun}}(t)}{2\,||\vec{w}(x,y)||}}\,, \tag{1.20}$$

see Figure 1.7, where the two vectors $\vec{w}$ and $\vec{v}_{\texttt{sun}}$ are represented for different heliostat positions.

Note that considering this formula, the highest value (1) and the lowest value (0) are reached when both vectors are parallel with the same and the opposite directions respectively. See [28, 31] for further details.

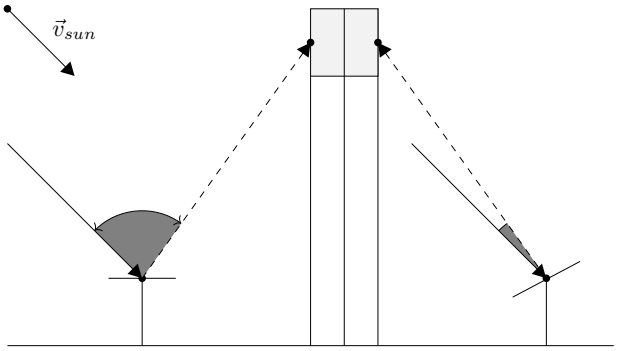

Figure 1.7: Cosine efficiency

4. **Interception efficiency**

The interception efficiency, also known as spillage factor, is the fraction of energy spot reflected by the heliostat that gets the receiver aperture. As said in [95], this value is calculated through an integration of the image shape produced by the heliostat over the receiver aperture. For simplicity, the receiver aperture is considered as a circular aperture. The interception efficiency is calculated as follows.

$$f_{sp}(t,x,y,\Theta) = f_1(t,x,y) \iint_S \exp\left(\frac{-f_2(u,v,x,y)}{2\,f_3^2(t,x,y,\Theta)}\right) du\,dv\,, \tag{1.21}$$

where S denotes the circular aperture and f_i with $i = 1,2,3$ are the following

functions:

$$f_1(t,x,y) = \frac{f_4(x,y)}{2\pi f_3^2(t,x,y)||\vec{w}(x,y)||^2}\,, \tag{1.22a}$$

$$f_2(u,v,x,y) = \frac{(u^2+v^2)}{2||\vec{w}(x,y)||^2}\left[(1+f_4^2(x,y)) + \frac{u}{\sqrt{(u^2+v^2)}}(1-f_4^2(x,y))\right]\,, \tag{1.22b}$$

$$f_3(t,x,y,\Theta) = \left[\mu_1^2 + \left(\frac{\mu_2(x,y)\,(1-f_{cos}(t,x,y,\Theta))}{4\,||\vec{w}(x,y)||}\right)^2\right]^{1/2}\,, \tag{1.22c}$$

$$f_4(x,y) = [\cos(\kappa(x,y))]_+ = \begin{cases} 0 & \text{if } \cos\kappa(x,y) \le 0 \\ \frac{\vec{w}(x,y)\cdot\vec{p}}{||\vec{w}(x,y)||} & \text{otherwise} \end{cases}\,, \tag{1.22d}$$

where μ_1 denotes a fixed coefficient related to the aberration factor (distortion due to the defocusing of the sun spot). The value μ_2 represents the diameter of the equivalent circle to the heliostat.

This integral is evaluated by means of a numerical approximation. Firstly, a change to polar coordinates is applied ($u = \rho\sin\phi$ and $v = \rho\cos\phi$), obtaining:

$$f_{sp}(t,x,y,\Theta) = f_1(t,x,y)\int_0^{2\pi}\int_0^r \exp\left(\frac{-f_2(\rho,\phi,x,y)}{2\,f_3^2(t,x,y,\Theta)}\right)\rho\,d\rho\,d\phi\,. \tag{1.23}$$

Then, integrating analytically over ρ:

$$f_{sp}(t,x,y,\Theta) = 2f_1(t,x,y)f_3^2(t,x,y))\int_0^{2\pi}\frac{1}{f_5(\phi,x,y)}\left(1-\exp\left(-\frac{r^2\,f_5(\phi,x,y)}{2\,f_3^2(t,x,y,\Theta)}\right)\right)\,d\phi\,. \tag{1.24}$$

where

$$f_5(\phi,x,y) = \frac{(1+f_4^2(x,y)) + \cos\phi(1-f_4^2(x,y))}{2||\vec{w}(x,y)||^2}\,. \tag{1.25}$$

Finally integrating numerically over ϕ, applying the Simpson's rule with $\phi_1 = (i-1/2)\pi/10$, one gets:

$$f_{sp}(t,x,y,\Theta) \cong \frac{\pi}{5}f_1(t,x,y)f_3^2(t,x,y))\sum_{i=1}^{10}\frac{1}{f_5(\phi_i,x,y)}\left(1-\exp\left(-\frac{r^2\,f_5(\phi_i,x,y)}{2\,f_3^2(t,x,y,\Theta)}\right)\right)\,, \tag{1.26}$$

see [26, 28, 30, 95] for further details.

5. **Shading and blocking efficiency**

The shading and blocking efficiency depends on the heliostats positions (the rel-

ative position between them) and the sun position. Therefore, it has to be calculated for each heliostat at each time instant.

In order to measure the shadow and blockage caused over a heliostat placed at position (x, y) (called *main heliostat*), one should take into account all the remaining heliostats in the field. However this option, although more precise, is very time consuming. It is usual in the literature to select a lower number of *neighbouring heliostats*, and calculate their effects over the main heliostat.

In the selected approach, the nearest 24 neighbouring heliostats are used, considering the Euclidean distance with respect the main heliostat center. Two types of interferences appear: shadow (a neighbouring heliostat inhibits the incident sunlight to reach the main heliostat) and blockage (the sunlight reflected by the main heliostat hit on a neighbouring heliostat and cannot reach the receiver aperture), see Figure 1.8. Note that for each heliostat and each time instant the calculation is repeated for each neighbouring heliostat.

From a computational point of view, the proportion of effective mirror area of the main heliostat (free of shadow and unblocked) is calculated following the Sassi's procedure, see [39, 94]. In this procedure one discretizes the mirror surface of the main heliostat into a grid, and projects there the centres of the neighbouring heliostats. Due to its quick computation, the following simplification of the process is applied: neighbouring heliostat planes are assumed to be parallel to the main heliostat plane at each time, see [28, 92]. As the main and neighbouring heliostat planes are considered parallel, the projections are rectangular shaped, which strongly simplifies the calculation.

The projection follows the direction vector given by the reflected ray $\vec{w}$ to obtain blockage and follows the inverse of the unit solar vector $-\vec{v}_{\mathtt{sun}}$, to obtain shadow. As result, the proportion of mirror area free of shadowing and blocking is obtained. As said in [28], one advantage of this strategy is the direct computation of overlapping situations when considering all the neighbouring heliostats.

1.3.4 Annual thermal energy

In the previous subsections all the necessary pieces to calculate the annual thermal energy have been described. In this subsection the annual thermal energy definition is given following three natural steps (incident solar energy, receiver outlet thermal power and annual thermal energy). Finally, some computational simplifications over the calculation of these functions are discussed.

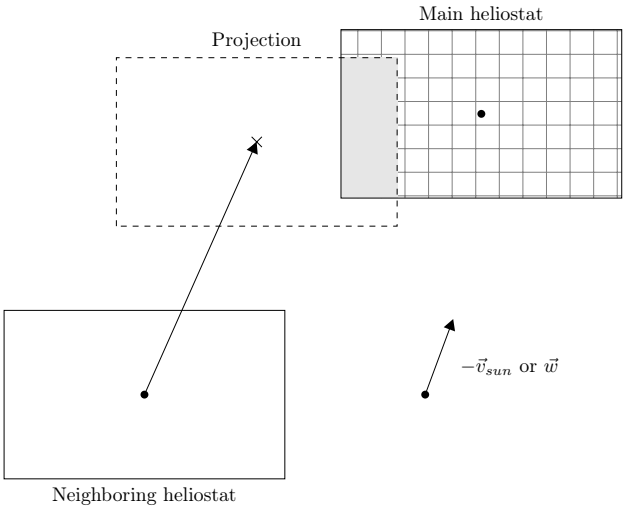

Figure 1.8: Shadow and blockage

Incident solar energy

The incident solar energy is the ideal solar power incident into the receiver, that is, the solar power collected if no energy losses are taken into account. Each heliostat located in the field receives over its heliostat area $A(x, y)$ a solar irradiation $I(t)$ at time t. The incident solar energy is calculated by adding the values collected at the field:

$$\Pi_t^*(\Theta, \mathcal{S}) = I(t) \sum_{(x,y)\in\mathcal{S}} A(x, y)\,. \tag{1.27}$$

Receiver outlet thermal power

The solar power collected into the receiver depends proportionally on the product of the so-called efficiencies functions. The efficiency functions are grouped in the function φ. The solar power into the receiver can be calculated as follows:

$$\tilde{\Pi}_t(\Theta, \mathcal{S}) = I(t) \sum_{(x,y)\in\mathcal{S}} \varphi(t, x, y, \Theta, \mathcal{S})\, A(x, y)\,, \tag{1.28}$$

where I is the so-called instantaneous direct solar irradiation, $A(x, y)$ is the area of the heliostat places at position (x, y), and the function φ can be detailed as follows:

$$\varphi(t, x, y, \Theta, \mathcal{S}) = f_{ref}(x, y)\, f_{at}(x, y)\, f_{cos}(t, x, y, \Theta)\, f_{sp}(t, x, y, \Theta)\, f_{sb}(t, x, y, \Theta, \mathcal{S})\,. \tag{1.29}$$

The receiver outlet thermal power value collected by the heliostat field $\mathcal{S}$ at time t

is calculated by subtracting thermal energy losses related to the receiver itself:

$$\Pi_t(\Theta, \mathcal{S}) = I(t) \sum_{(x,y)\in\mathcal{S}} \varphi(t, x, y, \Theta, \mathcal{S}) A(x, y) - \gamma_2 \pi r^2 \,, \tag{1.30}$$

where the constant γ_2 is a given constant related to the receiver aperture (which surface is πr^2).

Annual thermal energy

Once the solar power into the receiver collected by the heliostat field is calculated for each time instant, its integration over the whole year (interval $[0, T]$) results into the thermal annual energy of the SPT system.

$$\tilde{E}(\Theta, \mathcal{S}) = \int_0^T \tilde{\Pi}_t(\Theta, \mathcal{S})\, dt \,. \tag{1.31}$$

As already presented in (1.10), the thermal annual energy collected by a heliostat field $\mathcal{S}$ given the tower-receiver variables Θ is calculated as:

$$E(\Theta, \mathcal{S}) = \int_0^T \Pi_t(\Theta, \mathcal{S})\, dt - \gamma_1 \,, \tag{1.32}$$

where γ_1 is a given constant which measures final thermal losses appearing in the process.

Computational simplifications

It is usual in the literature to use some representative days and hours instead of computing the solar power at each time instant of the year, $t \in [0, T]$. Then the receiver outlet thermal power for the year estimation is obtained by fitting data, see [83], (for instance through a polynomial function). Finally, the total daily and annual energies are computed by integrating the hourly power output.

This simplification helps to perform a fast evaluation of the collected thermal annual energy function (and therefore of the objective function), which, though less accurate, allows one to evaluate the objective function in a reasonable time at each step of the optimization process.

Different strategies can be found in the literature on the selection of the representative days. For instance, in [91], five specific days (equinoxes and solstices among them) are considered. Four representative days, one of each season are used in [103] to perform the simulation, assuming that they have an equal weight in the interpolation. In [18], the computation time is sped up considering for each month of the year a single representative day. Based on the NSPOC approach, only a representative day per month

and 12 hours are considered in the numerical work, specifically the 21st of each month, and all of them are assumed to have equal weights in the interpolation.

Due to the complexity of the model, it seems very hard to measure in a rigorous way the error caused by such discretization. However, one can have an idea by checking how stable results are with respect to the grid used. For instance, if it is considered 5, 9 or 13 different hours to compute the daily thermal energy, for different fixed days the results shown in Table 1.1 are obtained. These results suggest that 1 or 2 decimal digits are acceptable and significant.

21th Month / E (MWth)	March	June	September	December
E_5	0.**3**71825	0.**4**05744	0.**37**4933	0.**2**72064
E_9	0.**3**67207	0.**4**06332	0.**37**1733	0.**2**68578
E_{13}	0.**3**64203	0.**4**10110	0.**37**0317	0.**2**44562

Table 1.1: Daily Thermal Energy

As it was mentioned before, firstly a polynomial fitting is applied over each selected day to obtain the monthly energy value. Then the resulting twelve polynomials, one for each month, are integrated over the solar hours given the corresponding monthly values. Secondly, a final polynomial fitting is performed over the obtained monthly values and integrated over the year obtaining the final annual value.

Based on the NSPOC approach, a quadratic polynomial had been used in both cases (monthly and annual integration). However, even for symmetrical solar irradiation data this fitting is not accurate at some months.

A particular emphasis should be made over the polynomial fitting itself, as it has to be accurate enough for any irradiation data. Symmetry or any other specific properties of the chosen site should not be used for a general case. For instance, when considering more than one receiver, see Chapter 4, this quadratic polynomial cannot be used, since it creates a strong distortion. Instead, it is simply computed the annual energy value of each representative day considering the receiver thermal power function as a piecewise constant function and applying the rectangular quadrature rule.

Chapter 2

A heuristic method for simultaneous tower and pattern-free field optimization on solar power systems

2.1 Introduction

The optimal design of an SPT system consists of determining the tower height, the shape and dimensions of the receiver aperture in the tower (*Tower Optimization*) and the location and number of the heliostats (*Field Optimization*) so as to optimize the annual thermal energy collected and the cost of the system.

Three challenging issues are the dimensionality of the field optimization problem, with (a priori unknown) hundreds or thousands of variables, the nonconvex constraints related to the location of heliostats (which prevent the heliostats from colliding), and the evaluation of the objective function. This evaluation is implicitly defined by the subroutine, and due to the nature of the process, is not smooth, multimodal and has no apparent mathematical structure which can help to choose an appropriate optimization algorithm.

Radially staggered pattern has been so far the most popular pattern used to solve the *Field Optimization* problem. By the pattern itself, access is guaranteed to all heliostats in the field for cleaning or repairing work, since roads are naturally given. Although pattern-free fields do not define roads in their layout, (see e.g. the recently built Ivanpah system [55]), one may impose, as it is done along this chapter, heliostats to be sufficiently apart from each other, so that access to all heliostats in the field is possible. This would not be needed if new strategies for cleaning the heliostats were developed, see [3].

Fixed-pattern strategies consider the number of heliostats to be located not given in

advance: an oversized field (i.e., a field with a sufficiently large number of heliostats), is built, and then those heliostats reflecting less solar energy into the receiver are sequentially removed while guaranteeing that a given receiver outlet thermal power is attained. This way, although the optimal parameters for the oversized field were obtained, there is a high risk that a strong distortion exists between the original and final fields.

A heliostats location procedure is presented which will not force to follow a specific geometrical pattern, and, instead, will be a pattern-free optimization strategy. With this algorithm an initial oversized field is not needed, the final number of heliostats is found during the optimization process. A possible drawback is that road design (to access heliostats for maintenance and cleaning) and building may be more expensive. Contrarily, pattern-free fields are much more flexible and can be adapted (as will be shown in Section 2.4.3) to many geographical circumstances.

Most articles in the literature focus on the *Field Optimization* problem, see [27, 91, 102], or on the *Tower Optimization* separately, see [45]. References to simultaneous optimization of the *heliostat field* and *tower-receiver system* are very scarce. [80] and [83] address the joint optimization by using a metaheuristic (genetic algorithm [46, 70] and simplex Nelder-Mead [58, 73]) improved by local searches (Powell descent method [41]), always under the assumption of a radially-staggered pattern for the field.

This chapter presents a pattern-free procedure for the field layout optimization, and an optimization algorithm including the optimization of both the tower-receiver system and the heliostat field.

The rest of the chapter is organized as follows. In Section 2.2, the main ingredients affecting the performance of the SPT system are described. In Section 2.3, the methodology proposed to solve the problem is explained. In Section 2.4, the optimization algorithms and analysis tools are applied to a typical SPT design, and finally, in Section 2.5, the main results of this chapter are summarized and the conclusions are presented.

2.2 Problem statement

In this Section, the SPT system, the variables used in the optimization process and the constraints that have to be satisfied are described. Finally, the two criteria involved in the objective function (energy and cost) and the optimization problem are presented.

2.2.1 Decision variables

As it was mentioned in Chapter 1, two types of decision variables appear, some associated with the height of the tower and the receiver aperture, and the remaining ones associated with the heliostats locations.

For simplicity, in this chapter only the two most relevant variables associated with the tower and the receiver design are considered, namely the *aperture size*, given by its radius r, and its height h in the tower. The two angles ξ and α defined in the previous chapter are considered as fixed parameters. Related to the heliostat field, the heliostats locations, given by the coordinates (x, y) of their centres, are the variables to be used.

Therefore, along this chapter Θ will denote the variables related to the tower-receiver system, i.e. $\Theta = (r, h)$, and by $\mathcal{S}$ the finite set of coordinates of the centres of the heliostats that define the heliostat field. The decision variables are Θ and $\mathcal{S}$.

2.2.2 Constraints

The feasible region related to the set of variables Θ is denoted by $\mathbf{\Theta}$ and defined in Eq. (1.8). The constraints related to the tower-receiver variables considered in this chapter can be rewritten as follows:

$$\mathbf{\Theta} = \{(r, h) \,:\, r_{min} \leq r \leq \min(h, r_{max}) \leq h_{max}\} \,. \tag{2.1}$$

Related to the heliostat field, the constraints described in Eg. 1.1, which defined the feasible region $\mathscr{S}$, have to be considered. The heliostats must be located within a given region $\Omega \subset \mathbb{R}^2$ and they have to rotate freely avoiding collisions between them, that is $\mathcal{S} \in \mathscr{S}$.

Regarding the additional constraints related to the allowable receiver outlet thermal power (see Eq. (1.12)), only a minimal power requirement Π_0 at T_d is considered, that is:

$$\Pi_{T_d}(\Theta, \mathcal{S}) \geq \Pi_0 \,. \tag{2.2}$$

2.2.3 Optimization problem

Two criteria are taken into account for the optimization of the SPT system: the total construction cost (see Eq. (1.9)) and the annual thermal energy collected (see Eq. (1.10)).

The annual thermal energy collected is computed using an algorithm similar to NSPOC procedure, that is described in [33]. The reader is referred to Chapter 1 and [13, 30, 31, 104], for further details.

No common optimum can be found for both criteria, so they are aggregated into one single objective, namely, the maximization of annual thermal energy collected per unit cost. Written this way, the addressed optimization problem is the following:

$$(\mathcal{P})\begin{cases}\max\limits_{\Theta,\mathcal{S}} & F(\Theta,\mathcal{S}) = E(\Theta,\mathcal{S})/C(\Theta,|\mathcal{S}|)\\ \text{subject to} & \Theta \in \mathbf{\Theta}\\ & \mathcal{S} \in \mathscr{S}\\ & \Pi_{T_d}(\Theta,\mathcal{S}) \geq \Pi_0\end{cases} \tag{2.3}$$

2.3 An alternating procedure to design the SPT system

In order to solve $(\mathcal{P})$, an alternating procedure is suggested, in which one sequentially optimizes the field layout for a given tower-receiver design and then, the tower-receiver system is optimized for the previously obtained field. In other words, the problems $(\mathcal{P}_\Theta)$ and $(\mathcal{P}_\mathcal{S})$ are alternatively solved. Both subproblems are described below.

A drawback of the alternating strategy is that, starting from a bad solution, the algorithm could converge to inefficient solutions. This risk can be prevented with a multistart of the alternating process, considering different random initial tower-receiver configurations as initial solutions. Although not formal proofs are given, empirical evidences appear which show that the algorithm converges to solutions outperforming heliostat fields such as **PS10**, **RPS10** and **Spiral** based, see Section 2.4.

The $(\mathcal{P}_\Theta)$ subproblem, that is, the optimization of the heliostat field for a fixed tower, can be written as follows:

$$(\mathcal{P}_\Theta) \quad \Theta \text{ fixed} \begin{cases}\max\limits_{\mathcal{S}} & F(\Theta,\mathcal{S})\\ \text{subject to} & \mathcal{S} \in \mathscr{S}\\ & \Pi_{T_d}(\Theta,\mathcal{S}) \geq \Pi_0\end{cases} \tag{2.4}$$

Observe that the cardinality of $\mathcal{S}$ (number of heliostats) is not fixed in advance in problems $(\mathcal{P})$ and $(\mathcal{P}_\Theta)$, thus they cannot be expressed as standard optimization problems in fixed dimension.

The other subproblem $(\mathcal{P}_\mathcal{S})$ given below describes the optimization of the tower-receiver when the field of heliostats $\mathcal{S}$ is fixed.

$$(\mathcal{P}_\mathcal{S}) \quad \mathcal{S} \text{ fixed} \begin{cases}\max\limits_{\Theta} & F(\Theta,\mathcal{S})\\ \text{subject to} & \Theta \in \mathbf{\Theta}\\ & \Pi_{T_d}(\Theta,\mathcal{S}) \geq \Pi_0\end{cases} \tag{2.5}$$

The alternating algorithm used to solve the optimization problem $(\mathcal{P})$ is described in Algorithm 1 and Figure 2.1. As it has been said, this algorithm alternatively solve the tower-receiver system and the heliostat field optimization problems. It is considered that the algorithm has performed a complete iteration when a tower problem and a field problem have been solved. Each time an optimization subproblem is solved, that is $(\mathcal{P}_\mathcal{S})$ or $(\mathcal{P}_\Theta)$, the highest value obtained for the objective function and the system

design associated with this value are stored in the variable $\Upsilon_{objective}$. At the end of each iteration, the relative error is calculated. If it is lower than a given value ϵ (positive and small), the algorithm stops and returns the highest computed value.

Algorithm 1 `Alternating algorithm`

Require: Θ^0 (feasible) and ϵ
  $k \leftarrow 0$
  $\mathcal{S}^0 \leftarrow$ solve $(\mathcal{P}_\Theta)$ given $\Theta = \Theta^0$
  $\Upsilon_{objective} \leftarrow F(\Theta^0, \mathcal{S}^0)$
  repeat
    $k \leftarrow k + 1$
    $\Theta^k \leftarrow$ solve $(\mathcal{P}_\mathcal{S})$ given $\mathcal{S} = \mathcal{S}^{k-1}$
    $\mathcal{S}^k \leftarrow$ solve $(\mathcal{P}_\Theta)$ given $\Theta = \Theta^k$
    $\Upsilon_{objective} = \min\{\Upsilon_{objective}, F(\Theta^k, \mathcal{S}^{k-1}), F(\Theta^k, \mathcal{S}^k)\}$
  until $||F(\Theta^k, \mathcal{S}^k) - F(\Theta^{k-1}, \mathcal{S}^{k-1})|| \leq \epsilon$
  return $\boxed{\Upsilon_{objective}}$

At the starting step, the initial value Θ^0 for the variable Θ is set randomly in the feasible region $\mathbf{\Theta}$. Once this initial value is calculated, the first heliostat field is obtained solving problem $(\mathcal{P}_\Theta)$, with $\Theta = \Theta^0$.

After the initial step is performed, both problems, $(\mathcal{P}_\mathcal{S})$ and $(\mathcal{P}_\Theta)$ are solved at each iteration in this same order. It is said that the alternating algorithm performs an iteration when both subproblems are solved. The optimization process is repeated until the value of the objective function increases or the difference between two consecutive iterates is irrelevant, that is, $||F(\Theta^k, \mathcal{S}^k) - F(\Theta^{k-1}, \mathcal{S}^{k-1})|| \leq \epsilon$ for a given ϵ.

In Subsection 2.3.1, the steps in the optimization of the heliostat field for a fixed tower-receiver (the $(\mathcal{P}_\Theta)$ subproblem) are detailed, since the other subproblem $(\mathcal{P}_\mathcal{S})$ is directly solvable by standard techniques as explained below.

The optimization of Θ is done applying a cyclic coordinate method, see [8]. It starts from an initial random solution in the feasible region, in this case $\mathbf{\Theta}$, at which the objective function is evaluated. The algorithm performs at each iteration two local searches using as search direction each coordinate axis. No difficulties are expected, since, from previous experiences, the function $F(\cdot, \mathcal{S})$ has a uni-modal shape, shown in Figure 2.2 using the reference field layout **PS10** given in [75].

2.3.1 Field optimization

The algorithm for solving problem $(\mathcal{P}_\Theta)$ is described in this subsection. Note that the number of variables (heliostats centres) is not fixed. Even fixing the number of heliostats, the high number of variables ($3,000$ in recent commercial plants [21]), together with the characteristics of the objective function (multi-modal, non-smooth and very time consuming) make this problem difficult to solve.

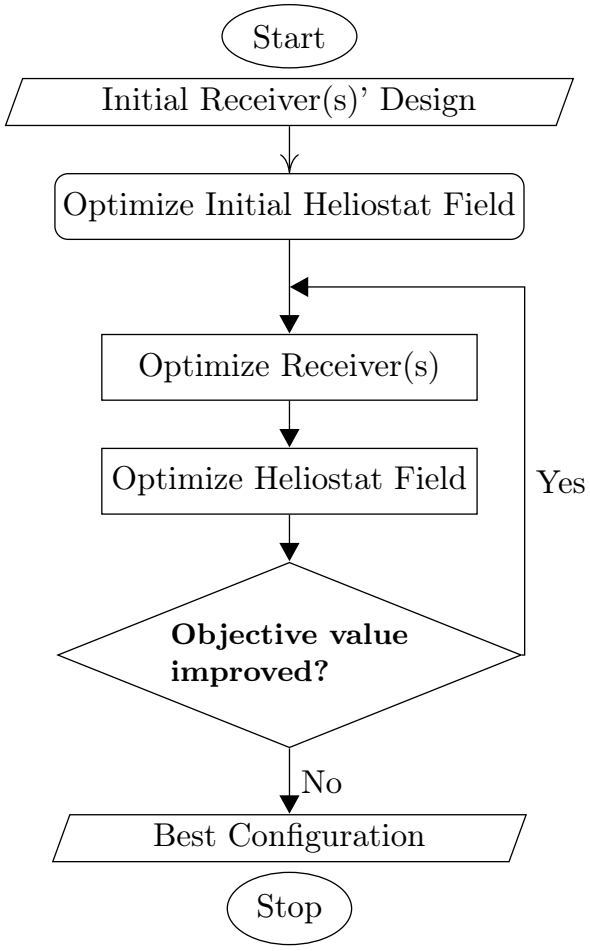

Figure 2.1: Diagram for the alternating algorithm

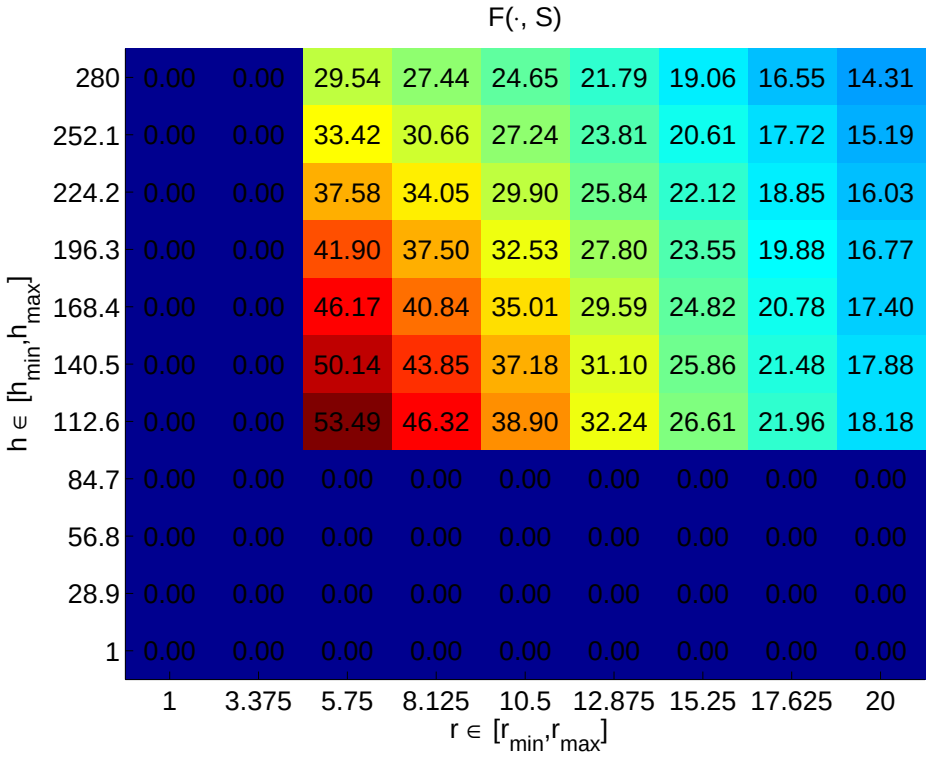

Figure 2.2: $F(\cdot, \mathcal{S})$ values fixed $\mathcal{S} = PS10$

As it has been already mentioned, there exist many approaches considering fixed-patterns to locate the heliostats. In [91], a greedy strategy is used to locate the heliostats in a fixed rectangular grid. In a first step, the annual thermal energy at any point of the grid is calculated. The heliostats are located at the best positions of the grid. To prevent future heliostats from being located in the optical path of those previously placed, a mirror image of the blocking effect is added without considering overlapping. They introduce a penalizing weight factor to favour the location of heliostats closer to the tower, due to the need of increasing the heliostat density given by the grid in the best region of the field (see Figure 2.3(a)).

The proposed procedure also uses a greedy strategy, although any fixed configuration to locate the heliostats is imposed. The process presented below is different from others in the literature in three aspects:

- No parametric form is used as a field pattern (e.g. the field is not assumed to possess a radially staggered shape), therefore the strategy can be extended directly to complex field regions, see Section 2.4.3.

- The number of heliostats is selected according to the thermal power requirements into the receiver, avoiding oversizing. This way computational time and distortion on the optimization results are removed.

- The procedure can be used to generate initial fields. The final result is susceptible of refinement with local improvements using, for instance, the method presented in [18].

A greedy based algorithm is presented which locates the heliostats one by one at the best feasible position, that is, the position where the annual thermal energy collected is highest for a given tower. The process is repeated until no improvement is reached in the annual thermal energy collected. The heliostats are located freely, without any pre-arranged distribution. Only two geometrical constraints have to be taken into account: the field shape constraint and the heliostat constraints to avoid collisions, see Eq. (1.1). At each step, the annual thermal energy collected into the receiver by each heliostat is modified due to the new shading and blocking effects that the heliostat is causing. This is the main reason of increase of the computing time. Once a new heliostat is located and the shading and blocking effects are incorporated, the process must be repeated.

Obviously, the first problem, $\left(\mathcal{P}_\Theta^0\right)$, involves locating the first heliostat centre when only the field shape constraint is considered:

$$\left(\mathcal{P}_\Theta^0\right) \quad \Theta \text{ fixed} \begin{cases} \max\limits_{(x,y)} & E(\Theta, \{(x,y)\}) \\ \text{subject to} & (x,y) \in \Omega \end{cases} \tag{2.6}$$

This problem has an easy-to-handle objective function, as plotted in Figure 2.3(a). In return, when (at least) one heliostat is located in the field and a field denoted by $\mathcal{S}_*^{k-1}$ (with $k-1$ heliostats which respects the constraints) is obtained, the problem $\left(\mathcal{P}_\Theta^k\right)$ described below is difficult to solve, since non-convex constraints are involved and the energy function has a complex behaviour due to the shading and blocking effects, see Figure 2.3(b).

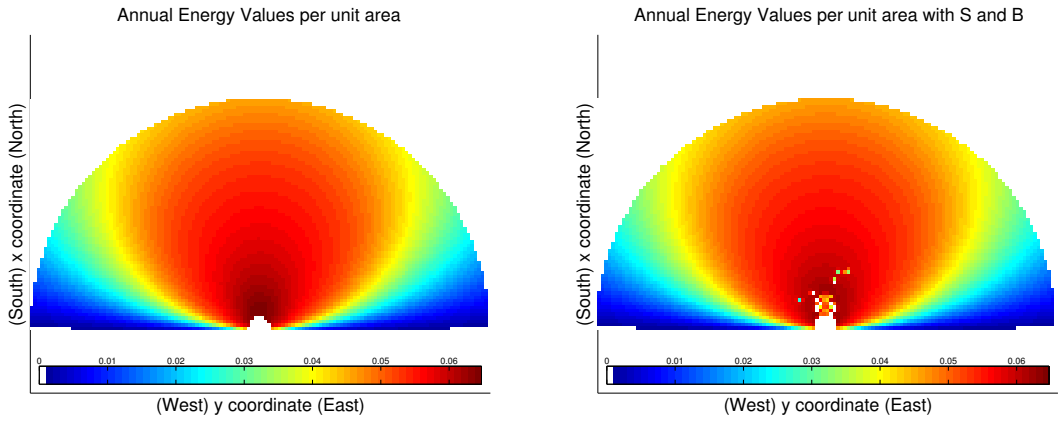

(a) $k = 0$ (b) $k = 25$

Figure 2.3: Annual thermal energy collected

The notation $\mathcal{S}_*^k = \left\{\mathcal{S}_*^{k-1}, (x,y)\right\}$ is introduced, where (x,y) denotes the decision variables in the optimization problem $\left(\mathcal{P}_\Theta^k\right)$:

$$\left(\mathcal{P}_\Theta^k\right) \quad \Theta \text{ fixed} \begin{cases} \max\limits_{(x,y)} & E(\Theta, \left\{\mathcal{S}_*^{k-1}, (x,y)\right\}) \\ \text{subject to} & (x,y) \in \Omega \\ & ||(x,y) - (x',y')|| \geq \delta_0 \quad \forall\, (x',y') \in \mathcal{S}_*^{k-1}\,. \end{cases} \tag{2.7}$$

As mentioned, the k-step the problem is equivalent to maximizing the annual thermal energy collected into the receiver by the new heliostat, because the cost function is fixed at each step. Note that, for simplicity, it is assumed that the heliostat cost is independent on its position in the field.

Now, this chapter focus on the resolution of the problem $\left(\mathcal{P}_\Theta^k\right)$, i.e. the location of one heliostat, and the *Greedy Algorithm* is introduced, see Algorithm 2, to solve it. It is well known that the energy function evaluation is computationally expensive, see Chapter 1 and [91]; that is why, in this algorithm, it is approximated by a much simpler function. Thus, instead of computing E as in (1.10), the receiver outlet thermal power (1.30) at the design point T_d is used; this is Π_{T_d}. More accurate approximations, as those suggested in [103, 116] based on calculating the receiver outlet thermal power at several time instants could be used, at the expense of increasing the already high computational cost.

Using Π_{T_d} as the objective function leads to more compact fields. The reduction on the shading and blocking effects at this time instant favours closer heliostat positions. In order to compensate for this, the safety distance value is modified. The new safety distance δ_0 is defined as the product of the initial safety distance δ and a new parameter $F_{\texttt{sep}}$ that can be in the range $[1,2]$. It depends on the selected design point, the heliostat size and the feasible region among others. For this reason, it has to be tuned for each problem.

To avoid local minima, the *Greedy Algorithm* considers $N_{\texttt{ini}}$ different random feasible initial solutions. The final solution is selected according to the receiver outlet thermal power at the design point collected by each new field layout.

The complete field is generated using the *Field Layout Algorithm* which scheme is given in Algorithm 3 and described below. In order to solve problem $(\mathcal{P}_\Theta)$, since the functions involved are highly multi-modal, and the output strongly depends on the starting points used on Algorithm 2, the complete process is repeated $N_{\texttt{sem}}$ times with different seed states. The initial data required are the fixed variables related to the tower-receiver size Θ, the number of times that the algorithm will be repeated $N_{\texttt{sem}}$, and the number of initial solution to be used in the greedy multi-start procedure $N_{\texttt{ini}}$.

In the first step of Algorithm 3 ($k = 0$, no heliostat in the field), there are not shading

Algorithm 2 `Greedy algorithm with multi-start`

Require: Θ and $\mathcal{S}_*^{k-1}$
  for $r = 1$ to N_{ini} **do**
    Random feasible point (x_r, y_r)
    $(\bar{x}_r, \bar{y}_r) \leftarrow$ solve $\left(\mathcal{P}_\theta^k\right)$ with initial solution (x_r, y_r)
    $\mathcal{S}_r^k = \left\{\mathcal{S}_*^{k-1}, (\bar{x}_r, \bar{y}_r)\right\}$
  end for
  $\mathcal{S}_*^k \leftarrow \max_r \left\{\Pi_{T_d}(\Theta, \mathcal{S}_r^k)\right\}$
  return $\boxed{\mathcal{S}_*^k}$

and blocking effects involving multi-modality in the objective function. Therefore no multi-start strategy is required, and the number of initial solutions is set to one. Once the first heliostat is located in the field ($k > 0$), the multi-modality of the problem appears and $N_{\texttt{ini}}$ different feasible random initial solution are considered. As it has been already described, the heliostats are located solving $\left(\mathcal{P}_\Theta^k\right)$ using Algorithm 2, with the corresponding $N_{\texttt{ini}}$ value.

When $k > 0$, two phases of Algorithm 3 can be differentiate, *Requirement Phase* and *Completion Phase*. Requirement Phase consists of locating heliostats using Algorithm 2 until the thermal power requirement Π_0 is reached. At the end of this phase the location of heliostats could be stopped, however it is continued by the Completion Phase applying a different stopping criterion. The location of heliostats is continued in this phase provided that the system annual thermal energy collected per unit cost increases.

It may happen that there exist some manufacturer requirements on the receiver outlet thermal power collected by the field in order to prevent damages, see Eq. (1.12). For this reason, Completion Phase should stop when a power upper limit, Π^+, is reached. In this case the heliostat field layout is stored in $\Upsilon_{design-B1}$. However, this field may be improved and forgetting this thermal power limitation. The algorithm continues until the system annual thermal energy collected per unit cost does not increase. In this case, the solution are the highest annual value attained $\Upsilon_{objective}$ and its tower and field configuration, Υ_{design}.

The proposed heuristic algorithm does not give an optimal solution, nor the ones proposed in the literature. Given the number of variables expected, a reasonable solution is obtained compared against the reference fields **PS10** and **RPS10**.

Note that the proposed greedy algorithm locates the heliostats one by one. This strategy can be extended to locate n heliostats in block, being n small to maintain the numerical treatability of the problem, as addressed in Chapter 3 with triangular structures.

Algorithm 3 `Field layout algorithm`

Require: $\Theta, N_{\texttt{sem}}, N_{\texttt{ini}}$
  for $\texttt{sem} = 1$ to $N_{\texttt{sem}}$ **do**
    test_stop $\leftarrow$ **true**
    $k \leftarrow 0$
    $N^*_{\texttt{ini}} \leftarrow 1$
    $\mathcal{S}^0_* \leftarrow$ solve $\left(\mathcal{P}^0_\Theta\right)$ with Algorithm 2
    while $\Pi_{T_d}(\Theta, \mathcal{S}^k_*) < \Pi_0$ **do**
      $k \leftarrow k + 1$ **Requirement Phase**
      $N^*_{\texttt{ini}} \leftarrow N_{\texttt{ini}}$
      $\mathcal{S}^k_* \leftarrow$ solve $\left(\mathcal{P}^k_\Theta\right)$ with Algorithm 2
    end while
    repeat
      $\Upsilon^0_{objective} \leftarrow F(\Theta, \mathcal{S}^k_*)$ **Completion Phase**
      $k \leftarrow k + 1$
      $\mathcal{S}^k_* \leftarrow$ solve $\left(\mathcal{P}^k_\Theta\right)$ with Algorithm 2
      $\Upsilon^1_{objective} \leftarrow F(\Theta, \mathcal{S}^k_*)$
      if $\Pi_{T_d}(\Theta, \mathcal{S}^k_*) > \Pi^+$ & test_stop **then**
        test_stop $\leftarrow$ **false**
        $\Upsilon_{design-B1} \leftarrow (\Theta, \mathcal{S}^k_*)$
      end if
    until $\Upsilon^1_{objective} < \Upsilon^0_{objective}$
  end for
  return $\begin{array}{lcl} \Upsilon_{objective} & \leftarrow & \Upsilon^0_{objective} \\ \Upsilon_{design} & \leftarrow & (\Theta, \mathcal{S}^{k-1}_*) \end{array}$

2.4 Results

A prototype of the algorithms has been developed in Matlab©, using `fminbnd` and `fmincon` as local search routines to solve the optimization sub-problems involved solving ($\mathcal{P}_\Theta$) and ($\mathcal{P}_\mathcal{S}$) respectively.

The accuracy and feasibility of the results have been confirmed by comparing to the heliostat fields obtained with benchmark procedures. Although in the greedy optimization procedure an approximation of the objective function (based on the thermal power collected at the design point) is used. When comparing the results, the accurate thermal energy function is used (see in the tables column label with E). Three fields are considered for comparison purposes, with a common tower-receiver design. Following [75], such test fields are called here **PS10**, **RPS10** (redefined PS10) and **Spiral**[1]. The values of the geographical, physical and geometrical parameters are given in Table 2.1.

Parameter	Default value	Ref.
Location and Time		
Site	Sanlúcar la Mayor (Seville)	[76]
Latitude	$37^o26'$ N	[75]
Longitude	$6^o15'$ W	[75]
Design Point T_d	21st March 12h	assumed
Design direct normal irradiance DNI	823.9 W/m^2	assumed
DNI model	cloudless sky	assumed
Receiver		
Aperture tilt	12.5^o	[75]
Receiver Technology	Saturated Steam	[76]
Heliostat		
Name	*Sanlucar*120	[75]
Width	12.84 m	[75]
Height	9.45 m	[75]
Optical height z_0	5.17 m	[76]
Minimal safety distance δ	diagonal	[18]
$\sigma_{optical}$	2.9 mrad	[75]
Field		
Slope	0^o	assumed
Shape	annulus	assumed
Minimum radius	50 m	assumed
Maximum radius	10^3 m	assumed
Maximum surface	156.68 ha	assumed

Table 2.1: Parameter values

[1]The author thanks C. J. Noone, M. Torrilhon, and A. Mitsos for providing the heliostat field configurations used to compare the results.

2.4.1 Heliostat field layouts comparison given a Tower-Receiver configuration

PS10, as given in [75], is an SPT system similar to a solar commercial plant located in Sanlúcar la Mayor, Spain, and it is one of the most popular test instances. The Tower-Receiver variables for the **PS10** are fixed as parameters, assuming a *tower height* of 100.50 m and an *aperture radius* of 6.39 m, that is $\Theta = (6.39, 100.5)$. **RPS10** is a variant suggested in [75], in which a local search is performed, taking the **PS10** layout as starting point, optimizing the parameters configuration of the system. Finally, **Spiral**, as introduced in [75], is another field layout obtained when a spiral pattern is given for the field layout and the parameters of the spiral are optimized.

In Figure 2.4, the previous heliostat field layouts and also the **GPS10** configurations, computed using the proposed greedy algorithm, are shown with the same number of heliostats. Such **GPS10** configuration has been obtained after performing different experiments varying $F_{\texttt{sep}}$ with $N_{\texttt{sem}} = 5$. The best configuration shown is obtained with $F_{\texttt{sep}} = 1.5$.

The receiver outlet thermal energy at the design point T_d, the annual thermal energy collected and annual thermal energy collected per unit cost for each field layout, are given in Table 2.2. Note that, in view of the results in Table 1.1, at best, it can be expected that the computations are 1% accurate, and this means that the differences of performance of **PS10**, **RPS10** and **Spiral** are between the error of calculation. **GPS10**-(Phase B) results in higher annual energy collection per unit cost, which implies that a larger number of heliostats results in lower cost.

If the results obtained are compared, fixing the same number of heliostats, **GPS10**-(Phase A), it can be seen that the algorithm provides similar results compared to **PS10**, **RPS10** and **Spiral** regarding the annual thermal energy, and better results than **Spiral** regarding the receiver outlet thermal energy at T_d. Note that **PS10** and **Spiral** fields are solutions of optimization problems in which a geometrical configuration pattern is imposed. However, the solutions so obtained, though optimal under the pattern based constraints, may be suboptimal if such constraints are removed.

Field	N	Π_{T_d}	E	F
PS10	624	0.43	0.12	0.50
RPS10	624	0.43	0.12	0.50
Spiral	624	0.42	0.12	0.50
GPS10 Requirement Phase	624	0.43	0.12	0.50
GPS10 Completion Phase	943	0.62	0.17	0.54

Table 2.2: Thermal power at T_d, annual thermal energy and annual thermal energy per unit cost. Π_{T_d} (MWth 10^{-2}) and E (GWHth 10^{-3})

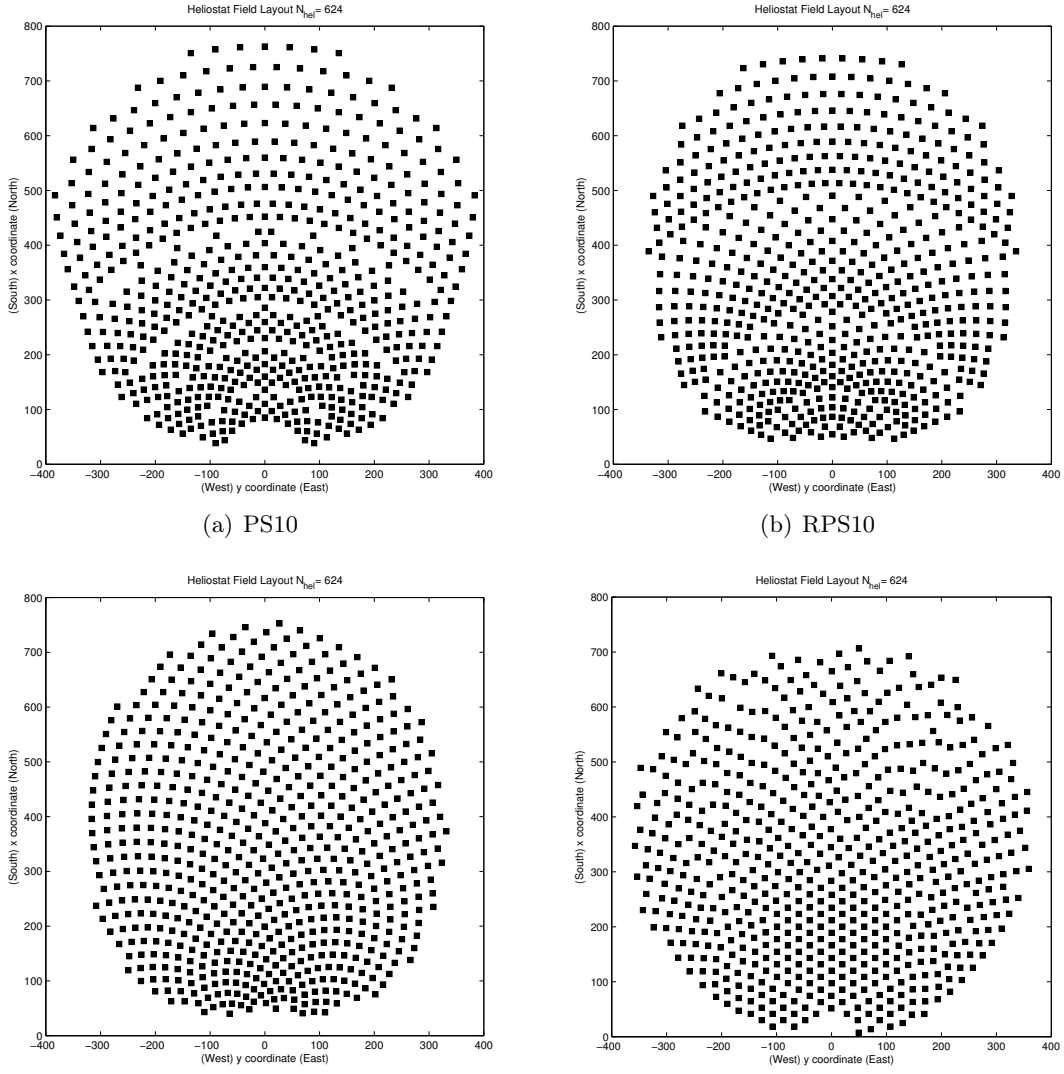

(a) PS10 (b) RPS10

(c) Spiral (d) GPS10 *Phase A*

Figure 2.4: Heliostat field layouts

The **RPS10** and **GPS10** fields are shown in Figure 2.5 with the heliostats coloured according to their contribution to the annual thermal energy collected.

In order to compare the four fields layouts, the heliostats of each field are sorted in terms of the amount of annual thermal energy collected by the receiver. Some results are described below, displaying the energy and the cost in terms of the number of heliostats. The annual thermal energy collected versus the number of heliostats located in the field is shown in Figure 2.6(a); the cost of the SPT system versus the number of heliostats is depicted in Figure 2.6(b), and Figure 2.6(c) shows the objective function, that is, the annual thermal energy collected per unit cost versus the number of heliostat. In these three figures the four fields have the same behaviour, but, when displaying the marginal annual thermal energy added by each heliostat in the field, see Figure 2.6(d), some differences can be observed due to the different heliostat location procedures.

The multi-modality of the problem is rather strong. In Figure 2.7, the field layouts obtained using the greedy algorithm without a multi-start procedure and with multi-start procedure are shown. When the greedy algorithm is used without a multi-start procedure, the heliostat field layouts obtained are not so regular. The use of different values for $N_{\texttt{ini}}$ and for $F_{\texttt{sep}}$ lead to different results, and the best results are not necessary matched with the field regularity. The results obtained are strongly dependant on the parameter $F_{\texttt{sep}}$, and thus this parameter must be carefully tuned.

2.4.2 Alternating procedure

When the tower-receiver variables are also optimized using the proposed alternating approach, the results shown in Table 2.3 and Figure 2.8 are obtained step-by-step. Using random feasible values as initial data for the tower-receiver configuration and the *Alternating Algorithm* 1, a more efficient SPT system is sought. To make a fair comparison, the receiver outlet thermal energy at T_d is fixed at 42.52 MWth, the same as the value obtained with the **PS10** configuration. The parameter $N_{\texttt{ini}}$ is set to 25, since this value gave the best results in some preliminary tests performed, and ϵ is set to 0.01.

From Table 2.3 it is concluded that the best solution $(\Theta^1, \mathcal{S}^1)$ found at the second step of the Alternating Algorithm collects a higher annual thermal energy per unit cost than the values of the three reference SPT systems. Note that the first heliostat field obtained in this example, see Figure 2.8(a), is not as compact as the heliostat fields obtained in next iterations. This effect is due to the low tower height value and the large receiver radius value obtained as initial random solution. When the alternating process continues this effect is corrected by the own algorithm.

Convergence of the alternating procedure is not shown. However, as can be seen in Table 2.3, starting from a "bad solution" (low tower and big aperture), the algorithm leads to a very reasonable solution compared against the benchmarks in the literature.

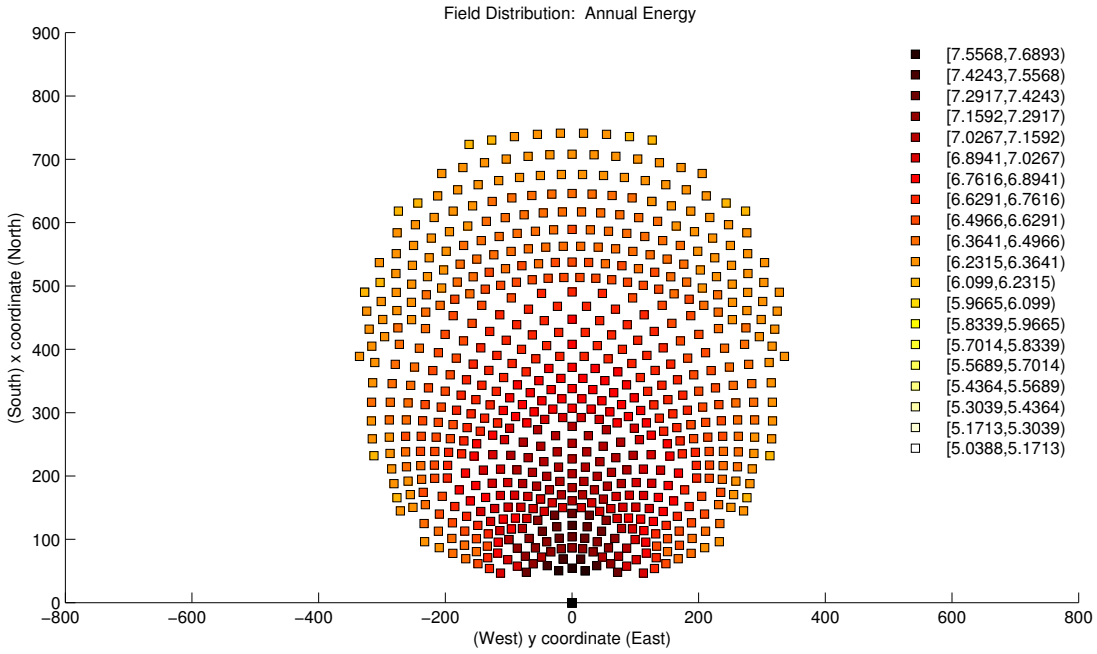

(a) RPS10

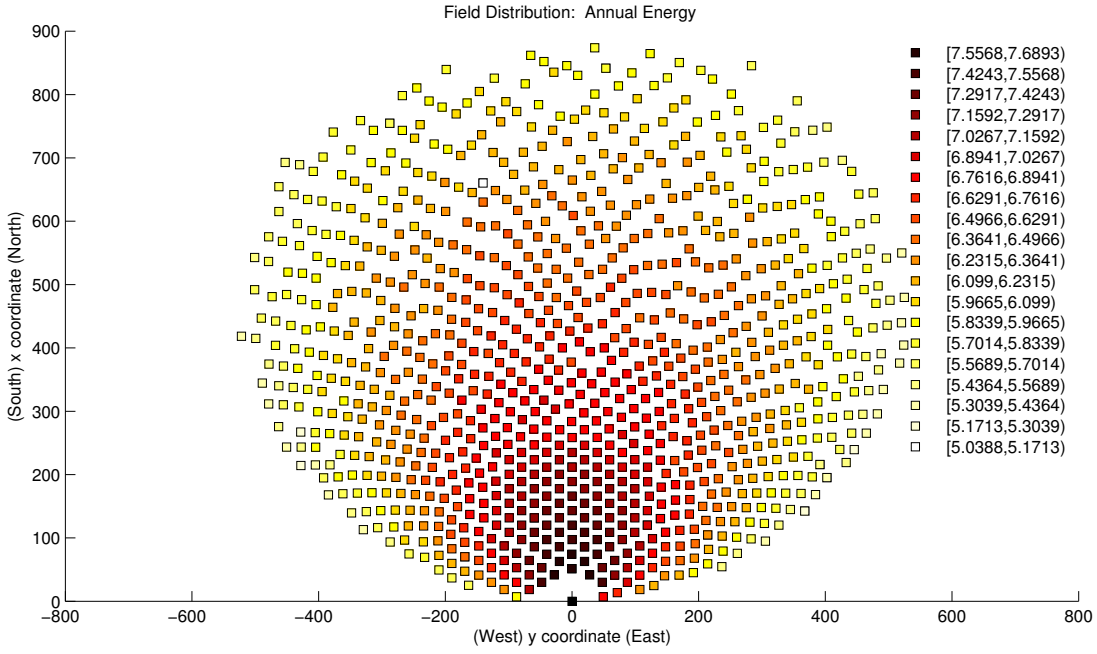

(b) GPS10 *Phase B*

Figure 2.5: Annual thermal energy collected per heliostat

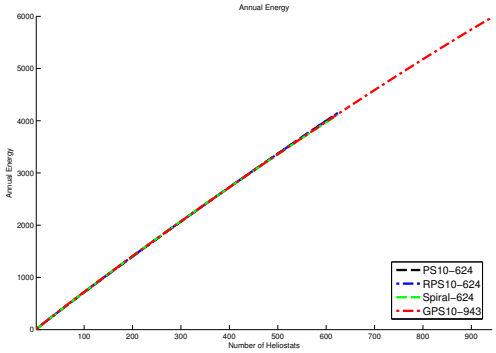

(a) Annual thermal energy per hel.

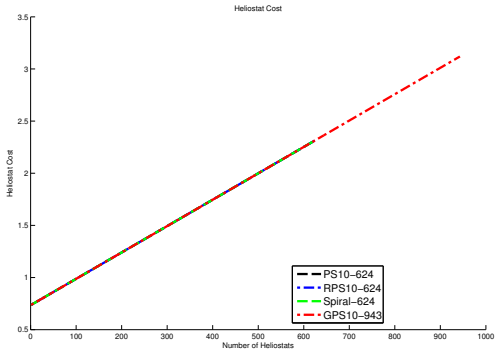

(b) Cost per heliostat

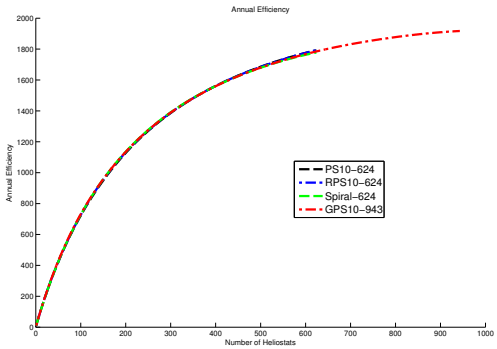

(c) Annual thermal energy per unit cost per hel.

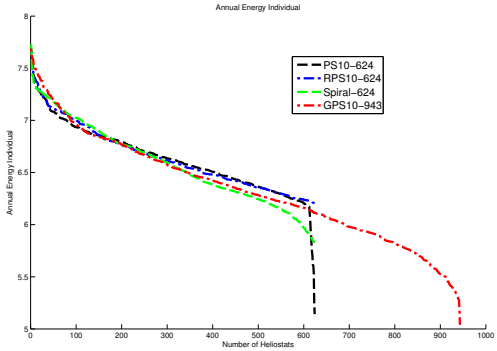

(d) Marginal annual thermal energy

Figure 2.6: Field layouts analysis

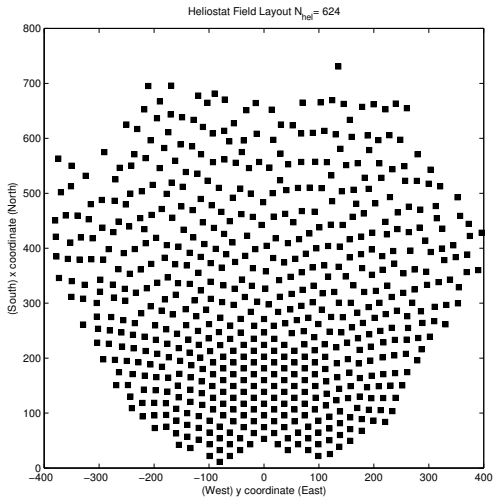

(a) $N_{\text{ini}} = 1$

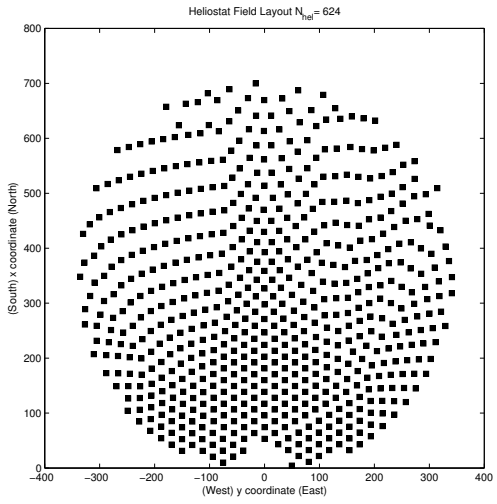

(b) $N_{\text{ini}} = 25$

Figure 2.7: Multistart analysis with $F_{\text{sep}} = 1.4$

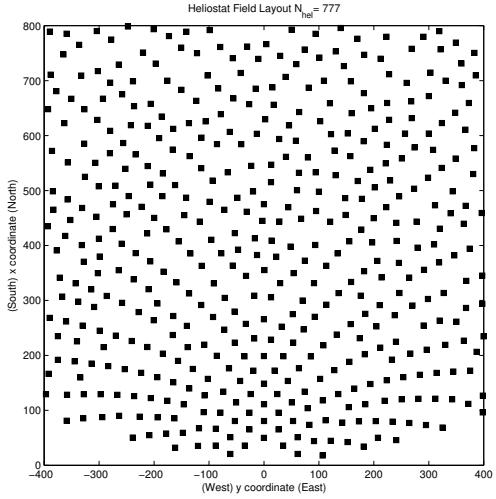

(a) $\mathcal{S}^0$

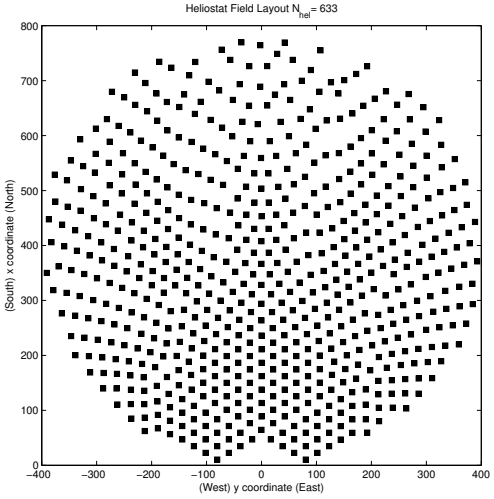

(b) $\mathcal{S}^1$

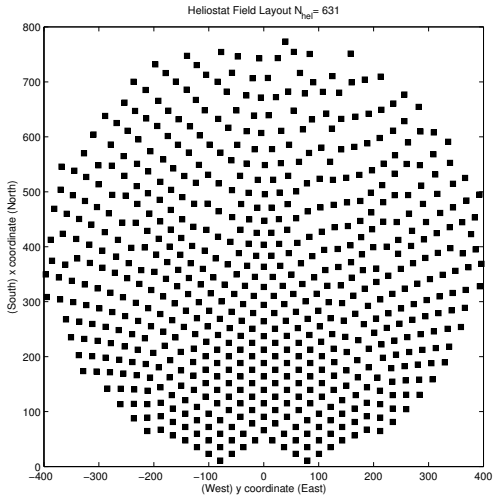

(c) $\mathcal{S}^2$

Figure 2.8: Alternating algorithm (Alg. 1): heliostat field layouts

Step	Problem	Θ^k	Fig.	$\lvert\mathcal{S}\rvert$	$\Pi_{T_d}(\Theta^k,\mathcal{S}^k)$	$E(\Theta^k,\mathcal{S}^k)$	$F(\Theta^k,\mathcal{S}^k)$	F_{sep}
k=0	Random Θ^0	(13.01,30.16)	-	0	-	-	-	-
	$\mathcal{S}^0$: Solve $(\mathcal{P}_\Theta)$	(13.01,30.16)	2.8(a)	477	0.43	0.12	0.31	2.0
$\Upsilon_{objective} = 0.31$ $\Upsilon_{design} = (\Theta^0, \mathcal{S}^0)$								
k=1	Θ^1: Solve $(\mathcal{P}_\mathcal{S})$	(5.81,84.22)	-	777	0.47	0.12	0.48	2.0
	$\mathcal{S}^1$: Solve $(\mathcal{P}_\Theta)$	(5.81,84.22)	2.8(b)	633	0.43	0.12	0.53	1.6
$\Upsilon_{objective} = 0.53$ $\Upsilon_{design} = (\Theta^1, \mathcal{S}^1)$								
k=2	Θ^2: Solve $(\mathcal{P}_\mathcal{S})$	(6.05,87)	-	633	0.45	0.12	0.52	1.6
	$\mathcal{S}^2$: Solve $(\mathcal{P}_\Theta)$	(6.05,87)	2.8(c)	631	0.43	0.12	0.52	1.6
$\mathbf{\Upsilon_{objective} = 0.53}$ $\mathbf{\Upsilon_{design} = (\Theta^1, \mathcal{S}^1)}$								

Table 2.3: Alternating algorithm results

The alternating algorithm could be embedded in a multi-start process, starting from different random initial solution Θ^0 and selecting as solution the best obtained configuration.

2.4.3 Different feasible regions

In real situations, the region selected to build the SPT system can have some terrain constraints. This means that some infeasible zones need to be excluded of the original feasible region. Using the field layout algorithm described in Algorithm 3, different regions can be considered. The heliostat location procedure remains exactly the same, since with the proposed algorithm the heliostat distribution is not parametrized, and the algorithm can adapt automatically the heliostat location to the selected region shape.

To illustrate the advantages of the proposed pattern-free method against pattern-based methods, three different possible feasible regions are considered and both procedures, radially-staggered parametrization and greedy algorithm, are compared in these regions. The three feasible regions that are considered are: a rectangular region (R), a perforated region (P) and a valley region (V), where the SPT system is supposed to be located near a river (see Figure 2.9).

As said before, the heliostat field is designed for each feasible region considering the receiver outlet thermal energy at T_d as $\Pi_0 = 42.52\ MWth$. The fields are obtained using Algorithm 3, and for each feasible region the different constraints associated are considered. In order to compare these fields, the **PS10** and **RPS10** configurations have been limited to the three different regions and evaluated the results.

In Figures 2.10-2.12, the heliostat fields for each feasible regions are shown. The different phases of the greedy algorithm, Requirement Phase and Completion Phase,

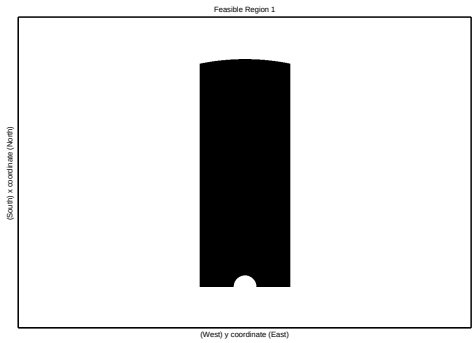

(a) Rectangular region (R)

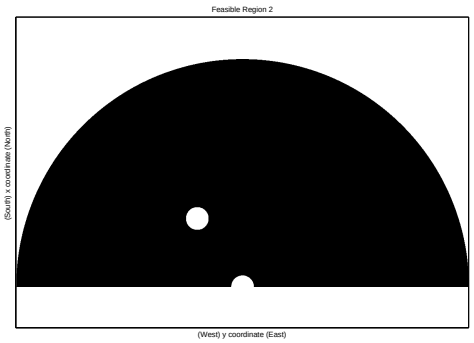

(b) Perforated region (P)

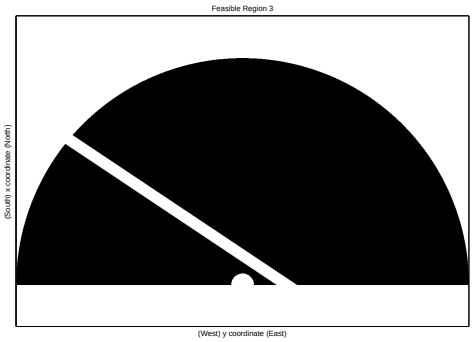

(c) Valley region (V)

Figure 2.9: Feasible regions

are detailed numerically in Table 2.4. From the results it is concluded that for most tests performed the annual thermal energy collected per unit cost improves with the greedy-based procedure, and in the case that this value is not improved solution is proposed.

Fixed-pattern algorithms ignore the shape of the feasible field region and are always limited to the geometrical pattern selected. By contrast, in Figure 2.11, the adaptation of the heliostat positions through the greedy algorithm around the circle perforation can be appreciated. Also, using the proposed pattern-free procedure the density of the field is automatically adapted to the field characteristics and takes advantage of the best region. These local adaptations are not automatically done using the original radially-staggered pattern.

		PS10						**RPS10**					
Reg	$\mathcal{S}$	$\lvert\mathcal{S}\rvert$	Π_{T_d}	Π^+	$E(\Theta,\mathcal{S})$	$F(\Theta,\mathcal{S})$	F_{sep}	$\lvert\mathcal{S}\rvert$	Π_{T_d}	Π^+	$E(\Theta,\mathcal{S})$	$F(\Theta,\mathcal{S})$	F_{sep}
R	Original	420	0.29	-	0.080	0.44	-	446	0.31	-	0.084	0.45	-
	Requirement Phase	419	0.29	0.31	0.079	0.44	1.5	448	0.31	0.33	0.084	0.45	1.5
	Completion Phase (Π^+)	-	-	0.31	-	-	1.5	-	-	0.33	-	-	1.5
	Completion Phase	425	0.30	-	0.081	**0.45**	1.5	452	0.31	-	0.085	0.45	1.5
P	Original	611	0.42	-	0.11	0.50	-	611	0.42	-	0.11	0.50	-
	Requirement Phase	607	0.42	0.44	0.11	0.50	1.5	612	0.42	0.44	0.11	0.50	1.5
	Completion Phase (Π^+)	639	0.44	0.44	0.12	0.50	1.5	645	0.44	0.44	0.12	0.51	1.5
	Completion Phase	745	0.50	-	0.14	**0.52**	1.5	824	0.55	-	0.15	**0.53**	1.5
V	Original	565	0.38	-	0.11	0.49	-	565	0.39	-	0.11	0.49	-
	Requirement Phase	562	0.38	0.40	0.10	0.48	1.6	566	0.39	0.41	0.11	0.49	1.6
	Completion Phase (Π^+)	592	0.40	0.40	0.11	0.49	1.6	597	0.41	0.41	0.11	0.49	1.6
	Completion Phase	856	0.56	-	0.15	**0.53**	1.6	916	0.60	-	0.16	**0.53**	1.6

Table 2.4: Annual thermal energy per unit cost: $F(\Theta,\mathcal{S}) = E(\Theta,\mathcal{S})/C(\Theta,|\mathcal{S}|)$

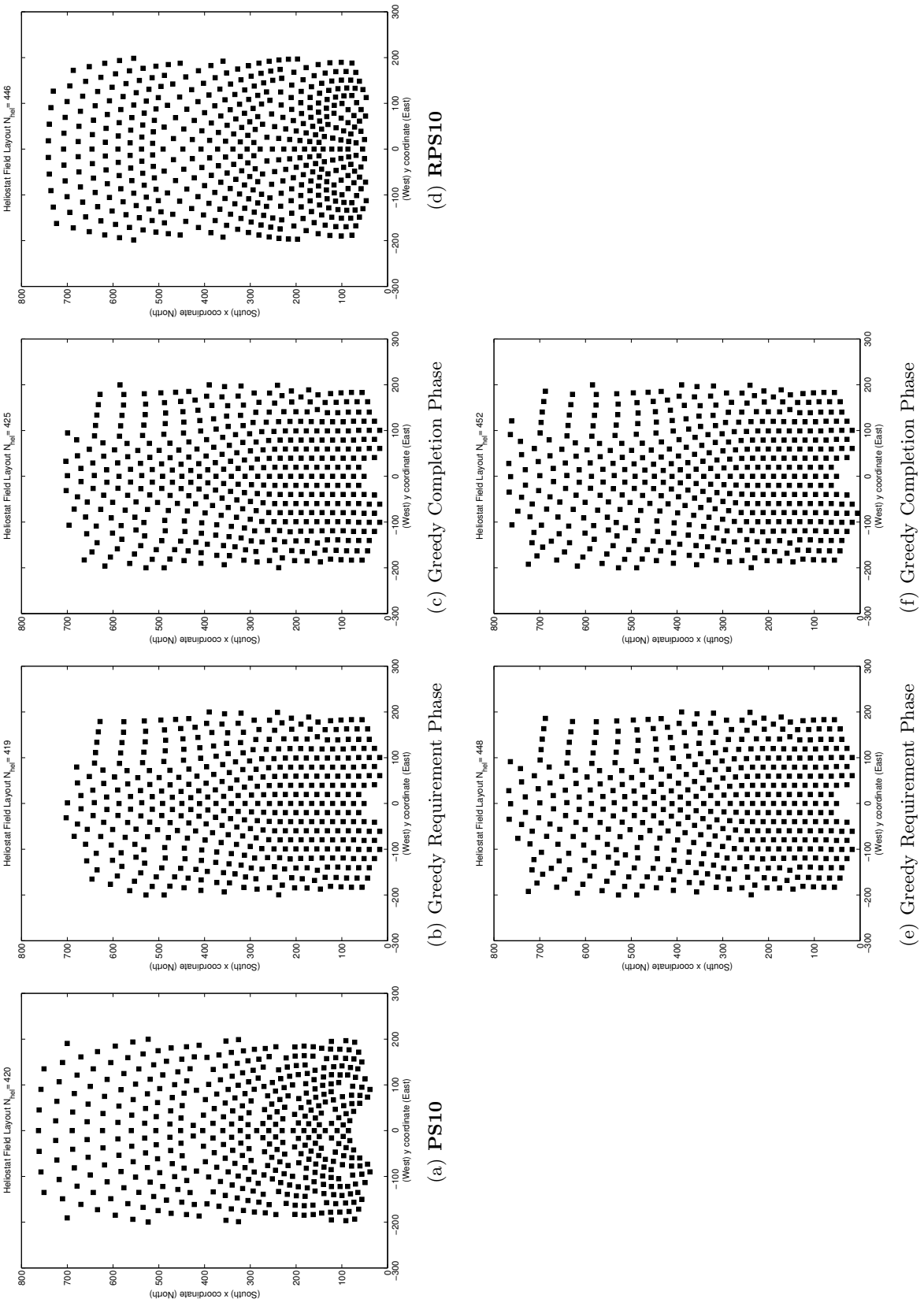

(a) **PS10** (b) Greedy Requirement Phase (c) Greedy Completion Phase (d) **RPS10**

(e) Greedy Requirement Phase (f) Greedy Completion Phase

Figure 2.10: Rectangular region

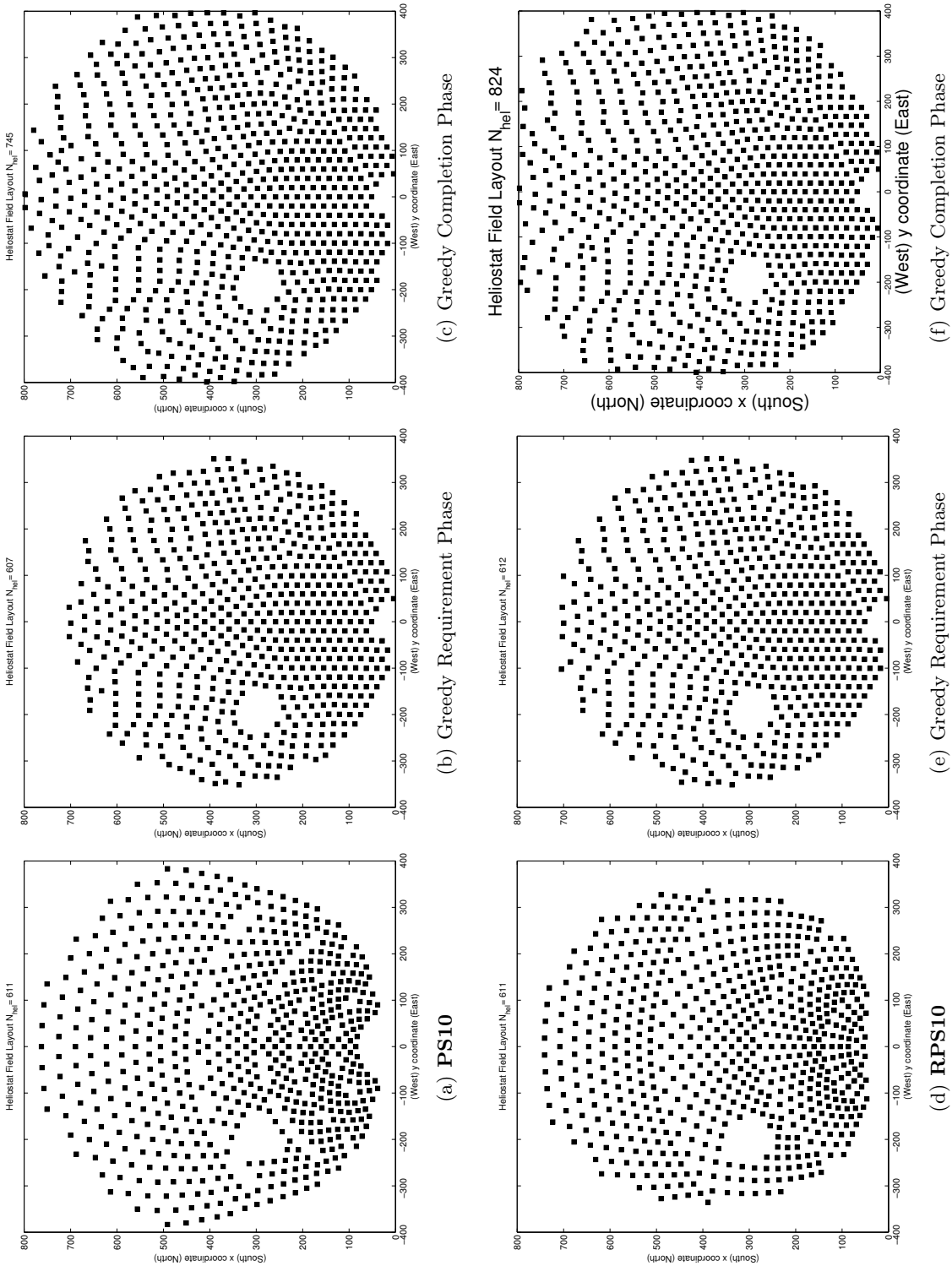

(a) **PS10** (b) Greedy Requirement Phase (c) Greedy Completion Phase

(d) **RPS10** (e) Greedy Requirement Phase (f) Greedy Completion Phase

Figure 2.11: Perforated region

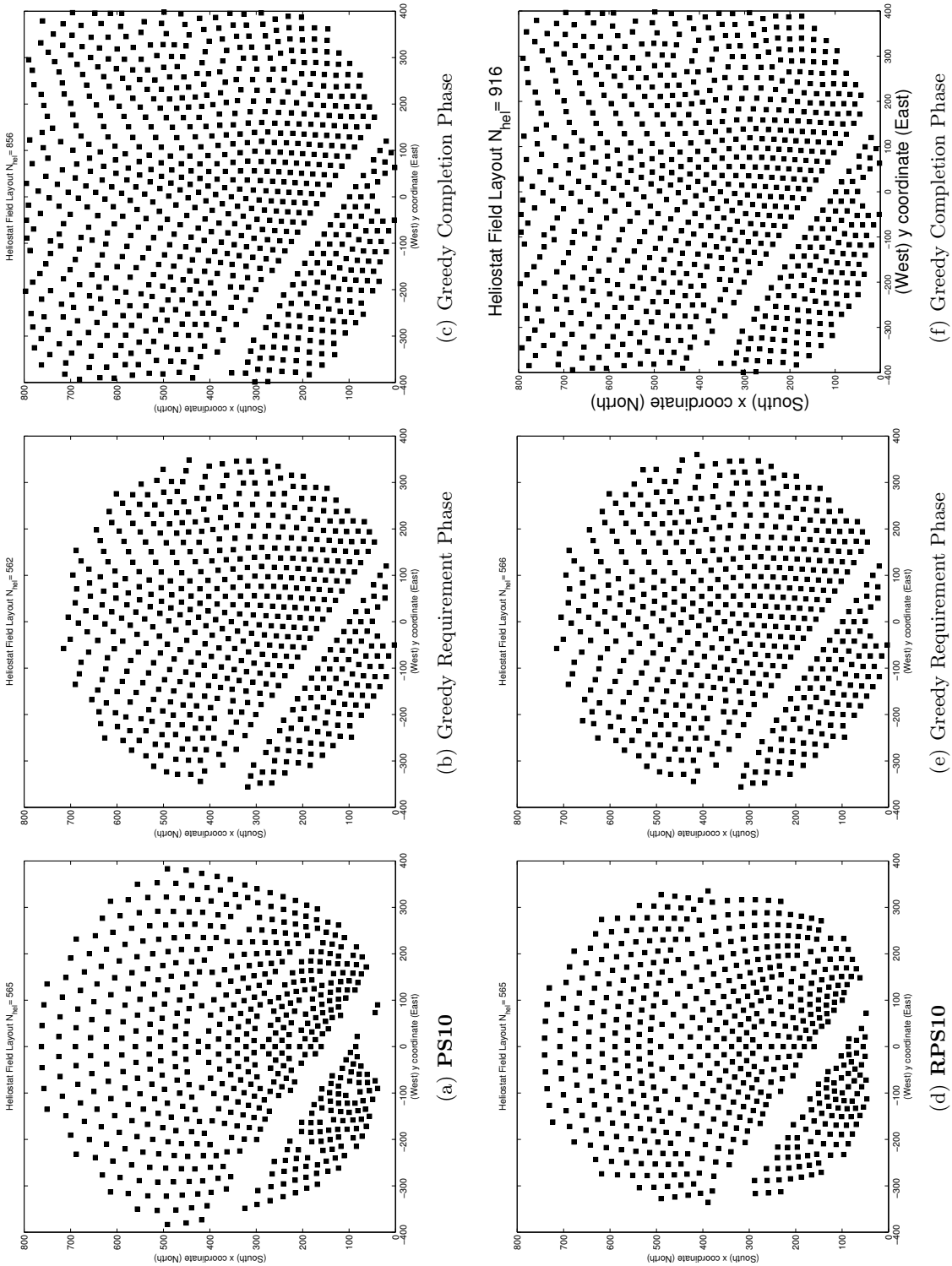

(a) **PS10** (b) Greedy Requirement Phase (c) Greedy Completion Phase

(d) **RPS10** (e) Greedy Requirement Phase (f) Greedy Completion Phase

Figure 2.12: Valley region

2.5 Conclusions

A pattern-free method for optimizing an SPT system has been proposed, in which both the location of the heliostats and the design of the solar tower-receiver system are simultaneously considered. Maximizing the thermal energy collected per unit cost leads to a difficult optimization problem, since it has non-convex constraints and a non-convex objective function, which is computationally expensive to evaluate.

An alternating greedy-based heuristic has been suggested. The proposed method provides competitive results against the standard results in the literature and it is more versatile, since it is not based on geometrical patterns which may be valid only under certain physical conditions.

Unfortunately, given the complexity of the model and the proposed heuristic methodology, it is not possible to easily perform an error analysis. However, using simpler models with a low number of heliostats, the quality of the solutions could be measured. As already mentioned, when considering a reduced number of heliostats a simultaneous heliostat location could be possible. This is a very interesting problem addressed in Chapter 3 with triangular structures called pod.

Chapter 3

Field-design optimization with triangular heliostat pods

This chapter presents an extension of the basic model described in Chapter 2, in which the location of heliostat pods (structures where several heliostats are placed using a common foundation) is addressed, instead of considering individual heliostats.

The greedy-based algorithm (introduced in Chapter 2) is adapted to handle with the design of fields with triangular heliostat pods. The proposed pattern-free method is compared with two different approaches: a pattern-based and a patter-free method developed by Stellenbosch University and Aachen University respectively, see further details in [38].

In the sequel, the triangular heliostat pod system is described, the heuristic approach used to locate the pods is discussed and compared. Finally, the optimization problem is addressed when considering the triangle length as an optimization variables as well, and concluding remarks are presented.

3.1 Triangular heliostat pod

The *Helio* pod used in this section corresponds to the triangular pod prototype used in the Helio100 plant, see [61, 107]. The facility, consisting of 20 triangular pods, has been constructed under the Technology Innovation Agency (TIA) for the Helio100 project at the University of Stellenbosch and serves as a testing and research facility of the triangular pod technology.

This Helio pod is an equilateral triangular structure with six small-size heliostats: three in the vertices and three in the midpoints, see Figure 3.1. It has been designed to reduce the associated costs and thereby improve the LCOE of the fields. Some important characteristics are the following: no foundations, operated by wireless, installation on uneven ground, easy manufacturing and assembly. All the parameters related to the

Helio pod prototype and to the field are detailed in Table 3.1.

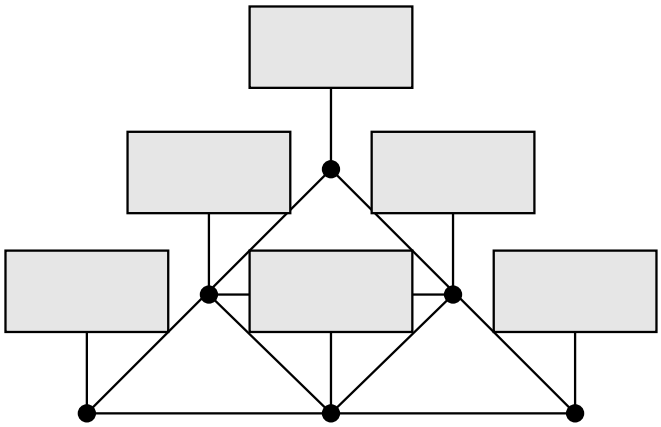

Figure 3.1: Triangular pod (Heliostat positions)

The function $\mathcal{E}$ which denotes the efficiency of the SPT system (tower-receiver and heliostat field) is defined as follows:

$$\mathcal{E}(\Theta, \mathcal{S}) = \frac{E(\Theta, \mathcal{S})}{\int_0^T \Pi_t^*(\Theta, \mathcal{S})\, dt}, \tag{3.1}$$

where E is the annual thermal energy defined in Eq. (1.10) and Π_t^* is the incident solar energy defined in Eq. (1.27).

The field efficiency collected with individual heliostat fields is slightly higher than for triangular pod fields, as can be seen in Figure 3.2. However, the low reduction in efficiency may be compensated by the expected cost reduction with pod systems.

3.2 Location problem

The optimization problem presented in this chapter deals with the location of triangular pods. Each triangular pod has six heliostats positioned at the vertices (3) and at the midpoints (3), see Figure 3.3(a).

Note that a specific enumeration is considered, as illustrated in Figure 3.3(a), where each heliostat position is identified with a number from 1 to 6. Each triangular pod can be uniquely defined by one of its vertex ($(x, y) \in \mathbb{R}^2$) and the tilt angle with respect to the vertical axis ($\gamma \in \mathbb{R}$), see in Figure 3.3(b).

Given the triangular pod described by (x, y, γ), $\Delta(x, y, \gamma)$ denotes the set of heliostats coordinates positioned on this pod:

Parameter	Default value
Location	
Site	Stellenbosch (South Africa)
Latitude	$33^o51'$ S
Longitude	$18^o49'$ E
DNI model	cloudless sky
Receiver	
Tower height	$12.20\,m$
Aperture Surface	$1\,m^2$
Heliostat	
Name	*Helio*
Width	1.83 m
Height	1.22 m
Optical height z_0	1.5 m
Minimal safety distance δ	diagonal
$\sigma_{optical}$	2.9 mrad
Pod	
Triangle Side	$6\,m$
# Heliostats per pod	6
Field	
Slope	0^o
Minimum radius	$1.04\ m$
# Heliostats	120

Table 3.1: Parameter values

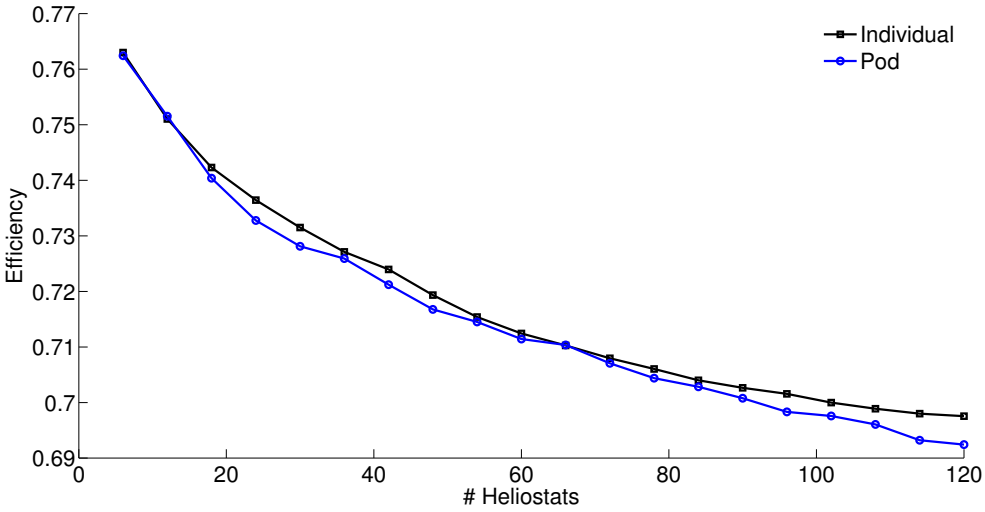

Figure 3.2: Field efficiency (individual heliostats vs triangular pods)

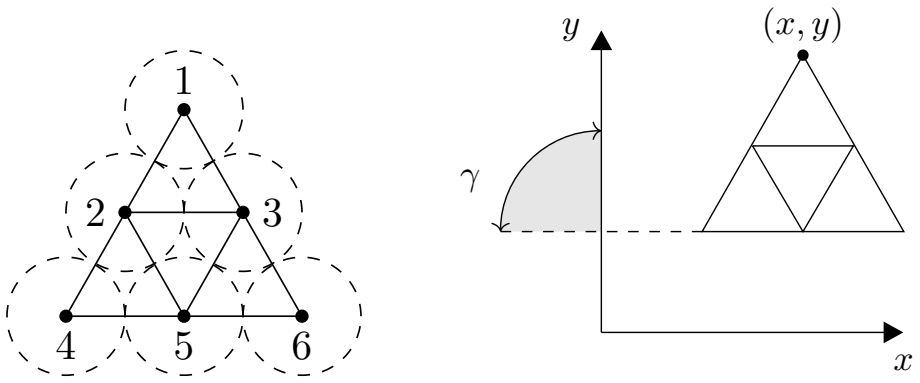

(a) Heliostats enumeration (b) Decision variables

Figure 3.3: Triangular pod

$$\Delta(x, y, \gamma) = \left\{(x^i, y^i)\right\}_{i=1}^{6} , \tag{3.2}$$

where the heliostats coordinates can be calculated as follows:

$$\begin{aligned}
&(x^1, y^1) = (x, y) \,, \\
&(x^2, y^2) = (x + 0.25\, l \cos\gamma - 0.5\, e \sin\gamma \,,\; y + 0.5\, e \cos\gamma + 0.25\, l \sin\gamma) \,, \\
&(x^3, y^3) = (x - 0.25\, l \cos\gamma - 0.5\, e \sin\gamma \,,\; y + 0.5\, e \cos\gamma - 0.25\, l \sin\gamma) \,, \\
&(x^4, y^4) = (x + 0.5\, l \cos\gamma - e \sin\gamma \,,\; y + e \cos\gamma + 0.5\, l \sin\gamma) \,, \\
&(x^5, y^5) = (x - e \sin\gamma \,,\; y + e \cos\gamma) \,, \\
&(x^6, y^6) = (x - 0.5\, l \cos\gamma - e \sin\gamma \,,\; y + e \cos\gamma - 0.5\, l \sin\gamma) \,.
\end{aligned} \tag{3.3}$$

The triangle side length is denoted by l, and e denotes the triangle height or elevation ($e = \sqrt{3}/2\, l$).

Note that two solutions can have different enumeration but have the same heliostat location. Therefore, two heliostat pods (x, y, γ) and (x', y', γ') are considered equal if $\forall\, (a, b) \in \Delta(x, y, \gamma)$ then $(a, b) \in \Delta(x', y', \gamma')$.

In order to maintain the same notation as in the rest of the dissertation, the set $\mathcal{S}$ (coordinates of the heliostat field) can be expressed as follows:

$$\mathcal{S} = \bigcup_{i=1}^{N'} \Delta(x_i, y_i, \gamma_i) \,, \tag{3.4}$$

where N' denotes the number of pods (number of heliostats divided by 6).

The optimization problem can be written as follows.

$$(\mathcal{P}_\Theta)\begin{cases}\max\limits_{\mathcal{S}} & E(\Theta,\mathcal{S})\\ \text{subject to} & \mathcal{S}\in\mathscr{S}\\ & 0\le\gamma_i\le\pi \quad \forall\, i=1,\dots,N',\end{cases} \tag{3.5}$$

where $\mathscr{S}$ corresponds to the same feasible region to locate heliostats described in (1.1), and Θ is the set of parameters related to the tower-receiver configuration selected.

Note that with the Helio pod prototype no further constraints are introduced as there is not enough space to locate heliostats inside the triangular structure. However, when the triangle side increases, overlapping effects between the pod systems appear, and additional geometrical constraints are needed. This will be discussed in the next section.

The so-called *Greedy Algorithm* (see Chapter 2) is going to be applied. Consequently, et each step of the algorithm, the following optimization problem is solved:

$$\left(\mathcal{P}^k_\Theta\right)\begin{cases}\max\limits_{(x_k,y_k,\gamma_k)} & E(\Theta,\Delta(x_k,y_k,\gamma_k))\\ \text{subject to} & (xi{\cdot}y^i)\in\Omega \quad \forall\,(x^i,y^i)\in\Delta(x_k,y_k,\gamma_k)\\ & ||(x^i,y^i)-(x,y)||\ge\delta \quad \forall\,(x^i,y^i)\in\Delta(x_k,y_k,\gamma_k) \quad \forall\,(x,y)\in\mathcal{S}^*_{k-1}\\ & 0\le\gamma_k\le\pi\,.\end{cases} \tag{3.6}$$

where Ω denotes the feasible area (see Section 1.2.1), δ denotes de security distance, and $\mathcal{S}^*_{k-1}$ denotes the positions of the heliostats located in the previous steps.

If the solution obtained for problem $\left(\mathcal{P}^k_\Theta\right)$ is denoted by (x^*,y^*,γ^*), then the heliostat field obtained at step k can be expressed as $\mathcal{S}^*_k=\mathcal{S}^*_{k-1}\cup\Delta(x^*,y^*,\gamma^*)$. Note that the number of decision variables is reduced to three due to the use of pod structures and that six heliostats positions are calculated at each step, reducing the number of problems to solve.

As done in the previous chapters, a multi-start strategy has been applied to avoid the local optima appearing because of the shading and blocking effects. However, in this approach, since six heliostats are introduced at each step, these effects become more complex, and a higher number (comparing to the location of individual heliostats) of initial solutions is needed to obtain good enough solutions.

3.2.1 Results

In this section the results obtained when applying the greedy algorithm are presented and compared against different field designs. The Helio100 field constructed in South Africa and two fields obtained with two different optimization procedures. A pattern-

free procedure (using a genetic-based algorithm [88]) and a pattern-based procedure with a parabolic pattern (using Nelder-Mead algorithm). Both algorithms are deeply explained in detail in [38].

See Table 3.2 and Figure 3.4, where the results obtained with the different field configurations are presented. The greedy algorithm is applied with 200 initial solutions in the multi-start procedure.

Field	E	$\mathcal{E}$
Helio100	0.413	0.67
Pattern-based	0.417	0.67
Genetic-based	0.422	0.68
Greedy-based	0.430	0.69

Table 3.2: Annual thermal energy E (GWHth) and field efficiency

Note that, despite the fact that both pattern-free approaches (genetic-based and greedy-based) have higher visual irregularities, they also collect higher annual thermal energy values. In this test case, this effect could be due to the fact that the annual energy maximum region, see Figure 3.5, is not symmetric. Note that for the irradiation data discussed in Chapter 2, the level curves of the energy function are symmetric, see Figure 2.3(a). Both pattern-free algorithms are capable to directly locate more heliostats into the east region (right part of the figures) of the field, taking advantage of this special situation. However, pattern-based approaches impose usually symmetry and therefore they need to be manually modified to handle this type of situations when detected.

3.3 Location and sizing problem

In this section the optimization of a field design with triangular pods including the triangle side as a decision variable is presented. The triangular Helio pod prototype has $6\,m$ side length. However, a deep study regarding this parameter has to be done including the cost associated with each possible side length. In Figure 3.6, a preliminary study when considering a heliostat field with different triangle sides is performed. The differences achieved regarding the annual thermal energy collected and the occupied land can be appreciated.

In previous calculations, the heliostat side, denoted by l, has been considered as a fixed parameter. This parameter was taken as the smallest possible value allowing the feasible location of the six heliostats into the triangle vertices and midpoints, see Figure 3.3(a). Taking into account the clear-out circle surrounding each heliostat (allowing the heliostat to rotate freely) the minimum triangle side can be easily calculated

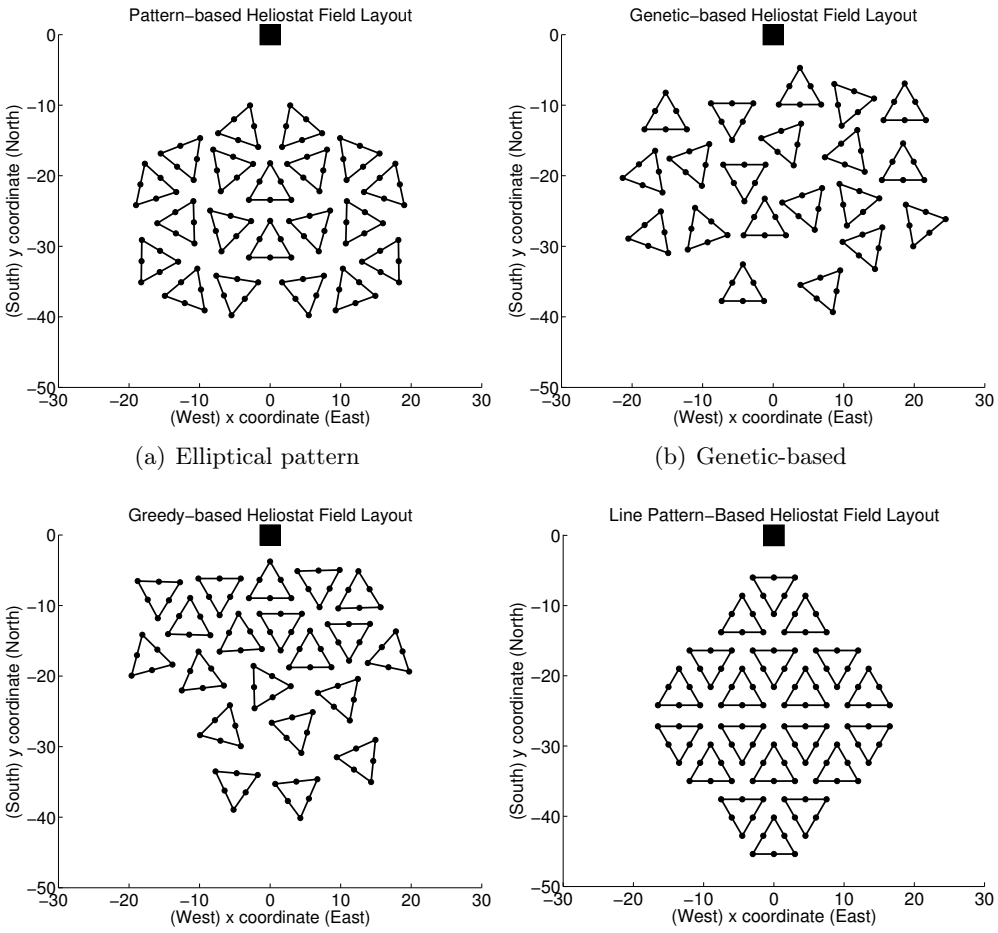

(a) Elliptical pattern

(b) Genetic-based

(c) Greedy algorithm

(d) Helio100

Figure 3.4: Triangular pod designs

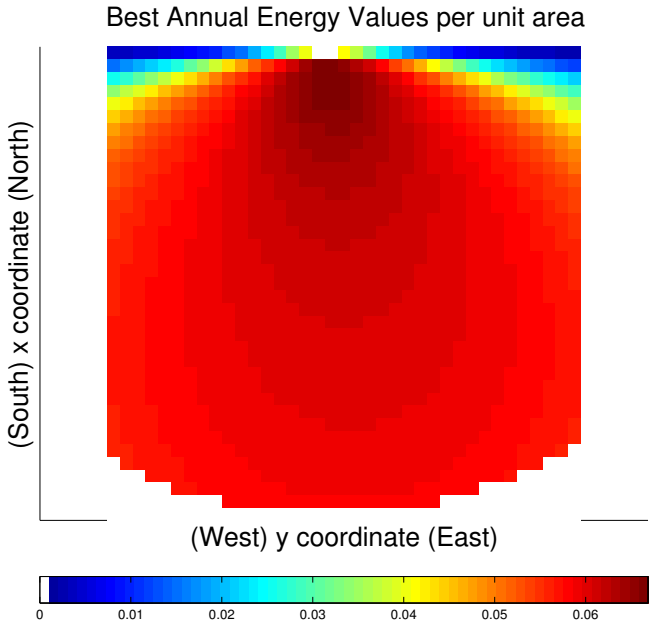

Figure 3.5: Annual energy values

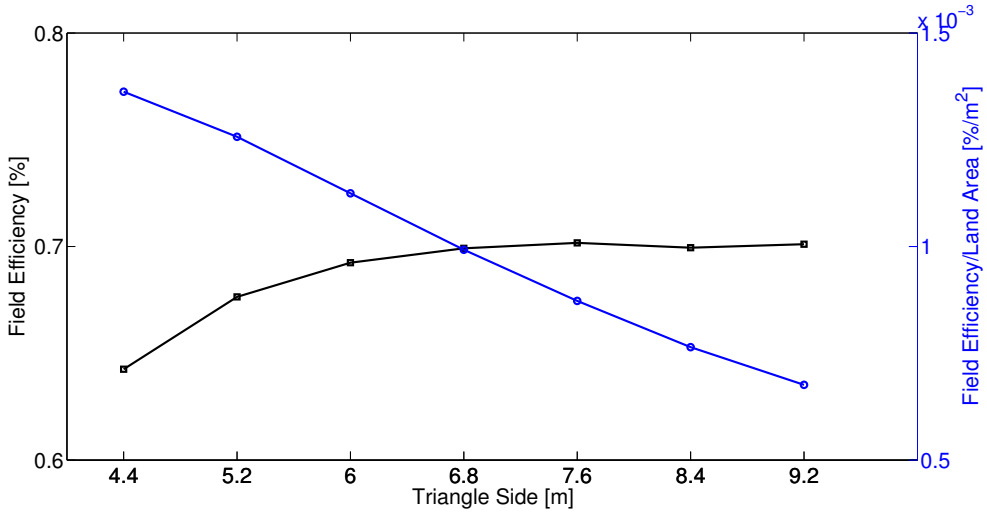

Figure 3.6: Different pod sides (field efficiency and occupied land)

as follows:

$$l_{\texttt{min}} = 2\,\delta^* \,. \tag{3.7}$$

If $l = l_{\texttt{min}}$ for all the triangular pods, the constraints to be considered in order to obtain a feasible solution can be reduced as the safety clear-out circle constraints as in the previous section. However, once the size of the triangle is $l > l_{\texttt{min}}$ (as can occur when it is included as an optimization variables) more constraints are needed to avoid overlap between the different pods. As can be seen in Figure 3.7, infeasible solutions are obtained considering only the previous constraints (overlapping triangles are highlighted in black).

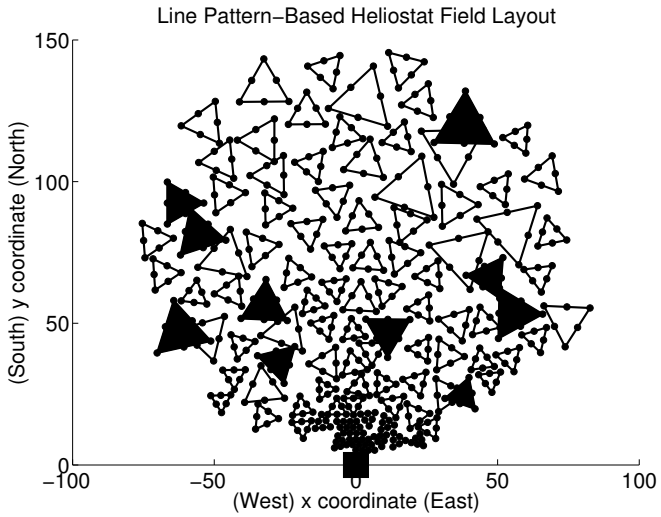

Figure 3.7: Overlapping effects

Therefore, additional constraints have to be included at each step of the greedy algorithm. At step k of the greedy algorithm (location of triangular pod $\Delta(x_k, y_k, \gamma_k)$ with the field $\mathcal{S}^*_{k-1}$ with $k-1$ heliostats is already located) the following constraint are added:

- Avoid vertices to be inside another triangle.

  For each vertex of $\Delta(x_k, y_k, \gamma_k)$, denoted as V_j for $j = 1, \ldots 6$, check if they are inside any another triangle $\Delta(x_i, y_i, \gamma_i)$ for $i = 1, \ldots (k-1)/6$ and vice versa.

  The vector product through the shoelace formulae, also known as the Surveyor's formula [16], is used to check if a point is or not inside a triangle. With this formula the triangle signed area is obtained allowing to calculate the relative position between the vertex V_j and the three sides of the triangle $\Delta(x_i, y_i, \gamma_i)$.

- Respect the security distance.

  The distance between the vertex V_j for $j = 1, \dots 6$ and the sides of the triangles already located $\Delta(x_i, y_i, \gamma_i)$ for $i = 1, \dots (k-1)/6$ has to be greater than the corresponding security distance.

3.3.1 Results

In this section the results obtained when the triangle side length is included as optimization variable are presented. The fixed parameters are the same as detailed in the previous section except for the site location (Sanlúcar la Mayor (Seville), latitude $37^o26'$ N and longitude $6^o15'$ W) and the tower height ($10.90\,m$). Note that in this case, the receiver is facing North as the site location is in the northern hemisphere.

With this, taking $N_{\texttt{ini}} = 200$, the field layout obtained as example is given in Figure 3.8, with an objective function of $E = 0.4372$ GWHth.

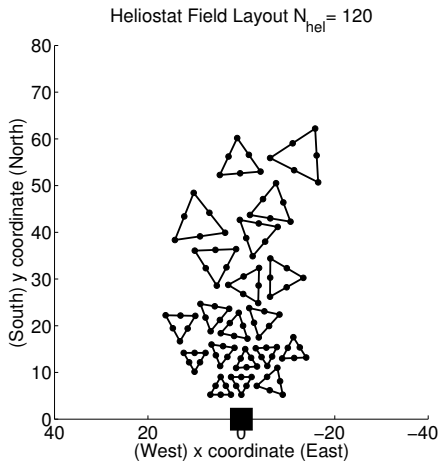

Figure 3.8: Triangular pod field with side length variable

3.4 Conclusions

Due to the recent development of pod systems, this chapter presents a first attempt to address the location problem. Hence, some simplifications have been made. In particular, the number of pods has been considered to be fixed, and just the energy collected by the field (see function E defined in Eq. (1.10)) is used.

Future work will consider the cost function as optimization criterion, as done in Chapter 2 for single heliostats.

Chapter 4

Optimization of multiple receivers solar power tower systems

4.1 Introduction

In recent years, higher power requirements are imposed on the SPT systems, calling for large-scale plants such as Gemasolar (19.9 MW and 2,650 hel. [21, 54]), Khi Solar One (50 MW and 4,120 hel. [56]) and Ivanpah (377 MW and 173,500 hel. [55]). Using one-receiver systems, as pointed out in [83, 95, 100], the large amount of heliostats forces to locate heliostats far from the tower, increasing atmospheric and spillage losses. The use of multiple receivers systems allows one to reach high temperatures, required to achieve conversion efficiency of solar energy to electricity [90], while reducing the thermal losses associated.

Regarding the spatial configurations of the multiple receivers, there are different proposals in the literature: vertical [93], circular [17, 28], same focal spot [19] and horizontal, see [95, 99].

Related to the heliostat field layout, different approaches have also been studied in the literature, see [11, 83, 90, 93, 95, 99]. A common approach relies on the field separation method: for each receiver a separate region where the heliostats will be placed, called aiming region, is identified, see [11]. The field separation strategy has already been used under radially-staggered layouts in [100].

The field separation method is mainly based on two facts: the varying heliostats performance regarding their position in the field [100], and the computational time reduction by implementing simplified methods to calculate shading and blocking effects [33, 92]. If, for instance, three aiming regions are considered, namely North, West and East, the West region will be most efficient at the beginning of the day and the East region in the afternoon. These performances imply that the optimal number and density of heliostats will not necessarily be the same for each selected region.

Different shapes are usually imposed to the aiming regions, such as concentric circular trapezoids [93] or ellipses [95, 99]. However, such aiming regions overlap, and it is not trivial how to fix a strategy to assign heliostats at the intersection of the regions.

The field and the receivers are interdependent, as pointed out in [93]. It is thus important to design both components simultaneously. This coupled optimization problem with multiple receivers has been addressed in the literature by different authors. In [95], a genetic-based algorithm is proposed to optimize the radial-stagger field layout parameters, the tower height and the receiver aperture size and tilt angle. In [83], eleven design variables are optimized through a variant of the Powell algorithm and a genetic-based algorithm. In a different way, in [100] the receiver is firstly selected to be as simple and cheap as possible, and then the radial-staggered field is limited to an ellipsoidal boundary which size is determined by the receiver. Finally, in [93], a reference field is fixed and the two receivers considered are placed in the best vertical arrangement found. Then, different two-zones heliostat field configurations are evaluated and the one reaching the best plant performance is selected.

In this chapter a new method to design a multiple receivers SPT system is presented, where the receivers and the heliostat field layout are simultaneously optimized. The variables related to the receivers and the heliostats (number and positions) are optimized through an alternating process to obtain a multiple receivers system that minimizes the LCOE.

The spatial configuration selected for the multiple receivers system is the horizontal distribution, and each receiver is characterized by its own height in the tower, aperture tilt angle, azimuth angle and aperture radius, see Figure 4.1. The separation method is applied to design the field layout and each aiming region is obtained by the algorithm without imposing any particular shape. For simplicity, the heliostats are considered aiming the same receiver regardless the instant of time. The methodology presented to solve the heliostat location problem is a greedy-based algorithm presented in Chapter 2. As far as the authors are aware of, these are novel issues in the literature.

The rest of the chapter is organized as follows. In Section 4.2, the SPT system is presented. Section 4.3 explains the optimization problem and the methodology proposed to solve it. The proposed algorithms are applied to a given configuration and the main results are discussed in Section 4.4. The last section is devoted to summarize the obtained results.

4.2 Decision variables and functions

The optimal design of a multiple receivers SPT system consists of determining the apertures dimensions and receivers positions in the tower and the location of the heliostats so as to minimize the LCOE. In the following subsections, the variables, the

feasible sets and the functions involved in the optimization problem will be presented.

4.2.1 Decision variables

Although the proposed approach is valid for any number of receivers, for simplicity three receivers are considered , called North, West and East, and numbered as receiver 1, 2 and 3 respectively.

The four most relevant variables associated with each receiver design are considered, namely the aperture *radius* r, the *height* h in the tower, the aperture *tilt* angle ξ (which measures the separation from the vertical line) and, the *azimuth* angle α (which measures the separation from the North axis), see Figures 4.1(a)-4.1(b). From now on Θ_i will denote the optimization variables related to receiver i, and Θ will denote the full collection of decision variables concerning the receivers:

$$\Theta = (\Theta_1, \Theta_2, \Theta_3) \in \mathcal{M}_{4\times 3} \text{ with } \Theta_i = (r_i, h_i, \xi_i, \alpha_i)^t \in \mathbb{R}^4 \quad \forall\, i = 1, 2, 3\,. \tag{4.1}$$

Some constraints, influenced by technical and legal regulations, determine the feasible region $\mathbf{\Theta}$. They are written as follows:

$$\mathbf{\Theta} = \left\{ \begin{array}{ll} \Theta \in \mathcal{M}_{4\times 3}\ : & r_{min} \le r_i \le \min(h_i, r_{max}) \le h_{max} \quad \forall\, i = 1, 2, 3 \\ & \xi_i \in [0, \pi/2] \\ & \alpha_i \in [\underline{\alpha}_i, \overline{\alpha}_i] \end{array} \right\}. \tag{4.2}$$

As presented in Chapter 1, r_{min} and r_{max} denote the minimum and maximum receiver radius and h_{max} is the maximum value for the tower height. The ranges for the variables α_i are calculated as follows:

$$\begin{array}{ll} \underline{\alpha}_1 = \max\{-\pi/2, \alpha_3 + \varsigma_3 + \varsigma_1\}\,, & \overline{\alpha}_1 = \min\{\pi/2, \alpha_2 - \varsigma_2 - \varsigma_1\}\,, \\ \underline{\alpha}_2 = \max\{0, \alpha_1 + \varsigma_1 + \varsigma_2\}\,, & \overline{\alpha}_2 = \min\{\pi, \alpha_3 - \varsigma_3 - \varsigma_2\}\,, \\ \underline{\alpha}_3 = \max\{-\pi, 2\pi + \alpha_2 + \varsigma_2 + \varsigma_3\}\,, & \overline{\alpha}_3 = \min\{0, \alpha_1 - \varsigma_1 - \varsigma_3\}\,, \end{array} \tag{4.3}$$

where the angles ς_i are obtained through the following equations:

$$\varsigma_i = \arcsin\left(\frac{r_i}{\sqrt{r_i^2 + d_{\mathtt{ap}}^2}}\right) \quad \forall\, i = 1, 2, 3\,. \tag{4.4}$$

The fixed parameter $d_{\mathtt{ap}}$ denotes the distance between each aperture and the center of coordinates, see Figures 4.1(a)-4.1(c).

In what concerns the field, the heliostat locations, given by the coordinates (x, y) of their centres, are the variables to be used. The finite collection of coordinates of the centres of the heliostats defines the heliostat field $\mathcal{S}$ within the feasible set $\mathscr{S}$ defined in Eq. (1.1).

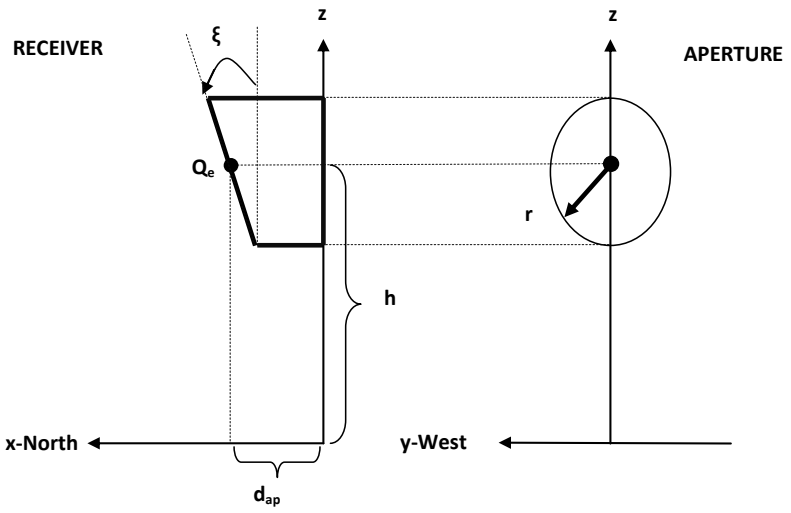

(a) h, ξ angle and r (front-lateral)

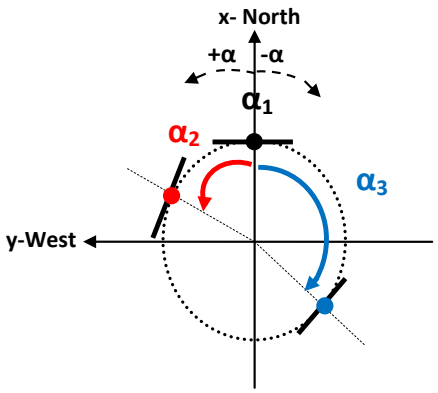

(b) α angle (top)

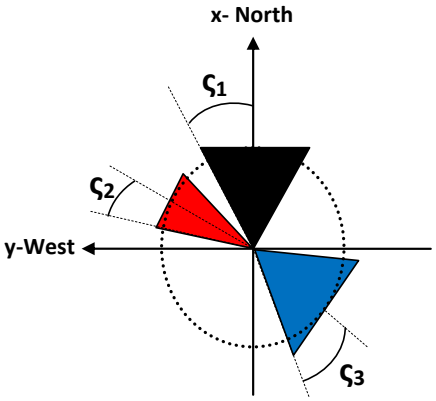

(c) ς angle (top)

Figure 4.1: Receivers variables

Note that the variable $\mathcal{S}$ is a set whose cardinality is not fixed in advance. As already mentioned, it is assumed that each heliostat is always aiming at the same receiver. The separate heliostat fields, denoted by $\mathcal{S}_i$ for $i = 1, 2, 3$, are expressed as follows:

$$\mathcal{S}_i = \{(x, y) \in \mathcal{S} \,:\, \text{heliostat at } (x, y) \text{ aims at receiver } i\} \text{ with } \mathcal{S} = \bigcup_{i=1}^{3} \mathcal{S}_i \,. \tag{4.5}$$

4.2.2 Functions

The function to be optimized is the LCOE, that is the maximization of the annual thermal energy collected per unit cost, calculated as $F = C(\Theta, |\mathcal{S}|)/E(\Theta, \mathcal{S})$.

The construction cost C is given by the function defined in Eq. (1.9), but slightly modified to take into account the three possible receiver heights:

$$C(\Theta, |\mathcal{S}|) = \beta_1(\max_i\{h_i\} + \kappa)^\sigma + \beta_2\pi \sum_{i=1}^{3} r_i^2 + c_{\mathtt{f}} + c|\mathcal{S}| \,, \tag{4.6}$$

where all the parameters are defined in Eq. (1.9).

The thermal annual energy collected by the field into the receiver is calculated following Eq. (1.10) in Chapter 2, which is based on the NSPOC procedure [33] with 12 representative days considered. In this chapter, however, a slight change is done: instead of using a polynomial fitting to obtain the annual value, the rectangular quadrature rule is applied since, in practice, each receiver energy value is calculated individually.

It is clear that the objective function, F, is a quantity that, at least at first sight, furnishes global information on the overall advantages and disadvantages of the construction cost needed to produce energy.

The approach proposed in this chapter uses such calculations as subroutines, but could thus be replaced by any alternative method such as e.g. ray-tracing methods [50].

4.3 Problem statement

The optimization problem is written as follows:

$$(\mathcal{P}) \begin{cases} \min\limits_{\Theta, \mathcal{S}} & F(\Theta, \mathcal{S}) = C(\Theta, |\mathcal{S}|)/E(\Theta, \mathcal{S}) \\ \text{subject to} & \Theta \in \boldsymbol{\Theta} \\ & \mathcal{S} \in \mathscr{S} \\ & \Pi_i^- \leq \Pi_{T_d}(\Theta_i, \mathcal{S}) \leq \Pi_i^+ \quad i = 1, 2, 3 \,. \end{cases} \tag{4.7}$$

Remind that two blocks of decision variables are considered: those related to the design of the receivers Θ, and those related to the field layout $\mathcal{S}$.

In order to handle problem $(\mathcal{P})$, it is first split in two sub-problems: the *Multiple Receivers Optimization* and the *Field Optimization*. The multiple receivers optimization problem, denoted by $(\mathcal{P}_\mathcal{S})$, describes the optimization of the multiple receivers when the heliostat field is fixed. Contrarily, the field optimization problem, denoted by $(\mathcal{P}_\Theta)$, describes the field optimization for a fixed multiple receivers configuration.

Both sub-problems are solved independently (following specific methods described in next subsections) and, finally, the alternating method (presented more in detail in Chapter 2) is applied to obtain a solution of the complete problem $(\mathcal{P})$.

The alternating algorithm, described in Algorithm 4, starts from an initial feasible solution $(\Theta^0, \mathcal{S}^0)$ and sequentially optimizes sub-problems $(\mathcal{P}_\mathcal{S})$ and $(\mathcal{P}_\Theta)$. In the following subsections the strategies devised to solve problems $(\mathcal{P}_\Theta)$ and $(\mathcal{P}_\mathcal{S})$ independently are presented.

Algorithm 4 `Alternating algorithm`

Require: Θ^0 and ϵ_0
  $k \leftarrow 0$
  $\mathcal{S}^0 \leftarrow$ solve $(\mathcal{P}_\Theta)$ given $\Theta = \Theta^0$
  $\Upsilon_{obj} \leftarrow F(\Theta^0, \mathcal{S}^0)$
  repeat
    $k \leftarrow k + 1$
    $\Theta^k \leftarrow$ solve $(\mathcal{P}_\mathcal{S})$ given $\mathcal{S} = \mathcal{S}^{k-1}$
    $\mathcal{S}^k \leftarrow$ solve $(\mathcal{P}_\Theta)$ given $\Theta = \Theta^k$
    $\Upsilon_{obj} = \min\{\Upsilon_{obj}, F(\Theta^k, \mathcal{S}^{k-1}), F(\Theta^k, \mathcal{S}^k)\}$
  until $||F(\Theta^k, \mathcal{S}^k) - F(\Theta^{k+1}, \mathcal{S}^{k+1})|| \leq \epsilon_0$
  return $\boxed{\Upsilon_{obj}}$

4.3.1 Multiple receivers optimization

This section focus on the first sub-problem $(\mathcal{P}_\mathcal{S})$, where the heliostat field is considered fixed and the optimization variables are those connected to the multiple receivers configuration:

$$(\mathcal{P}_\mathcal{S}) \quad \mathcal{S} \text{ fixed} \begin{cases} \min\limits_{\Theta} & F(\Theta, \mathcal{S}) \\ \text{subject to} & \Theta \in \boldsymbol{\Theta} \\ & \Pi_i^- \leq \Pi_{T_d}(\Theta_i, \mathcal{S}) \leq \Pi_i^+ \quad i = 1, 2, 3\,. \end{cases} \tag{4.8}$$

In general, to solve sub-problem $(\mathcal{P}_\mathcal{S})$ the Multiple Receivers Algorithm described in Algorithm 5 is applied. This algorithm performs an iteration once all the receivers have been optimized. The algorithm stops after an iteration when no improvement in the objective function is found or the difference between the obtained configuration

and the previous one is insignificant, i.e. $||\Theta^k - \Theta^{k+1}||_\infty \leq \epsilon_1$ for a given ϵ_1. The power requirements are included in the objective function by penalizing the non-feasible solutions.

Individually, the different receivers are optimized sequentially, and the set of variables associated with each receiver Θ_i are optimized using the cyclic coordinate method. This method performs at each receiver variable ($r_i, h_i, \xi_i,$ and α_i) a local search in the corresponding feasible interval given by the feasible set $\boldsymbol{\Theta}$ described in (4.2). While optimizing receiver i the following stopping rule is applied: $||\Theta_i^k - \Theta_i^{k+1}||_\infty \leq \epsilon_2$ for a given ϵ_2. In other words, the cyclic coordinate method stops when the difference between two consecutive solutions is irrelevant, see [8] for further details.

Algorithm 5 `Multiple receivers algorithm`

Require: Π_i^-, $\mathcal{S}$, ϵ_1 and Θ^0 (feasible)
  $k \leftarrow 0$
  $F_0 \leftarrow F(\Theta^0, \mathcal{S})$
  $\Upsilon_{obj} \leftarrow F_0$
  repeat
    $k \leftarrow k + 1$
    for $i = 1:3$ **do**
      $r_i^k \leftarrow$ solve $\max_{r_i} F(\Theta, \mathcal{S})$ with $r_i \in [r_{min}, \min(h_i, r_{max})]$
      $h_i^k \leftarrow$ solve $\max_{h_i} F(\Theta, \mathcal{S})$ with $h_i \in [r_i, h_{max}]$
      $\xi_i^k \leftarrow$ solve $\max_{\xi_i} F(\Theta, \mathcal{S})$ with $\xi_i \in [0, \pi/2]$
      $\alpha_i^k \leftarrow$ solve $\max_{\alpha_i} F(\Theta, \mathcal{S})$ with $\alpha_i \in [\underline{\alpha}_i, \overline{\alpha}_i]$
      $\Theta_i^k \leftarrow (h_i^k, \xi_i^k, \alpha_i^k, r_i^k)$
    end for
    $\Theta^k \leftarrow (\Theta_1^k, \Theta_2^k, \Theta_3^k)$
    $F_k \leftarrow F(\Theta^k, \mathcal{S})$
    $\Upsilon_{obj} = \min\{\Upsilon_{obj}, F(\Theta^k, \mathcal{S})\}$
  until $F_k > F_{k-1}$ or $||\Theta^k - \Theta^{k+1}||_\infty \leq \epsilon_1$
  return $\boxed{\Upsilon_{obj}}$

4.3.2 Field optimization

This section focus on the heliostat field optimization sub-problem, when the variables related to the receiver are fixed, that is, the resolution of problem $(\mathcal{P}_\Theta)$:

$$(\mathcal{P}_\Theta) \quad \Theta \text{ fixed} \begin{cases} \min\limits_{\mathcal{S}} & F(\Theta, \mathcal{S}) \\ \text{subject to} & \mathcal{S} \in \mathscr{S} \\ & \Pi_i^- \leq \Pi_{T_d}(\Theta_i, \mathcal{S}) \leq \Pi_i^+ \quad i = 1, 2, 3\,. \end{cases} \tag{4.9}$$

This is a difficult large-dimensional multi-modal black-box optimization problem. Therefore, heuristic methods are applicable. These do not necessarily guarantee that a globally optimal solution is found, but are fast enough and do not require much knowledge about the function itself. For simplicity, three receivers and a different aiming region for each receiver are considered. The resolution of problem $(\mathcal{P}_\Theta)$ is divided in two stages: the division of the feasible region Ω into three aiming regions and the location of heliostats within each aiming region.

Aiming regions calculation

Given a multiple receivers configuration Θ, the field optimization procedure starts from discretizing the feasible region Ω in order to separate it into three regions of empty intersection. Firstly, for each point (x, y) of the discretization, the energy generated by a heliostat centred at (x, y) and aiming at receiver i, for $i = 1, 2, 3$, is calculated. Then, the optimal aiming of this point, if no other heliostat existed in the field, is identified as the receiver where the maximum thermal energy is collected, i.e. $\arg\max_i\{E(\Theta_i, \{(x, y)\})\}$.

This section is illustrated with some examples obtained after applying the proposed method to an annulus shaped feasible region Ω and the following multiple receivers configuration:

$$\Theta = \begin{pmatrix} 100.5 & 100.5 & 100.5 \\ 12.5 & 12.5 & 12.5 \\ 0 & 90 & -90 \\ 6.39 & 6.39 & 6.39 \end{pmatrix}, \tag{4.10}$$

with units detailed in Table 4.2.

Since Ω is infinite, a finite grid is chosen in the discretization, obtaining plots such as the one in Figure 4.2(a), yielding the maximum energy values, and Figure 4.2(b), yielding the split given by the optimal aiming: red, black and blue correspond to the West, North and East receiver.

Once a discretization of Ω is obtained, the three sets of boundary points are selected and a polynomial fit is applied to each set. Three polynomial fits are applied to the following boundary points: North-West, North-East and West-East; obtaining p, q and s polynomials respectively. In the given example, the south region is fairly separated by the x axis as can be seen in Figure 4.2(a).

The regions have not the same influence over the objective function. North region reaches better values if the system is in the northern hemisphere, see Figure 4.2(a) and different power requirements are considered for each receiver. A simple process without considering different possible regions may not lead to the best field configuration. Therefore, different weights are applied to the obtained energy values in order to give more or less priority to the northern region. That is, for each point (x, y) and each

weight $w \in \mathbb{R}^+$, the optimal aiming is calculated as the receiver where the maximum value is achieved, i.e. $\max\{wE(\Theta_1, \{(x,y)\}), E(\Theta_2, \{(x,y)\}), E(\Theta_3, \{(x,y)\})\}$.

Given the weight $w \in \mathbb{R}^+$ and following the previous notation, each aiming region is denoted by Ω_i^w and expressed as follows:

$$\Omega_1^\omega = \left\{ \begin{array}{ll} (x,y) \in \Omega : & x \geq 0 \\ & q_\omega(x) \leq y \leq p_\omega(x) \end{array} \right\}, \tag{4.11}$$

$$\Omega_2^\omega = \left\{ \begin{array}{lll} (x,y) \in \Omega : & y \geq p_\omega(x) & \text{if } x \geq 0 \\ & y \geq s_\omega(x) & \text{if } x < 0 \end{array} \right\}, \tag{4.12}$$

$$\Omega_3^\omega = \left\{ \begin{array}{lll} (x,y) \in \Omega : & y \leq q_\omega(x) & \text{if } x \geq 0 \\ & y \leq s_\omega(x) & \text{if } x < 0 \end{array} \right\}. \tag{4.13}$$

As a first example, ω is set to 1, i.e. no prioritized region is considered. After applying the procedure, p_1, q_1 and s_1 are obtained as shown in Figure 4.2(c), where the West-East polynomial s_1 corresponds to the x axis. If five different weights $w_k \in \mathbb{R}_+$ are considered, for each weight the corresponding three polynomials p_{ω_k}, q_{ω_k} and s_{ω_k} are obtained, which define three different aiming regions. As can be seen in Figure 4.2(d), considering $\omega = 1.010$ (resp. $\omega = 0.990$), more priority (resp. less priority) is given to the North region.

Then, the heliostat location problem is solved for the aiming regions obtained corresponding to the various weights. At the end of the process, the field layout which reaches the best objective value is selected as final solution.

Heliostats location

Once the three aiming regions are obtained for a given weight w, the second goal is to calculate the heliostat field layout, that is, $\mathcal{S}_i \in \mathscr{S}_i^\omega$, where the feasible sets are given by $\mathscr{S}_i^\omega = \mathcal{S} \cap \Omega_i^\omega$ for $i = 1, 2, 3$. The algorithm starts locating heliostats at the most favourable region (Ω_1^ω if the system is in the northern hemisphere) leading to $\mathcal{S}_1$. This first location problem is denoted by $\left(\mathcal{P}_\Theta^1\right)$ and is described below:

$$\left(\mathcal{P}_\Theta^1\right) \quad \Theta \text{ fixed} \left\{ \begin{array}{ll} \min\limits_{\mathcal{S}_1} & F(\Theta, \mathcal{S}_1) \\ \text{subject to} & \mathcal{S}_1 \in \mathscr{S}_1^\omega \\ & \Pi_{T_d}(\Theta_1, \mathcal{S}_1) \geq \Pi_0^1 \,. \end{array} \right. \tag{4.14}$$

After $\mathcal{S}_1$ is obtained, the procedure continues by solving $\left(\mathcal{P}_\Theta^2\right)$ and $\left(\mathcal{P}_\Theta^3\right)$ simultaneously, to obtain $\mathcal{S}_2$ and $\mathcal{S}_3$. For $i = 2, 3$, both problems are described below.

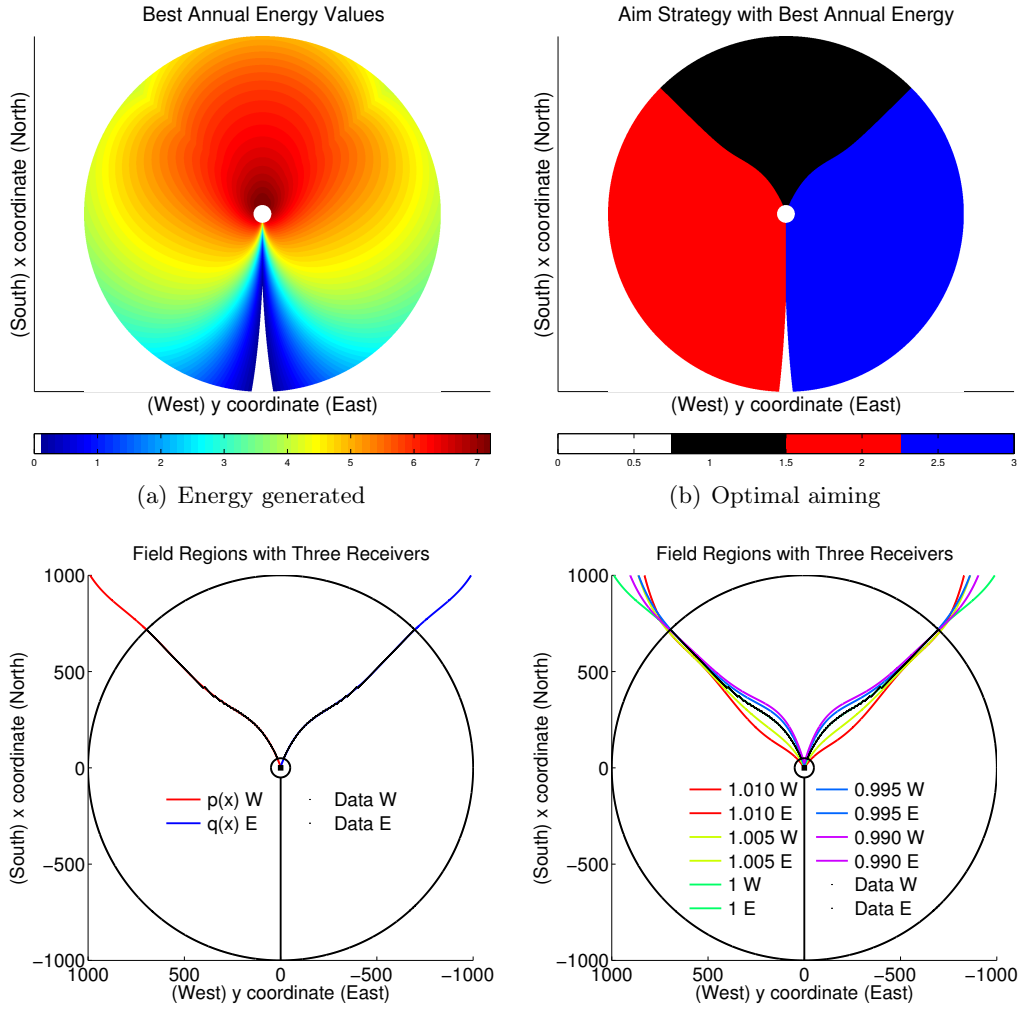

(a) Energy generated

(b) Optimal aiming

(c) Aiming regions for $\omega = 1$

(d) Aiming regions for several ω

Figure 4.2: Aiming regions calculation

$$\left(\mathcal{P}^i_\Theta\right) \quad \Theta \text{ fixed} \begin{cases} \min\limits_{\mathcal{S}_i} & F(\Theta, \mathcal{S}) \\ \text{s.t.} & \mathcal{S}_i \in \mathscr{S}_i^\omega \\ & ||(x,y)-(x',y')|| \geq \delta \quad \forall\,(x,y) \in \mathcal{S}_i\,,\,(x',y') \in \mathcal{S}_1 \\ & \Pi_{T_d}(\Theta_i, \mathcal{S}_i) \geq \Pi_0^i\,. \end{cases} \tag{4.15}$$

Note that problem $\left(\mathcal{P}^i_\Theta\right)$ includes constraints motivated by the heliostat positions from $\mathcal{S}_1$. Collisions between heliostats must be avoided including those located near the boundaries of the aiming regions.

Following the location algorithm described later on, at a first phase the heliostats are located at each aiming region until the minimal power requirement for the corresponding receiver is reached. This step is called the *Requirement Phase*, where a feasible solution of problem $(\mathcal{P}_\Theta)$ is obtained.

However, a second phase, called *Completion Phase*, is applied where the location of the heliostats continues if the value of the objective function improves and the maximal power requirement is not attained. Unlike the requirement phase, where heliostats are located at the corresponding aiming region, in the completion phase the three aiming regions are considered simultaneously and the heliostats are located at the best of one of the three possible positions if and only if the objective value of the system improves and the maximal power requirements are not attained. If none of the three new positions improves the LCOE of the system or any of the maximal power requirements is achieved, the algorithm stops and gives as solution the field obtained so far.

For several reasons, the greedy-based strategy seems very reasonable: at each step, the number of variables to optimize is small, which allows one a quick resolution; moreover, it permits to determine the total amount of heliostats without any a priori requirement. Furthermore, it has been tested successfully in the framework of one-receiver fields, see Chapter 2.

The complete heliostat location algorithm proposed to solve problem $(\mathcal{P}_\Theta)$ with multiple receivers is detailed in Algorithm 6. Note that $\left(\mathcal{P}^i_\Theta\right)^k$ denotes the problem of locating heliostat number k at the aiming region i, where there are already $k-1$ heliostats. At each step of the algorithm, the corresponding field is updated with the new position obtained by the Greedy Algorithm. In the requirement phase, the North field is first calculated followed by the East and West fields, that are calculated simultaneously reducing the computational time. Then, in the completion phase, the final number of heliostats and the final field are obtained.

Following the example with weight $\omega = 0.990$, after the *Requirement Phase* the algorithm gives as solution the field shown in Figure 4.3(a), where heliostats aiming different receivers are highlighted with different colors, and heliostats located at the *Completion Phase* are highlighted with white asterisks. The product of the efficiency

coefficients (cosine, shading and blocking, interception and atmospheric) for each heliostat at different time instants are shown in Figure 4.3(b)-4.3(d), where the different variations over the day can be appreciated.

Algorithm 6 `Heliostat location algorithm for multiple receivers`

Require: Θ, Ω

$\mathcal{S} =$ **Requirement Phase**

$k \leftarrow 0$

for $i = 1, 2, 3$ **do**

  while $\Pi_{T_d}(\Theta, \mathcal{S}_i) < \Pi_i^-$ **do**

    $k \leftarrow k + 1$

    $(x^k, y^k) \leftarrow$ solve $\left(\mathcal{P}_\Theta^i\right)^k$ with Greedy Alg.

    $\mathcal{S}_i \leftarrow \mathcal{S}_i \cup \{(x^k, y^k)\}$

  end while

  $\mathcal{S} \leftarrow \mathcal{S} \cup \mathcal{S}_i$

end for

$\mathcal{S}^k \leftarrow \mathcal{S}$ **Completion Phase**

repeat

  $k \leftarrow k + 1$

  for $i = 1, 2, 3$ **do**

    $(x_i^k, y_i^k) \leftarrow$ solve $\left(\mathcal{P}_\Theta^i\right)^k$ with Greedy Alg.

    $\mathcal{S}_i^k \leftarrow \mathcal{S}^k \cup \{(x_i^k, y_i^k)\}$

  end for

  $j \leftarrow \max_i\{E(\Theta, \mathcal{S}_i^k)\}$

  $\mathcal{S}^k \leftarrow \mathcal{S}_j^k$

until $F(\Theta, \mathcal{S}^k) > F(\Theta, \mathcal{S}^{k-1})$ or $\Pi_{T_d}(\Theta_i, \mathcal{S}^k) > \Pi_i^+$ for $i \in [1, 2, 3]$

return $\boxed{\mathcal{S}^{k-1}}$

4.4 Results

The SPT system is assumed to be placed at the same location of the reference plant called **PS10**, see [75]. In Table 4.1, all the fixed parameters are detailed. The lack of results available in the literature in this multiple receivers approach has made impossible to carry out a comparison of the obtained results with possible competitors. As all the algorithms in this dissertation, these have been implemented in Matlab© to have a user-friendly and easily adaptable prototype.

The minimal and maximal power requirements are set to $\Pi^0 = 38.27\ MWth$ and $\Pi^+ = 40.18\ MWth$ respectively and equal for the three receivers.

In this section the iterations performed by the proposed alternating algorithm are detailed. As explained in Section 4.3.2-Figure 4.2(d), five different weights have been considered in previous experiments, and the best results were found with $\omega = 0.990$.

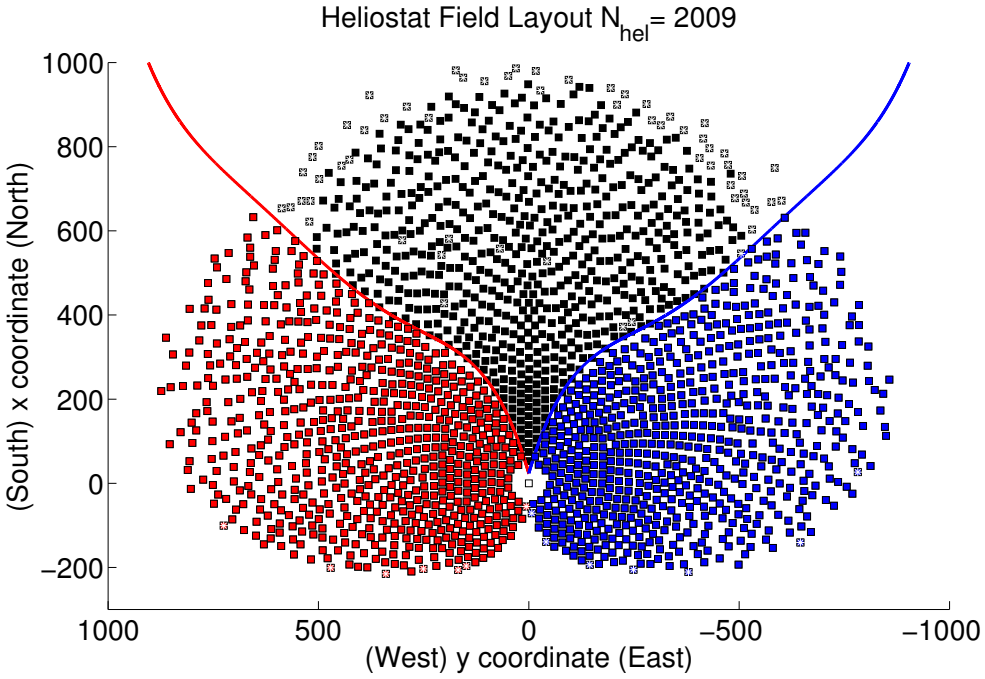

(a) $\mathcal{S}^0$ with $\omega = 0.990$ and Θ^0 fixed

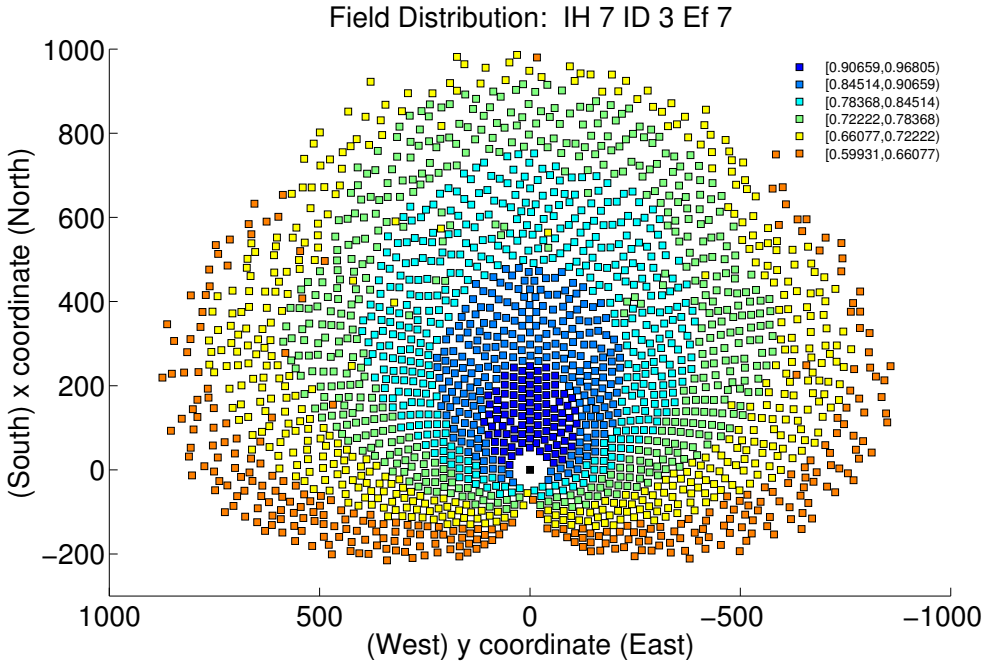

(b) $\mathcal{S}^0$ (21st March 12h)

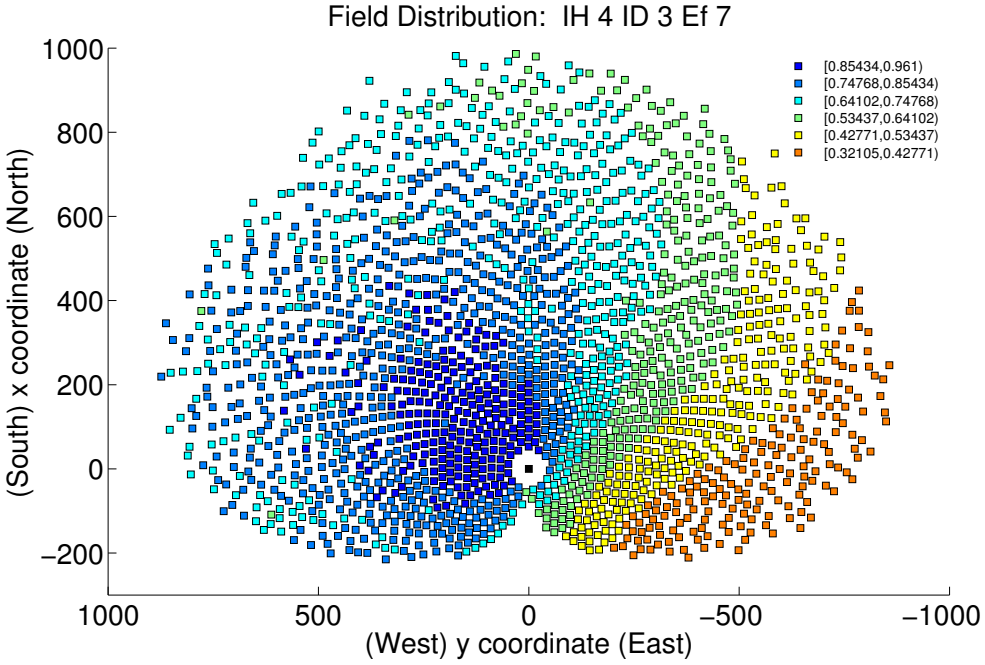

(c) $\mathcal{S}^0$ (21st March 09h)

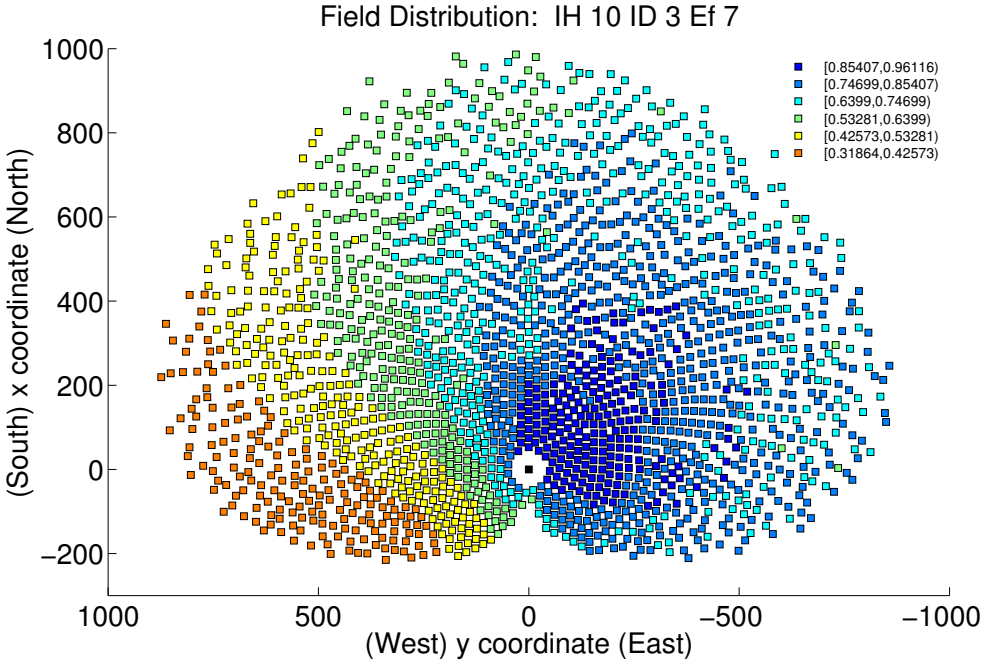

(d) $\mathcal{S}^0$ (21st March 15h)

Figure 4.3: Heliostat field $\mathcal{S}^0$. Efficiency coefficients product at different time instants

Parameter	Default value	Ref.
Location and Time		
Site	Sanlúcar la Mayor (Seville)	[76]
Latitude	$37^o26'$ N	[75]
Longitude	$6^o15'$ W	[75]
Design Point T_d	21st March 12h	assumed
Design direct normal irradiation DNI	823.9 W/m^2	assumed
DNI model	cloudless sky	assumed
Heliostat		
Name	$Sanlucar120$	[75]
Width	12.84 m	[75]
Height	9.45 m	[75]
Optical height z_0	5.17 m	[76]
Minimal safety distance δ	heliostat diagonal+d_s	[18]
$\sigma_{optical}$	2.9 mrad	[75]
Field		
Slope	0^o	assumed
Shape	annulus	assumed
Minimum radius	50 m	assumed
Maximum radius	10^3 m	assumed

Table 4.1: Parameter values

This value constant is maintained, and the Alternating algorithm is applied, taking as initial solution Θ^0, detailed in Table 4.2.

The Alternating algorithm performs three complete iterations and stops when $||F(\Theta^1, \mathcal{S}^1) - F(\Theta^2, \mathcal{S}^2)|| < \epsilon_0$, with $\epsilon_0 = 0.001$. The three heliostat fields obtained during the process, $\mathcal{S}^0$, $\mathcal{S}^1$ and $\mathcal{S}^2$, are shown in Figures 4.3(a)-4.4(a)-4.4(b), respectively.

As shown in Table 4.3 and Figure 4.5, the algorithm achieves a reduction on the LCOE value. Note that the label enumeration corresponds to the configurations detailed in Table 4.3 (column 2) and that heliostats aiming different receivers are highlighted with different colors.

During the optimization process (see Table 4.2), the aperture sizes are reduced, and the receivers positions are modified, unlike the receivers height, that remains approximately constant. The aiming regions, location and number of heliostats in the different fields have also been modified by the algorithm according to the receivers changes. The final solution is configuration number (3), which corresponds to $(\Theta^1, \mathcal{S}^1)$ where the minimum LCOE value is achieved.

Note that due to the differences between the azimuth angles of East and West receivers in the different iterations, the location of heliostats in the southern part of the field changes. With the initial solution Θ^0, where receivers East and West have a bigger azimuth angle, heliostats are located in the southern part, see field $\mathcal{S}^0$. However, with

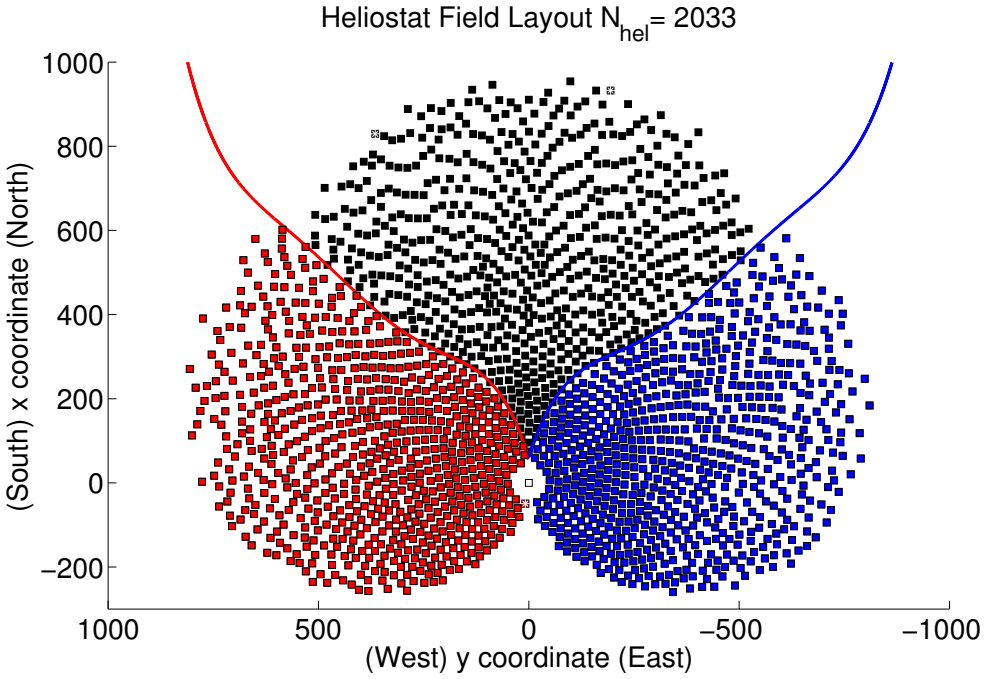

(a) $\mathcal{S}^1$ (Θ^1 fixed). Final field

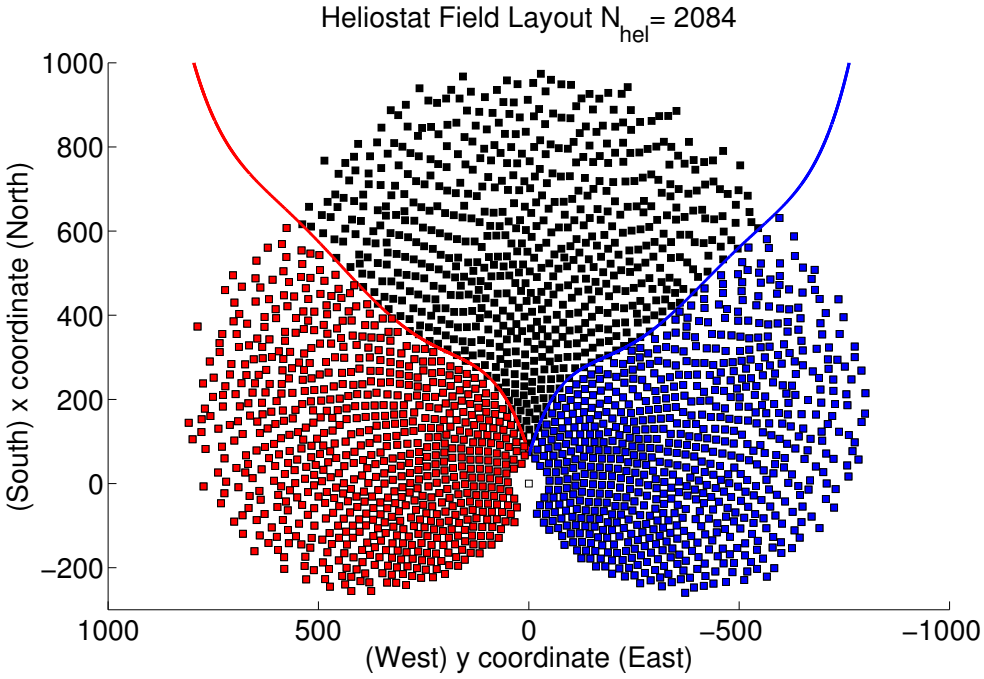

(b) $\mathcal{S}^2$ (Θ^2 fixed)

Figure 4.4: Heliostat field layouts

Step		h [m]	ξ [grad]	α [grad]	r [m]
Θ^0	Θ_1	100.50	12.50	0	6.39
	Θ_2	100.50	12.50	90	6.39
	Θ_3	100.50	12.50	-90	6.39
Θ^1	Θ_1	100.53	8.72	-0.81	4.83
	Θ_2	100.50	17.24	80.94	4.44
	Θ_3	100.50	17.96	-81.32	4.48
Θ^2	Θ_1	100.50	10.71	-0.26	4.44
	Θ_2	100.50	17.50	75.41	4.11
	Θ_3	100.50	17.43	-76.09	4.11

Table 4.2: Alternating algorithm results: receivers

Step	Pb	$\lvert\mathcal{S}\rvert$	Π_{T_d}	E	C	C/E
$k=0$	$1:(\Theta^0,\mathcal{S}^0)$	2009	118.7550	326.83	5.9984	0.01835
	$2:(\Theta^1,\mathcal{S}^0)$	2009	112.0731	310.62	5.3916	0.01736
$k=1$	$3:(\Theta^1,\mathcal{S}^1)$	2033	115.0178	314.55	5.4445	0.01731
	$4:(\Theta^2,\mathcal{S}^1)$	2033	110.4583	306.45	5.3443	0.01744
$k=2$	$5:(\Theta^2,\mathcal{S}^2)$	2084	114.8432	312.30	5.4567	0.01747

Table 4.3: Alternating algorithm results: configurations. Π_{T_d} (MWth), E (GWHth) and C (M€)

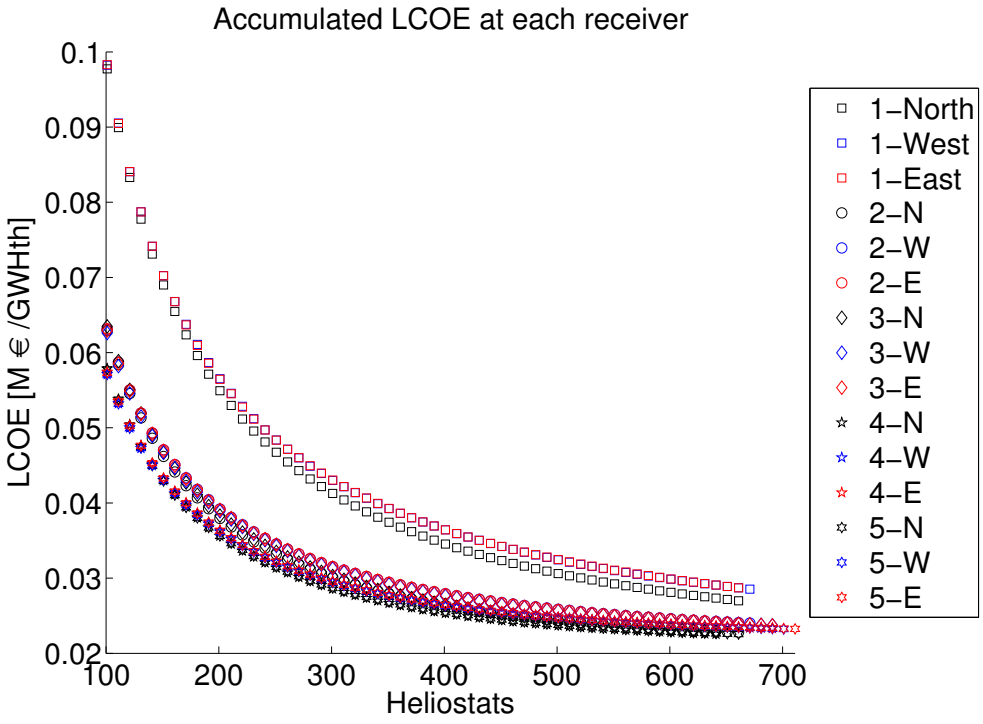

Figure 4.5: Alternating process: LCOE (M€/GWHth)

configurations Θ^1 and Θ^2 (smaller azimuth angle between the receivers) the number of heliostats located in the southern region is reduced, see fields $\mathcal{S}^1$ and $\mathcal{S}^2$.

Regarding the obtained heliostat field layouts, some irregularities appear at the boundaries. The shape of the final field could be smoothed by using, for instance, a non-restricted refinement method [18] or selecting continuous piecewise linear polynomials to better adapt the boundaries discontinuities.

The provided results are not yet validated through an experimental or equivalent procedure and they may not be verified. However, the computational experience shows how promising this new method is for this kind of problems.

4.5 Conclusions

In this chapter, a method to design multiple receivers SPT systems is proposed, where the receivers and the heliostat field are simultaneously optimized. The method identifies the aiming areas (field areas with the same aiming receiver) and calculates their boundaries without imposing any prefixed shape. Heliostats are located freely at different regions following a pattern-free procedure called Greedy Algorithm.

The proposed method is applied with a three receivers initial configuration, showing that the design of multiple receivers systems can be optimized using pattern-free strategies. A new heliostat field layout and a new multiple receivers configuration are obtained at the end of the process successfully reducing the LCOE value of the initial configuration.

Chapter 5

An optimization approach to the design of multi-size-heliostat fields

The optimization of the heliostat field to minimize the LCOE function is a challenging problem as already pointed out in Chapter 2. Usually, the heliostat size has been considered as a fixed parameter, that is, all the heliostats are assumed to have identical size. However, this choice may not lead to optimal fields, as already pointed out in [34]. This chapter focus on the optimization of the multi-size-heliostat field (heliostat field with different heliostat sizes) using a pattern-free method.

For simplicity, the tower-receiver configuration is considered given (to address the whole optimization problem see Chapter 2) and the pedestal height is considered the same for all heliostat sizes. Usually, when addressing the field layout problem, all heliostats are assumed to be focused into the same target point: the aperture centre.

Different heliostat geometries have been studied in order to improve the heliostats performance and cost (hexagonal [97], bubble [52], mini-mirror array [47] and other geometries [59, 67, 115]). The design of heliostat fields using different heliostat sizes together remains, as far as the authors are aware of, unexplored.

The following examples aim to illustrate the effects of the heliostat size in the annual energy collected (when the rest of the parameters are fixed (see Table 5.1). To do that, a *large-size* heliostat (called `HSanlucar120`) and a *small-size* heliostat (called `HTiny`) are selected, whose area and dimensions are one-ninth approximately, and conserve the same aspect ratio (see the details in Table 5.2).

The annual energy per unit area generated by one single heliostat is very similar for both sizes; although they have different behaviour depending on the position. In Figure 5.1 it can be appreciated that the ellipsoidal contour lines differ, specially in regions below the two quadrant diagonals, which furnishes better results with the small-size heliostat (thick lines). This behaviour is due to the interception efficiency (also known as spillage) which measures the amount of reflected energy which fit inside the

receiver aperture.

Considering the tower parameters detailed in Table 5.1, the maximum thermal energy value is reached at coordinates $(74.41, 0)$. That is 0.74 tower heights to the North, this value is according with the interval $[0.5, 1]$ given in [63]. Therefore, as can be also appreciated in Figure 5.1, this region (near the tower) is the most favourable to locate heliostats and where a higher density of heliostats seems preferable, as pointed out in [75, 98].

If a set of heliostats of each selected size are located in this region, a slightly different performance is obtained. As an illustration, take 400 small-size heliostats (`HTiny`) and 43 large-size heliostats (`HSanlucar120`), corresponding with approximately the same reflective area. The positions are obtained applying the patter-free *Greedy Algorithm* (presented in Chapter 2) and can be seen in Figure 5.2. Along this Chapter small-size and large-size heliostats are denoted by points and squares respectively. In this example the annual energy per unit of reflective surface is 1.9671 $MWHth/m^2$ (`HTiny`) and 1.9708 $MWHth/m^2$ (`HSanlucar120`) respectively.

Note that for all heliostat sizes the safe distance remains the same as it is a positive constant related to installation errors and heliostat accessibility. So although the small-size heliostats will have less shadow and blocking because of their relatively larger separation, the large-size heliostats will be more densely packed in the best region of the field, providing a better average performance of 0.2%. For this reason, the iterative algorithm is selected to start from a large-size heliostats field and complement it with small-size heliostats, advantageous at specific positions, aiming to improve the LCOE value of the SPT system.

The rest of the chapter is organized as follows. In Section 5.1, the main ingredients affecting the behaviour and performance of the SPT system are described. The methodology presented to solve the optimization problem is explained in Section 5.2. In Section 5.3, the proposed algorithm and analysis tools are applied to a typical plant design with two different size examples and finally, in Section 5.4, the main results are summarized.

5.1 Problem statement

In this Section, the variables involved in the optimization process are explained, the energy and cost function to handle with different heliostat sizes and the optimization problem itself.

5.1.1 Variables

All heliostats are assumed to be rectangular and to have the same pedestal height, although they can have different dimensions. This last assumption also helps to re-

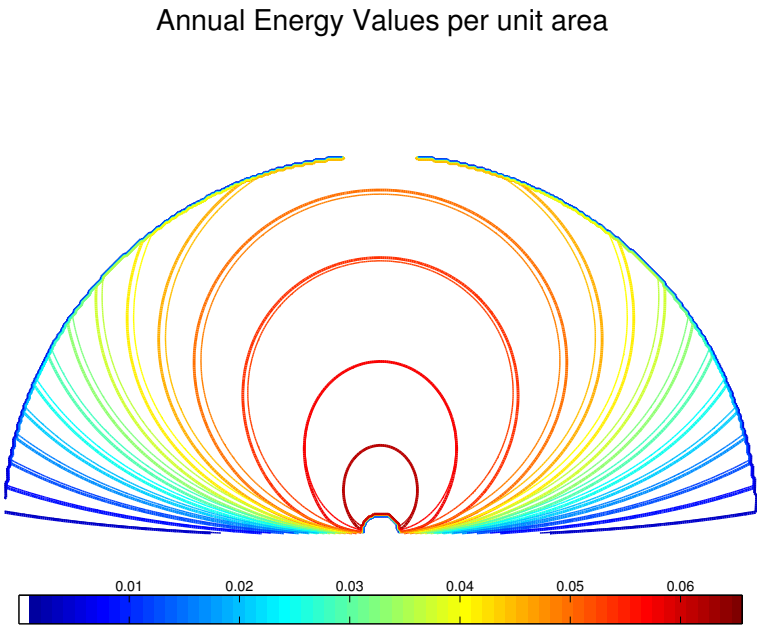

Figure 5.1: Overlapping annual energy per heliostat unit area of small-size (thick lines) and large-size (GWHth/m^2). Outer semicircle has a radius of 9.95 tower heights (1 km).

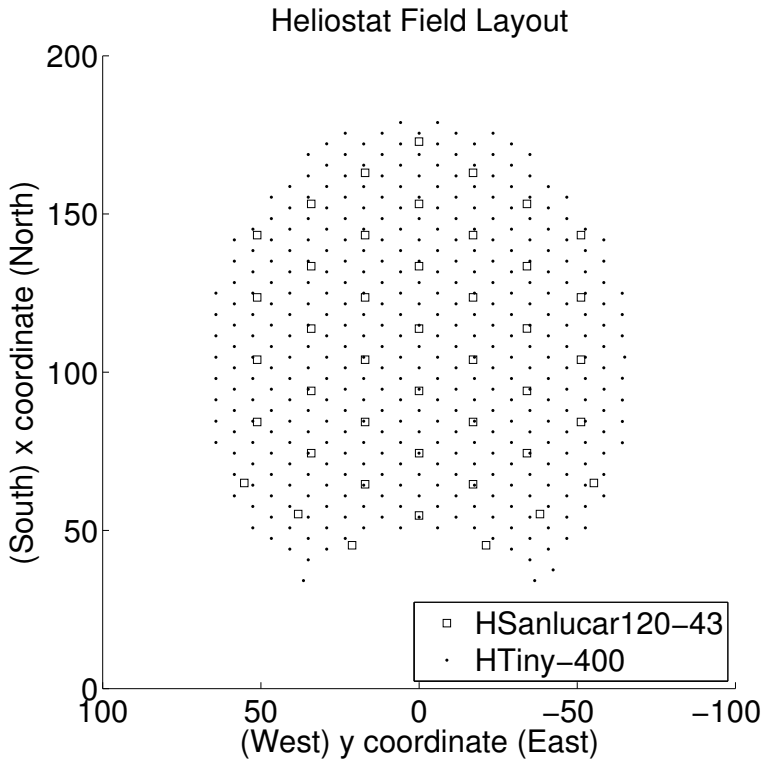

Figure 5.2: Small-size (`HTiny`, 13.21 m^2) vs large-size (`HSanlucar120`, 121.34 m^2)

duce the shading and blocking effects caused by large-size heliostats over the smaller ones. Including pedestal heights as optimization variables and the aiming strategy are interesting problems that need to be studied in the future.

The set $\mathcal{D}$ of all the possible heliostats dimensions is assumed to be given and to consist of two different sizes. From now on Z will denote the collections of coordinates of the centres and sizes of the heliostats, namely (x, y, w). The set Z is described as follows, where N denotes the total number of heliostats, $\mathcal{S}$ denotes the set of heliostats coordinates and $\mathcal{D}$ the set of heliostat sizes:

$$Z = \{(x_i, y_i, w_i) \text{ for } i \in [1, N] \text{ with } (x_i, y_i) \in \mathcal{S} \text{ and } w_i \in \mathcal{D}\} \ .$$

For simplicity, it is assumed that the tower and receiver dimensions are given, see Chapter 2 to include the in the optimization and address the full optimization problem.

5.1.2 Functions

The cost function C defined in Eq.(1.9) can be rewritten as follows:

$$C(\Theta, Z) = K(\Theta) + c_{\mathtt{f}} + \Psi(Z)\,, \tag{5.1}$$

where the function K groups all the terms related to the tower-receiver system (which are fixed along this chapter), $c_{\mathtt{f}}$ is a constant which represents the cost associated with the land (purchasing and preparing), and function Ψ involves all the costs related to the heliostat field.

The annual energy input function E is obtained as explained in Chapter 1, taking into account in the calculations that each heliostat could have a different size. Therefore, the energy function has been adapted in order to be capable to assess the different heliostat sizes properly, and in particular the shading and blocking effects.

5.1.3 Optimization Problem

The optimization problem addressed can be written as follows, where the LCOE function is considered as objective function and denoted by F:

$$(\mathcal{P}) \begin{cases} \min\limits_{Z} & F(\Theta, Z) = C(\Theta, Z)/E(\Theta, Z) & \\ \text{subject to} & Z \subset \Omega \times \mathcal{D} & \\ & ||(x, y) - (x', y')|| \geq \delta(w) + \delta(w') & \text{for } (x, y, w), (x', y', w') \in Z \\ & & (x, y) \neq (x', y') \\ & \Pi_{T_{\mathtt{d}}}(\Theta, Z) \geq \Pi_0\,. & \end{cases} \tag{5.2}$$

An additional power requirement at the design point is considered as explained in

Section 1.2.4. As usual, the heliostats located in the field have to rotate freely avoiding collisions with other heliostats. Note that in this approach the security distance function δ defined in Eq.(1.6) depends on the heliostat size, that is:

$$\delta(w) + \delta(w') = d_w/2 + d_{w'}/2 + d_{\mathtt{s}}\,, \tag{5.3}$$

where d denotes the heliostat diagonal, which depends on each heliostat size w, and $d_{\mathtt{s}}$ is a positive constant, called safe distance and related to installation errors and heliostat accessibility, which remains equal for all the heliostat sizes.

Some of the heliostat efficiency functions are dependent on the heliostat area (interception efficiency, see Eq.(1.21)) or its position in the field (atmospheric efficiency, see Eq.(1.19)). Hence the heliostats annual energy per unit area values are different depending on their size and position, as can be seen in Figure 5.1.

5.2 Field optimization

The goal is to solve problem ($\mathcal{P}$), that is to design a field of heliostats when different heliostat sizes are involved. The proposed procedure, called *Expansion-Contraction Algorithm*, starts with a large-size heliostat field and complements it by inserting small-size heliostats. Large-size heliostat will be located first because, as already explained, they reach a higher performance in the most favourable region.

As initial step the algorithm generates a large-size heliostat field following the *Greedy Algorithm* explained in Chapter 2. Following this algorithm large-size heliostats will be located at the best positions taking advantage of the most favourable region near the tower. Then two phases, *Expansion* and *Contraction*, are applied into this initial field and repeated up to the maximum number of iterations. At the *Expansion Phase*, small-size heliostats are inserted with the *Greedy Algorithm*. At the *Contraction Phase* the best heliostats are selected according to their LCOE per unit area values and the worst are sequentially deleted. The *Expansion-Contraction Algorithm* is explained in detail in the next section.

5.2.1 Expansion-Contraction Algorithm

The *Expansion-Contraction Algorithm* starts with a feasible large-size heliostat field that reaches the power input constraint and then makes a series of *Expansion-Contraction* steps.

The *Expansion Phase* consists of oversizing the large-size field using small-size heliostats until a certain power input value Π_0^+, greater than Π_0, is reached. The small-size heliostats are located one by one following the *Greedy Algorithm*, recalculating the shading and blocking effects at each step. Small-size heliostats are expected to fill-in possible

holes between the large-size heliostats already located due to their smaller area. Moreover, they are also expected to reach higher energy per unit area values in lateral regions than large-size heliostats, see Figure 5.1.

Once the oversized multi-size-heliostat field is obtained, the heliostats are arranged according to their LCOE per unit area values. At the *Contraction Phase* the heliostats reaching worst values are (sequentially) deleted and the number of selected heliostats is given by the power input constraint Π_0. This phase has to follow a sequential procedure because once a heliostat is deleted, the shading and blocking effects over its neighbours changed and thus, their values have to be recalculated and the heliostats sorted again. This process can be done selecting carefully the active neighbours in order to avoid the recalculation of the annual energy of the whole field reducing the computational time. These procedures, oversizing and selection, are well-known in the field layout problem, as they are used with some fixed-pattern strategies to obtain the final number of heliostats, see [28, 65, 75, 111].

The *Expansion-Contraction Algorithm* is described in Algorithm 7. As initial data the power values Π_0 and Π_0^+ are required. At the initial step the field Z^0 is designed using *Greedy Algorithm* reaching the power value Π_0. The LCOE value at each step is denoted by F_k, and during the process the best field layout obtained and the objective value are stored in Υ_{field} and Υ_{obj} respectively. Z_+^k, respectively Z_-^k, denotes the fields obtained at each *Expansion*, resp. *Contraction*, phase at step k. The algorithm continues up to the maximum number of iterations $k_{\texttt{max}}$ or when no improvement is found, and returns as solution the best field obtained Υ_{field}.

5.3 Results

The *Expansion-Contraction* algorithm described in Section 5.2.1 has been implemented in Matlab©, using the `fmincon` routine to solve the involved local optimization sub-problems. The power input required at the design point Π_0 is set to 45.03 MWth and the maximum number of iterations is set to 14 iterations, that is $k_{\texttt{max}} = 14$. The specific values for the tower-receiver and site parameters are shown in Table 5.1. Two different examples have been considered in which the heliostat cost function, the safe distance, the aspect ratio and the sizes have been modified. The results obtained applying the proposed algorithm to both examples are detailed in the following sections.

5.3.1 First example

Two different heliostat sizes are going to be considered, called small-size and large-size. From now on, large-size heliostats will be the usual heliostats used in the literature with this tower-receiver configuration ($121.34\,m^2$, called `HSanlucar120`), much bigger than small-size heliostats, selected by the author for experimental studies ($4.35\,m^2$,

Algorithm 7 `Expansion-Contraction algorithm`

Require: Θ, Π_0 and Π_0^+

$\boxed{Z^0} \leftarrow \begin{cases} \text{Create initial field using large-size heliostats with } \textit{Greedy Algorithm.} \\ \text{Stop when } \Pi_0 \text{ is reached.} \end{cases}$

$F^0 \leftarrow F(\Theta, Z)$

$\Upsilon_{obj} \leftarrow F^0$

$\Upsilon_{field} \leftarrow Z^0$

$stop \leftarrow 0$

$k \leftarrow 0$

while $k \leq k_{\texttt{max}}$ & $stop = 0$ **do**

Expansion Phase:

$\boxed{Z_+^k} \leftarrow \begin{cases} \text{Oversize } Z^k \text{ using small-size heliostats with } \textit{Greedy Algorithm.} \\ \text{Stop when } \Pi_0^+ \text{ is reached.} \end{cases}$

Contraction Phase:

$\boxed{Z_-^k} \leftarrow \begin{cases} \text{Sort } Z_+^k \text{ according to: LCOE per unit area.} \\ \text{Select the best heliostats until } \Pi_0 \text{ is reached.} \end{cases}$

Update:

$k \leftarrow k + 1$

$F^k \leftarrow F(\Theta, Z_-^k)$

$Z^k \leftarrow Z_-^k$

if $F^k \geq \Upsilon_{obj}$ **then**

$\Upsilon_{obj} \leftarrow F^k$

$\Upsilon_{field} \leftarrow Z^k$

else

$stop \leftarrow 1$

end if

end while

return $\boxed{\Upsilon_{field}}$

Parameter	*Default value*	*Reference*
Location and Time		
Emplacement	Sanlúcar la Mayor (Seville)	[76]
Latitude	$37^o26'$ N	[75]
Longitude	$6^o15'$ W	[75]
Design Point $T_{\mathtt{d}}$	March 21st 12h	assumed
Design direct normal irradiation DNI	823.9 W/m^2	assumed
DNI model	cloudless skies	assumed
Tower and Receiver		
Tower optical height h	100.50 m	[75]
Aperture radius r_a	6.39 m	assumed
Aperture slope ξ	12.5	[75]
Minimum radius of the field	50 m	assumed
Receiver Technology	Saturated Steam	[76]
Thermal receiver minimal power input at $T_{\mathtt{d}}$	45.0334 MWth	assumed
Field		
Slope	0^o	assumed
Feasible region shape	annulus	assumed
Maximum size	156.68 ha	assumed

Table 5.1: Parameter values

called `HSmaller`). In this section, the safe distance considered is 1.70 m, the heliostat sizes considered have a different aspect ratio (see Table 5.2), and the heliostat cost function considered is detailed as follows.

$$\Psi(Z) = \sum_{w \in \mathcal{D}} c_w N_w \,, \tag{5.4}$$

where the number of heliostats of each size is denoted by N_w and c_w denotes the cost per heliostat of size w. All costs associated with the heliostats (mirror modules, support structure, drives, pedestal, foundation, field wiring, etc.) are included in c_w and for simplicity they are suppose to be independent on the heliostat position.

The value for the upper limit Π_0^+ is set to 49.51 MWth (an increase of 10% on Π_0). In order to compare the obtained results, a reference field layout called **PS10** achieving Π_0 is used, similar to a solar commercial plant located in Seville, see Figure 5.3(a). The initial field Z^0, see Figure 5.8(a), is obtained with the *Greedy Algorithm* considering the power requirements Π_0. Note that any heliostat field could be used in its place, multi-size or single-size field. As detailed in Figure 5.1 and Table 5.1, the feasible region considered has an annulus shape. However, note that in the following examples the heliostats are located by the algorithms automatically at the north area, where higher energy values are reached.

The numerical studies so far show that small heliostat has a smaller cost per unit

Heliostat Parameter		*Large-size*	*Small-size*
Name		`HSanlucar120`	`HSmaller`
Width	$[m]$	12.84	3.21
Height	$[m]$	9.45	1.36
Optical height z_0	$[m]$	5.17	5.17
$\sigma_{optical}$	$[mrad]$	2.9	2.9
Diagonal d_w	$[m]$	15.94	3.48
Safe distance d_s	$[m]$	1.70	1.70
Security distance $\delta(w)$	$[m]$	17.64	5.18
Aspect Ratio (width /height)		1.36	2.36
Total Area A_w	$[m^2]$	121.34	4.35

Table 5.2: Heliostat parameter values

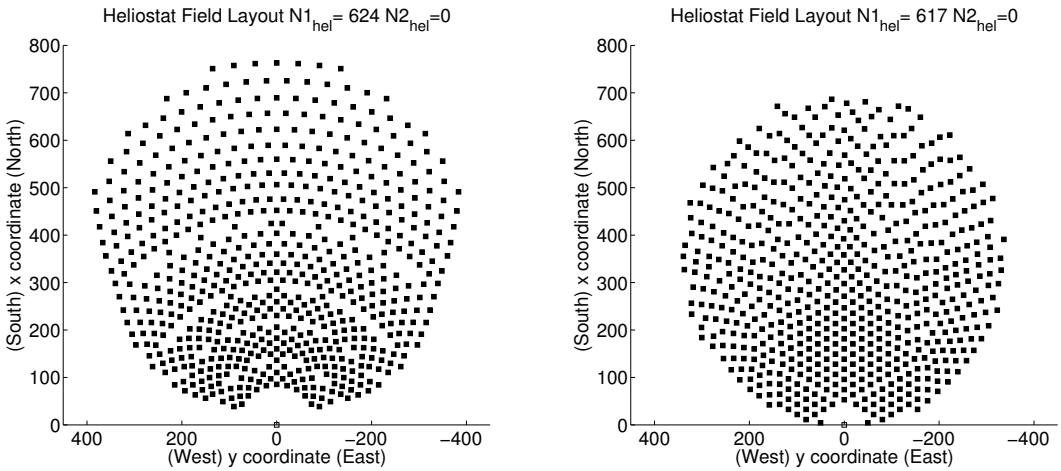

(a) **PS10** (b) Z^0

Figure 5.3: **PS10** and Z^0 (`HSanlucar120`)

area than larger heliostats, see [14, 52]. Therefore, in this section, 2 different costs scenarios are studied, in which the heliostat cost per unit area of small-size being is considered the same as the heliostat cost per unit area of large-size (100%) or the 80% respectively. These scenarios are called Scenario 100% and Scenario 80%. At each scenario, the LCOE function is denoted by F_{100} and F_{80} respectively.

In Figure 5.4 the contraction process of Z^0 is detailed for the two different scenarios. The heliostats highlighted in red are the heliostats selected to be eliminated due to their low LCOE per unit area values. As expected, the number of large-size heliostats deleted increases as the heliostat cost per unit area of small size decrease and different solutions are obtained for each cost scenario.

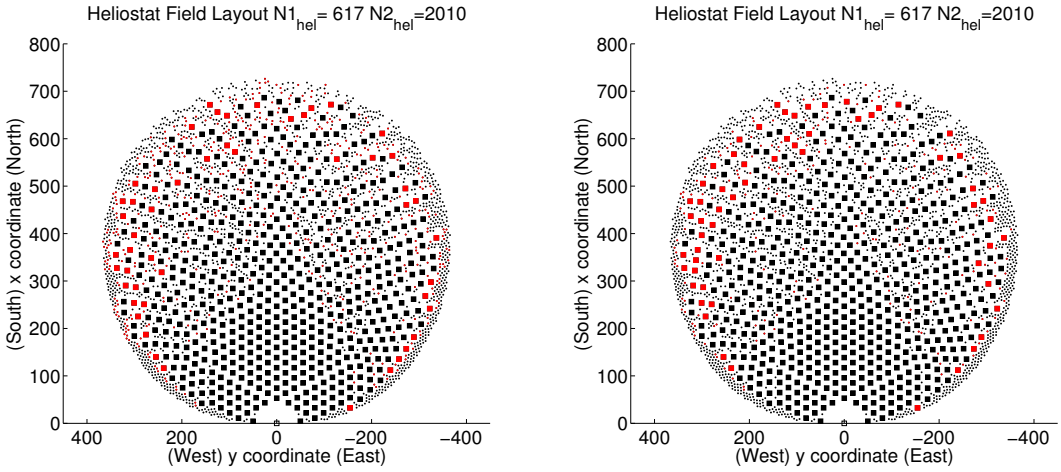

(a) Scenario 100% (b) Scenario 80%

Figure 5.4: Detail of *Expansion-Contraction* phases for Z^0

At each scenario, the algorithm stops when no improvement in the LCOE value is found. The results and final fields obtained using the *Expansion-Contraction Algorithm* for the different scenarios are shown in Figures 5.5-5.6 and Tables 5.3-5.4, where N_{dif} denotes the number of large-size heliostats deleted by the algorithm at each iteration.

The LCOE result obtained at the worst scenario (Scenario 100%, Table 5.3) is similar to the reference plant **PS10** and shows an improvement over Z^0. In this scenario, the best field is obtained with Z^5. In Table 5.4, the results obtained using Scenario 80% show a reduction of approximately 10% on the LCOE of the reference field, and it is achieved with Z^{12}.

Considering the heliostats sizes already detailed and Scenario 80%, a multi-size-heliostat field reaching better LCOE value than the reference field is obtained. Note that, with the same heliostats sizes, if the heliostat cost per unit area of small-size is reduced (for instance applying Scenario 60%), multi-size-heliostat fields does not seem to be advantageous, as, it is preferable to work with single-size-heliostat fields. Moreover,

although in this section we are given such fields as the final output, these fields can be used as input of another procedure. For instance, a pattern-free refinement process, see e.g. [18], can be applied to further improve the objective function and correct the visual irregularities. As can be seen in the resulting fields, there exist some holes (due to final heliostat(s) deleted on the last iteration) and visual irregularities (areas where large-size heliostat have been deleted and small-size heliostat re-positioned).

The numerical experiments show the effects of combining heliostats of different sizes, according to various costs per unit area.

Field	N	N_{small}	N_{large}	N_{dif}	Π_{T_d}	E	F_{100}
PS10	592	0	592	0	45.03	127.4	0.018153
Z^0	617	0	617	0	45.06	126.0	0.018218
Z^1	2077	1509	568	49	45.08	126.6	0.018224
Z^2	3265	2741	524	44	45.07	126.9	0.018184
Z^3	3737	3231	506	18	45.03	127.0	0.018172
Z^4	4005	3509	496	10	45.04	127.0	0.018164
Z^5	4138	3647	491	5	45.04	127.0	0.018159
Z^6	4191	3702	489	2	45.04	127.0	0.018159

Table 5.3: Results Scenario 100%. Π_t (MWth) and E (GWHth)

Field	N	N_{small}	N_{large}	N_{dif}	Π_{T_d}	E	F_{80}
PS10	592	0	592	0	45.03	127.4	0.018153
Z^0	617	0	617	0	45.06	126.0	0.018218
Z^1	2359	1801	558	59	42.56	126.6	0.017976
Z^2	3991	3493	498	68	45.07	127.0	0.017692
Z^3	5670	5233	437	61	45.04	127.3	0.017427
Z^4	7361	6983	378	59	45.08	127.8	0.017191
Z^5	9094	8775	319	59	45.07	128.2	0.016988
Z^6	10822	10560	262	57	45.10	128.7	0.016811
Z^7	12077	11857	220	42	45.04	128.8	0.016701
Z^8	12763	12567	196	24	45.05	128.9	0.016613
Z^9	13201	13020	181	15	45.06	129.0	0.016558
Z^{10}	13358	13183	175	6	45.03	129.0	0.016532
Z^{11}	13455	13283	172	3	45.08	129.2	0.016509
Z^{12}	13439	13322	171	1	45.11	129.3	0.016501
Z^{13}	13526	13357	169	2	45.04	129.1	0.016504

Table 5.4: Results Scenario 80%. Π_t (MWth) and E (GWHth)

5.3.2 Second example

In this section, the value for the upper limit Π_0^+ is set to 46 MWth (an increase of 2.15% on Π_0) and the function Ψ considered (which represents the heliostat cost function) is the following:

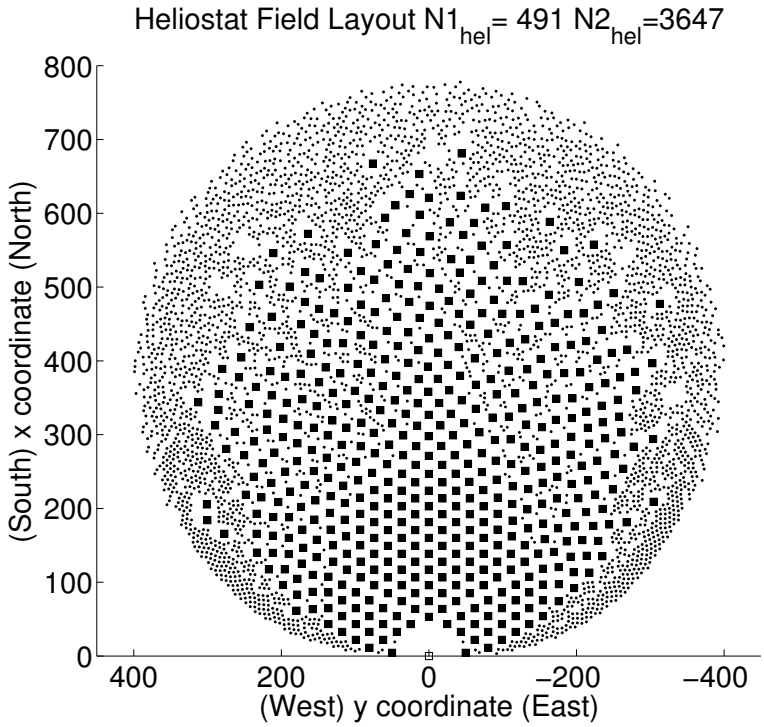

Figure 5.5: Final Field: Z^5 Scenario 100%

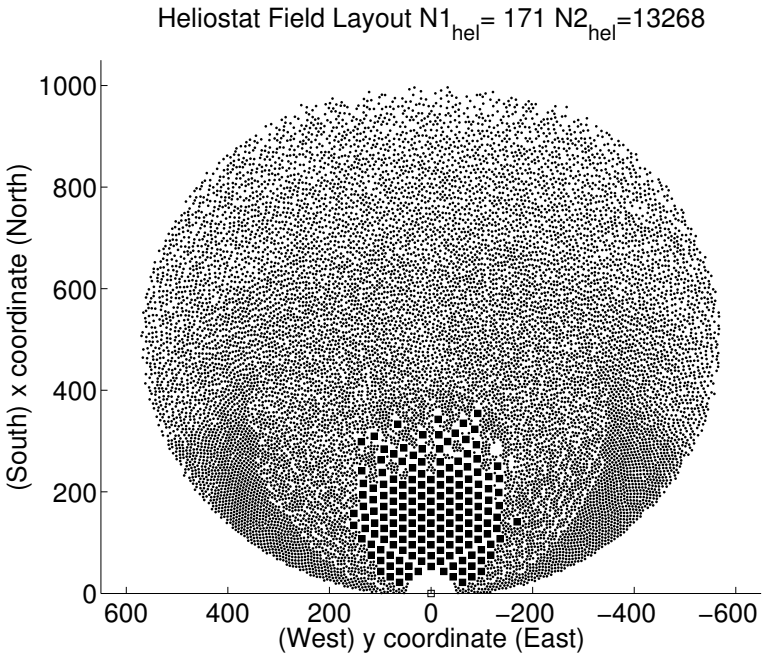

Figure 5.6: Final Fields: Z^{12} Scenario 80%

$$\Psi(Z) = \sum_{w \in \mathcal{D}} c(A_w) N_w \,. \tag{5.5}$$

where N_w represents the number of heliostat of size w and $c(A_w)$ denotes the cost per heliostat, which is a function of the heliostat size. All costs associated with the heliostats are included in c and for simplicity they are supposed to be independent of the heliostat position.

Following the analysis in [14] for uniform wind speed, the heliostat cost function can be written as follows:

$$c(A_w) = c_1(A_w)A_w + c_2(A_w)A_w^{3/2} + c_3(A_w)\,, \tag{5.6}$$

where A_w denotes the are of heliostat size w. The constants c_1, c_2 and c_3 are given values associated with one of the three costs categories considered in [14] and different for each heliostat size. The three categories are: (1) hardware costs (constant per mirror area unit), (2) load-bearing components (dependent on mirror area unit: pedestal, foundation, drive units, etc.), and (3) electronics (independent of mirror area unit: controllers, processors, field wiring costs,etc.).

The reference heliostat costs selected are distributed as detailed in [60] for a reference heliostat area $A_* = 148\ m^2$ which cost per unit area is set to $167.49\,\$/m^2$. The values associated with each cost category are: $v_1 = 39.24\,\$/m^2$, $v_2 = 117.94\,\$/m^2$ and $v_3 = 10.31\,\$/m^2$, where $B(A_*) = (v_1 + v_2 + v_3)A_*$. That is, the three cost categories, Category 1, Category 2 and Category 3 are distributed with the 23.4%, 70.4% and 6.2% respectively.

Given any heliostat area A, it can be expressed in terms of the reference area and the heliostat cost function can be easily written as:

$$B(A) = c(A)\,A\,, \text{ with } c(A) = v_1 + v_2\sqrt{A/A_*} + v_3 A_*/A\,. \tag{5.7}$$

As detailed in [14], the optimum area (for the minimum cost per unit area), can be calculated as follows:

$$A_{min} = (2v_3/v_2)^{2/3}\ A_*\,. \tag{5.8}$$

In this section, the large-size heliostat `HSanlucar120` is considered again and the heliostat cost per unit area value is 158.61 $\$/m^2$ accordingly to Eq.(5.7). A small-size heliostat, called `HSmall` and having the same cost per unit area (area 20.10 m^2), is considered. The optimum area given by Eq.(5.8) corresponds with 46.28 m^2, and the corresponding small-size heliostat is called as `HMin`. Finally, a smaller heliostat (13.21 m^2) is chosen, having a higher cost per unit area (190 $\$/m^2$), called `HTiny`.

Three small-size heliostats are going to be considered in this example, called `Hmin`,

`HSmall`, and `HTiny` with parameter values given in Table 5.5. The heliostat cost per unit area function is detailed in Figure 5.7, where: `HTiny` corresponds with the blue circle, `HSmall` with the black circle, `HMin` with the green circle and `HSanlucar120` with the black square. The black diamond corresponds with the reference area A_* and its corresponding cost.

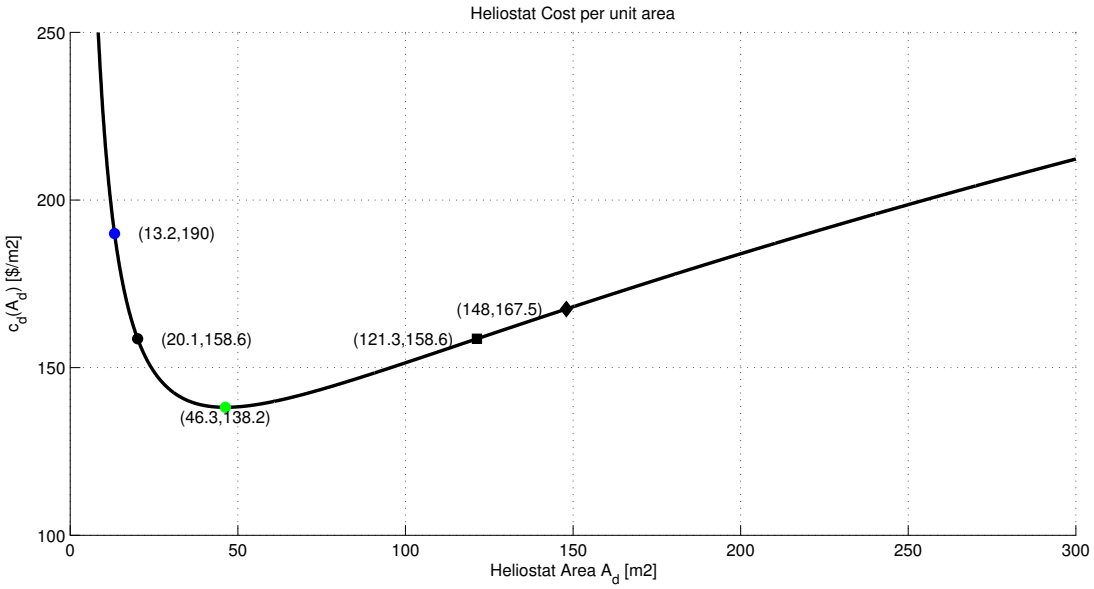

Figure 5.7: Detail of function $c(w)$

The presented algorithm is applied for the pairs `HSanlucar120-Hmin`, `HSanlucar120-HSmall` and `HSanlucar120-HTiny`, yielding for each scenario the optimal field with a different mix of large-size, small-size heliostats. Note that in this example, all the heliostat sizes will have the same elevation axis height, safe distance value and aspect ratio (in order to make a fair comparison).

In order to compare the obtained results the reference plant **PS10** is used again. The initial field Z^0, see Figure 5.8(a), is obtained with the *Greedy Algorithm* considering the power requirements Π_0. The study of the different scenarios where the different combinations are selected is detailed in Tables 5.6-5.7. The algorithm stops when no improvement in the LCOE value is found or the maximum number of iterations is reached.

At the first phase of the Expansion-Contraction Algorithm it can be observed that with scenarios `HSanlucar120-HTiny` and `HSanlucar120-HSmall`, the large-size heliostats prevail and no small-size heliostats are selected due to their higher cost per unit area, giving as result the field Z^1 that is the field **GHSan** shown in Figure 5.8(a). The algorithm stops at this step due to the stopping criteria (no improvement found in the LCOE value of the field).

The operation of the Expansion-Contraction algorithm is detailed in Table 5.7 for

Heliostat Parameter		*Large-size*	*Small-size*		
Name		`HSanlucar120`	`HMin`	`HSmall`	`HTiny`
Width	$[m]$	12.84	7.93	5.23	4.24
Height	$[m]$	9.45	5.84	3.85	3.12
Optical height z_0	$[m]$	5.17	5.17	5.17	5.17
$\sigma_{optical}$	$[mrad]$	2.9	2.9	2.9	2.9
Diagonal d_w	$[m]$	15.94	9.85	6.49	5.26
Safe distance $d_{\mathtt{s}}$	$[m]$	0.30	0.30	0.30	0.30
Security distance $\delta(w)$	$[m]$	16.24	10.15	6.79	5.56
Aspect Ratio (width /height)		1.36	1.36	1.36	1.36
Total Area A_w	$[m^2]$	121.34	46.28	20.10	13.21
Relative Area		1	0.381	0.166	0.109
Cost per unit area $c(A_w)$	$[\$/m^2]$	158.61	138.16	158.61	190
Relative Cost per unit area		1	0.882	1	1.198

Table 5.5: Heliostats parameter values

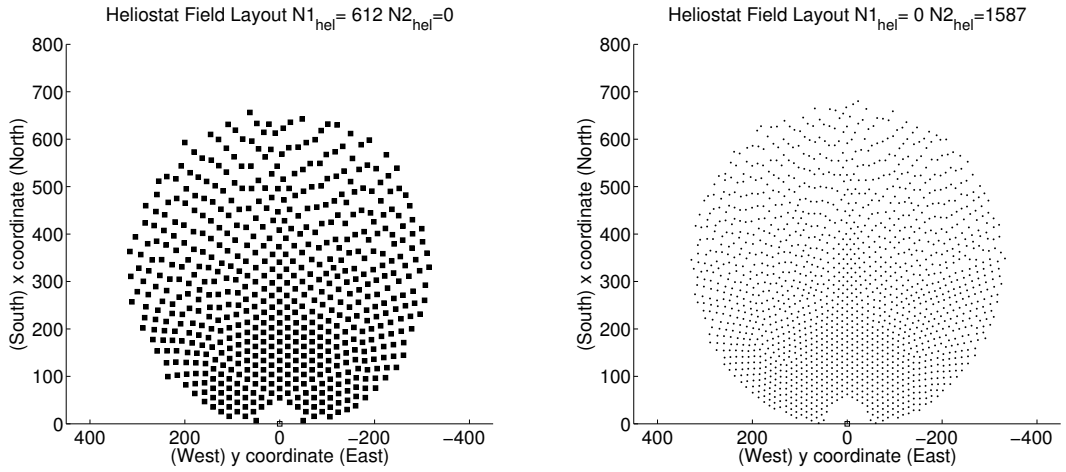

(a) **GHSan** (b) **GHMin**

Figure 5.8: **GHSan** and **GHMin** fields

Scenario `HSanlucar120-HMin`. At this scenario the algorithm reaches at the last iteration of the algorithm better LCOE values, considering both heliostat sizes, than the reference plant **PS10**. $Z^{10} - R$ is the result from refining the last iteration relocating the small-size heliostats. However, although the heliostat location in the field $Z^{10} - R$ is more compact, the objective value gets worse due to the shading and blocking effects.

When considering scenario `HSanlucar120-HMin`, small-size heliostas prevail reaching better LCOE values than the initial field **GHSan** and the reference field **PS10** selected, see Figure 5.8(b).

Size(s)	Field	N	N_{large}	N_{small}	Π_{T_d}	E	F
`HSanlucar120`	**PS10**	624	624	0	45.03	127.4	0.016555
`HSanlucar120`	**GHSan**	612	612	0	45.04	123.7	0.016834
`HMin`	**GHMin**	1587	0	1587	45.05	124.2	0.015275
`HSanlucar120-HTiny`	Z^1	612	612	0	45.04	123.7	0.016834
`HSanlucar120-HSmall`	Z^1	612	612	0	45.04	123.7	0.016834
`HSanlucar120-HMin`	Z^{14}	907	429	478	45.03	124.2	0.016350

Table 5.6: Results final fields. Π_t (MWth), E (GWHth) and C (M€)

Field	N	N_{large}	N_{small}	Π_{T_d}	E	C/E
Z^1	615	610	5	45.04	123.7	0.016832
Z^2	637	596	41	45.26	131.6	0.016803
Z^3	659	582	77	45.05	123.5	0.016796
Z^4	681	568	113	45.04	123.3	0.016778
Z^5	703	554	149	45.03	123.3	0.016742
Z^6	726	540	186	45.05	123.5	0.01669
Z^7	748	526	222	45.03	123.6	0.016637
Z^8	771	512	259	45.04	123.7	0.016589
Z^9	794	498	296	45.04	123.8	0.016547
Z^{10}	817	485	332	45.09	124.1	0.016496
Z^{11}	838	471	367	45.04	124	0.016465
Z^{12}	861	457	404	45.04	124.0	0.016429
Z^{13}	884	443	441	45.03	124.1	0.016389
Z^{14}	907	429	478	45.03	124.2	0.016350
$Z^{14} - R$	907	429	478	45.1	123.8	0.016401

Table 5.7: Results scenario `HSanlucar120-HMin`. Π_t (MWth), E (GWHth) and C (M€)

All the LCOE results obtained show an improvement over the initial field **GHSan** value. The result Z^{14} obtained with scenario `HSanlucar-HMin` achieves an improvement over the reference field **PS10**. However, the best LCOE value is reached with the single-size-heliostat field calculated with the optimum heliostat area, `HMin`. This field (Figure 5.8(b)) for which the cost/m^2 of heliostat is 82% of `HSanlucar120` shows a reduction of approximately 8.51% on the LCOE of the reference field **PS10**.

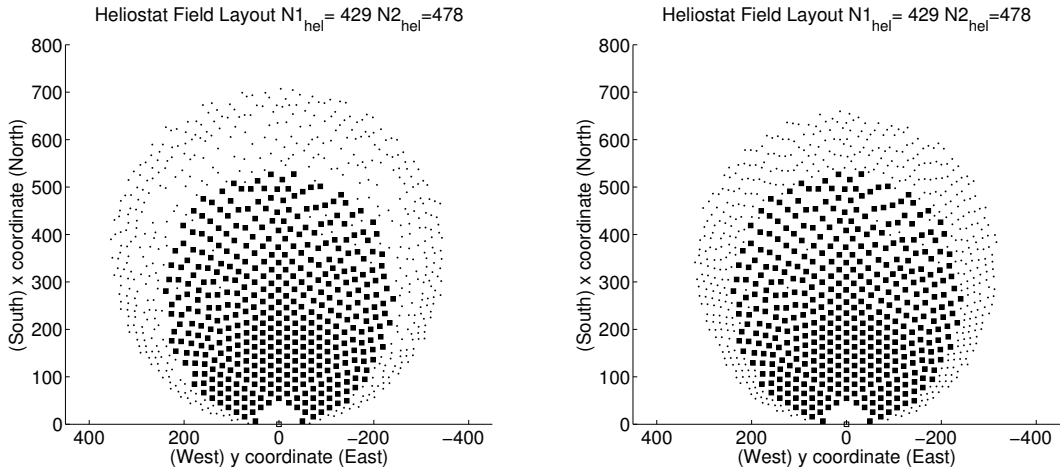

(a) Z^{14} (b) $Z^{14} - R$

Figure 5.9: Final fields for scenario `HSanlucar120-HMin`

In all scenarios, as detailed in Table 5.6, combining both heliostats sizes is not useful, better values are reached with the corresponding single-size-heliostat fields. Therefore, multi-size-heliostat fields does not seem to be advantageous with the examples considered in this section, as, it is preferable to work with single-size-heliostat fields.

5.4 Conclusions

An algorithm for optimizing a multi-size-heliostat field has been proposed, in which both the location and the size of the heliostats are simultaneously considered. The algorithm proposed tends to locate large-size heliostats in the most efficient regions of the field, and small-size heliostats, in the borders and to fill-in the holes between large sizes heliostats when advantageous. If the smaller heliostats are also lower cost/m^2 the tend to replace all the larger, more expensive ones. Using the *Expansion-Contraction Algorithm*, a detailed comparative study is performed, taking into account different heliostats sizes, showing the usefulness of multi-sized-heliostat or single-size-heliostat fields at each scenario.

Using the proposed algorithm, a detailed comparative study can be performed, taking into account the different heliostats sizes (heliostat height or width, aspect ratio, cost per unit area, etc.) available at the time of building an SPT system, although same pedestal height.

Following the idea of the procedure presented in this chapter, heliostat fields with more than two heliostat sizes could also be calculated.

Chapter 6

Conclusions and further work

This dissertation deals with an optimization problem coming from the solar industry: the design of SPT plants and, more precisely, the tower-receiver and heliostat field design. This is a large-scale optimization problem with non-convex constraints and a non-convex objective function involving a computationally expensive evaluation. Due to the complexity of the problem, the exact solution is unknown and exact optimization approaches are not available. Along the previous chapters, appropriate heuristic algorithms have been presented.

A greedy-based heuristic algorithm has been proposed to design the heliostat field. This differs from the usual methods found in the literature so far in several points:

- First, the organization of the heliostat field is not forced to follow a specific geometrical pattern; instead, it obeys a pattern-free optimization strategy.

- On the other hand, an initial oversized field is not needed, since the final amount of heliostats is found during the optimization process.

The flexibility of the proposed algorithm is a key feature. Accordingly, it can be adapted and combined with different optimization procedures. This way, it can be used to solve the problems proposed in the previous chapters (for instance, it leads to the design of a heliostat field with triangular pods and/or multiple receivers).

The fields obtained with the pattern-free strategies here presented are less regular than the traditional pattern-based fields. However, new cleaning and maintenance strategies can be used for fields of this kind (see [3]) and, if necessary, road access can be directly included without essentially modifying the algorithm.

The proposed greedy algorithm might be improved by adding more sophisticated techniques at each iteration, for instance in the selection at each step in the new solution. In the GRASP procedure, see [87, 114], randomness is incorporated to this selection. Furthermore, the proposed strategy can be considered to obtain an initial field for

other algorithms (such as the one in [20]) and can be extended to address many other situations (some of them are briefly described below).

Several extensions of the work carried out in Chapter 3 are possible, in some cases, with not much effort. For instance, combining the triangular pods with the multiple-receivers systems.

Throughout Chapter 4, independent power threshold levels have been considered for the different receivers, each measured at one (common) design point. It is straightforward to extend the proposed method to the case in which overall power threshold levels, or multiple design points are considered. The computation of the optimal number of receivers and their related variables is another possible extension.

As it has been mentioned along this dissertation, one of the major issues of developing heuristic techniques to successfully solve the proposed problems is the high computing time needed to evaluate one of the optimization criteria considered (annual thermal energy). The need to develop new codes to simulate and evaluate the SPT system accurately in a short time has been detected and new codes have been under development during the last years, see for instance [44, 50, 88]. Note that in [50, 84], fast and accurate algorithms are studied to compute the shadowing and blocking effects without the parallelism simplifications that have been mentioned above.

The selected optimization criteria, the LCOE of the system, is an aggregation of the two involved criteria, the investment cost and the annual thermal energy function. Because of the high computational time needed to evaluate the annual thermal energy function, in this dissertation this multi-objective optimization problem is addressed as a mono-objective problem.

However, addressing the problem with multi-objective optimization techniques permits to approximate the efficient frontier for the bi-objective problem; see [88, 103], where a promising first approach is proposed. This way different configurations will be given to the users, which can study the different options. Since the optimization of the SPT can be performed for different purposes, in a early stage of a solar project, this possibility can facilitate and speed up the design process.

In this dissertation, all the receivers have been considered to be located at the same (unique) tower. Multi-towers configurations are an interesting innovation in SPT systems, see [4, 96]. In a multi-tower problem, several towers are placed in the same region and both the optimal tower/heliostat characteristics and the aiming strategies have to be determined. This leads to a very interesting and complex optimization problem. This may be addressed with a suitable adapted version of the methods presented here.

Also, taking into account the effect of the tower shading over the field is an additional improvement to be done. In practice, this plays and important role in the design of multi-tower systems.

The aiming strategy has been considered fixed all along this dissertation. Heliostats

have been assumed to be always aiming the aperture centre. This assumption, although usual when addressing the heliostat field design, implies unrealistic situations in the operating phase.

In this dissertation, a homogeneous flux distribution has been assumed, see [19]. However, differences in flux density will occur over the absorber area and the distribution will also vary during the day and the seasons. An appropriate control is required to adapt the mass flow in the absorber to the solar distribution because a uniform heat flux distribution is required.

The design of an appropriate aiming strategy yields a continuous non-linear constrained optimization problem of very large dimensions which deserves further analysis, see for instance [53, 86]. This problem is usually considered as an independent problem from the heliostat field design; see for instance [10] where the ant colony optimization meta-heuristic is applied to solve this problem. However, when addressing the multiple-receivers or multi-tower design problem, the aiming strategy selected to operate the plant is highly connected with the optimal design.

Note that the SPT site location problem is not considered in the proposed approach, although it is an important and interesting problem, see [74, 113]. Site humidity, dust particles, clouds and legal regulations (among others) will affect the selected location and will strongly modify the optimization criteria behaviour.

The heliostat field design in regions with ground irregularities is also a very interesting problem. In this case, one possible approach is to include the heliostat height as an optimization variable. This upgrade can be also used to solve the multi-size-heliostat field problem allowing heliostats to have different pedestal heights.

Thermal energy storage systems and their operation have been studied recently for improving the system performance and self-sufficiency, see [45, 101]. In [90], the idea of subdivided solar field used, in Chapter 4, is applied to a storage system with solar power systems based on parabolic trough collector. A similar concept could be applied using SPT technology.

Finally, another interesting problem is to take into consideration variable (stochastic) meteorological data, see [81].

References

[1] G. Abal and V. Duranona. *Manual Técnico de Energía Solar Térmica. Volumen I: Fundamentos.* Facultad de Ingeniería, Universidad de la República Uruguay, 2013.

[2] U.S. Energy Information Administration. Levelized Cost and Levelized Avoided Cost of New Generation Resources in the Annual Energy Outlook 2015. Technical report, EIA, 2015. http://www.eia.gov/forecasts/aeo/electricity_generation.cfm.

[3] L. Alon, G. Ravikovich, M. Mandelbrod, U. Eilat, Z. Schop, and D. Tamari. Computer-based management of mirror-washing in utility-scale solar thermal plants. In *Proceedings of ASME 2014 (8th International Conference on Energy Sustainability and 12th International Conference on Fuel Cell Science, Engineering and Technology)*, volume 1, July 2014.

[4] G. Augsburger. *Thermo-economic optimisation of large solar tower power plants.* PhD thesis, École Polytechnique Fédérale de Lausanne, 2013.

[5] G. Ausiello, P. Crescenzi, G. Gambosi, V. Kann, A. Marchetti-Spaccamela, and M. Protasi. *Complexity and Approximation.* Springer, Berlin, 1999.

[6] A. L. Avila-Marin, J. Fernandez-Reche, and F. M. Tellez. Evaluation of the potential of central receiver solar power plants: Configuration, optimization and trends. *Applied Energy*, 112:274–288, 2013.

[7] J. Bang-Jensen, G. Gutin, and A. Yeo. When the greedy algorithm fails. *Discrete Optimization*, 1:121–127, 2004.

[8] M. S. Bazaraa, H. D. Sherali, and C. M. Shetty. *Nonlinear Programming: Theory and Algorithms.* John Wiley and Sons, Hoboken, New Jersey, 2006.

[9] O. Behar, A. Khellaf, and K. Mohammedi. A review of studies on central receiver solar thermal power plants. *Renewable and Sustainable Energy Reviews*, 23:12–39, 2013.

[10] B. Belhomme, R. Pitz-Paal, and P. Schwarzbözl. Optimization of heliostat aim point selection for central receiver systems based on the ant colony optimization metaheuristic. *Journal of Solar Energy Engineering*, 136(011005):(7 Pages), 2014.

[11] R. Ben-Zvi, M. Epstein, and A. Segal. Simulation of an integrated steam generator for solar tower. *Solar Energy*, 86:578–592, 2012.

[12] S. M. Besarati, D. Y. Goswami, and E. K. Stefanakos. Optimal heliostat aiming strategy for uniform distribution of heat flux on the receiver of a solar power tower plant. *Energy Conversion and Management*, 84:234–243, 2014.

[13] F. Biggs and C.N. Vittitoe. The HELIOS model for the optical behavior of reflecting solar concentrators. Technical Report SAND76–0347, Sandia National Labs., 1976. http://prod.sandia.gov/techlib/access-control.cgi/1976/760347.pdf.

[14] J. B. Blackmon. Parametric determination of heliostat minimum cost per unit area. *Solar Energy*, 97:342–349, 2013.

[15] A. Boubault, C. K. Ho, A. Hall, T. N. Lambert, and A. Ambrosini. Levelized cost of energy (lcoe) metric to characterize solar absorber coatings for the csp industry. *Renewable Energy*, 85:472–483, 2015.

[16] B. Braden. The surveyor's area formula. *The College Mathematics Journal*, 17(4):326–337, 1986.

[17] J. G. Broze, S. Ranade, and H. W. Prengle. An approximate model for sizing and costing a solar thermal collector-central receiver system. *Solar Energy*, 34:341–350, 1985.

[18] R. Buck. Heliostat field layout improvement by nonrestricted refinement. *Journal of Solar Energy Engineering*, 136(021014):(6 Pages), 2014.

[19] R. Buck, C. Barth, M. Eck, and W. Steinmann. Dual receiver concept for solar tower. *Solar Energy*, 80:1249–1254, 2006.

[20] R. Buck, A. Pfahl, and T. H. Roos. Target aligned heliostat field layout for non-linear flat terrain. In *Proceedings of the First Southern African Solar Energy Conference (SASEC2012)*, 2012.

[21] J. I. Burgaleta, S. Arias, and D. Ramirez. GEMASOLAR, the first tower thermosolar commercial plant with molten salt storage. In *Proceedings of SolarPaces 2011*, 2011.

[22] E. Carrizosa, C. Domínguez-Bravo, E. Fernández-Cara, and M. Quero. An optimization approach to the design of multi-size-heliostat fields. Technical report, IMUS, 2014. www.optimization-online.org/DB_HTML/2014/05/4372.html.

[23] E. Carrizosa, C. Domínguez-Bravo, E. Fernández-Cara, and M. Quero. A heuristic method for simultaneous tower and pattern-free field optimization on solar power systems. *Computers & Operations Research*, 57:109–122, 2015.

[24] E. Carrizosa, C. Domínguez-Bravo, E. Fernández-Cara, and M. Quero. Optimization of multiple receivers solar power tower systems. *Energy*, 90:2085–2093, 2015.

[25] K. Chen, N. X. Song, Z. Y. He, and X. Zhang. Wind turbine positioning optimization of wind farm using greedy algorithm. *Journal of Renewable and Sustainable Energy*, 5(023128):(15 Pages), 2013.

[26] F. J. Collado. Quick evaluation of the annual heliostat field efficiency. *Solar Energy*, 82(4):379–384, 2008.

[27] F. J. Collado. Preliminary design of surrounding heliostat fields. *Renewable Energy*, 34(5):1359–1363, 2009.

[28] F. J. Collado and J. Guallar. Campo: Generation of regular heliostat fields. *Renewable Energy*, 46:49–59, 2012.

[29] F. J. Collado and J. Guallar. A review of optimized design layouts for solar power tower plants with campo code. *Renewable and Sustainable Energy Reviews*, 20:142–154, 2013.

[30] F. J. Collado and J.A. Turégano. An analytic function for the flux density due to sunlight reflected from a heliostat. *Solar Energy*, 37:215–234, 1986.

[31] F. J. Collado and J.A. Turégano. Calculation of the annual thermal energy supplied by a defined heliostat field. *Solar Energy*, 42:149–165, 1989.

[32] J-F. Cordeau, M. Gendreau, G. Laporte, J-Y. Potvin, and F. Semet. A guide to vehicle routing heuristics. *The Journal of the Operational Research Socitey*, 53:512–522, 2002.

[33] L. Crespo and F. Ramos. NSPOC: A New Powerful Tool for Heliostat Field Layout and Receiver Geometry Optimizations. In *Proceedings of SolarPaces 2009*, 2009.

[34] L. Crespo, F. Ramos, and F. Martínez. Questions and answers on solar central receiver plant design by NSPOC. In *Proceedings of SolarPaces 2011*, 2011.

[35] A. Danielli, Y. Yatir, and O. Mor. Improving the optical efficiency of a concentrated solar power field using a concatenated micro-tower configuration. *Solar Energy*, 85:931–937, 2011.

[36] K. Deb, F. Ruiz, M. Luque, R. Tewari, J. M. Cabello, and J. M. Cejudo. On the sizing of solar thermal electricity plant for multiple objectives using evolutionary optimization. *Applied Soft Computing*, 12(10):3300–3311, 2012.

[37] C. Domínguez-Bravo. Problemas de optimización global en el diseño de plantas solares con tecnología de torre. Master's thesis, Facultad de Matemáticas. Universidad de Sevilla, 2012.

[38] C. Domínguez-Bravo, B. Sebastian-James, G. Heiming, P. Richter, E. Carrizosa, E. Fernández-Cara, M. Frank, and P. Gauché. Field-design optimization with triangular heliostat pods. In *Proceedings of SolarPaces 2015*, 2015.

[39] U. Facchini, G. Sassi, F. Parrini, and A. Longhetto. Determination of the interference between the elements of a Central-Receiver Solar System. *Il Nuovo Cimento C*, 5:84–98, 1982.

[40] T. A. Feo and M. G. C. Resende. Greedy randomized adaptative search procedures. *Journal of Global Optimization*, 6:109–133, 1995.

[41] R. Fletcher and M. J. D. Powell. A rapidly convergent descent method for minimization. *The Computer Journal*, 6:163–168, 1963.

[42] X. Gandibleux. *Multiple criteria optimization: state of the art annotated bibliographic surveys*. Springer Science & Business Media, 2002.

[43] P. Garcia, A. Ferriere, and A. Bezian. Codes for solar flux calculation dedicated to central receiver system applications: A comparative review. *Solar Energy*, 82:189–197, 2008.

[44] C. Gertig, A. Delgado, C. Hidalgo, and R. Ron. Sofia - a novel simulation tool for central receiver systems. *Energy Procedia*, 49:1361–1370, 2014.

[45] A. Ghobeity and A. Mitsos. Optimal Design and Operation of a Solar Energy Receiver and Storage. *Solar Energy Engineering*, 134(031005):9 pages, 2012.

[46] D. E. Goldberg and J. Richardson. Genetic algorithms with sharing for multimodal function optimization. In *Proceedings of the Second International Conference on Genetic Algorithms*, 1987.

[47] J. Göttsche, B. Hoffschmidt, S. Schmitz, M. Sauerborn, R. Buck, E. Teufel, K. Badst´ubner, D. Ifland, and C. Rebholz. Solar Concentrating Systems using Small Mirror Arrays. *Solar Energy Engineering*, 132:011003–011007, 2010.

[48] A. Grosso, A. R. M. J. U. Jamali, M. Locatelli, and F. Schoen. Solving the problem of packing equal and unequal circles in a circular container. *JOGO*, 47:63–81, 2010.

[49] S. Guha and S. Khuller. Greedy strikes back: Improved facility location algorithms. *Journal of Algorithms*, 31(1):228–248, 1999.

[50] M. Izygon, P. Armstrong, N. Nilsson, and N. Vu. TieSOL – a GPU-based suite of fsoftware for central receiver solar power plants. In *Inproceedings of SolarPaces 2011*, 2011.

[51] N. Jelley and T. Smith. Concentrated solar power: Recent developments and future challenges. *Journal of Power and Energy*, 0:1–21, 2015.

[52] J. G. Kolb, S. A. Jones, M. W. Donnelly, D. Gorman, R. Thomas, R. Davenport, and R. Lumia. Heliostat Cost reduction study. Technical Report SAND2007-3293, Sandia National Labs., 2007.

[53] A. Kribus, I. Vishnevetsky, A. Yogev, and T. Rubinov. Closed loop control of heliostats. *Energy*, 29:905–913, 2004.

[54] National Renewable Energy Laboratory. Gemasolar thermosolar plant. Sener www.nrel.gov/csp/solarpaces/project_detail.cfm/projectID=40, 2011.

[55] National Renewable Energy Laboratory. Ivanpah solar electric generating system. BrightSource Energy www.nrel.gov/csp/solarpaces/project_detail.cfm/projectID=62, 2014.

[56] National Renewable Energy Laboratory. Khi solar one. Abengoa Solar www.nrel.gov/csp/solarpaces/project_detail.cfm/projectID=244, 2014.

[57] National Renewable Energy Laboratory. Power tower projects. Technical report, NREL, 2015. www.nrel.gov/csp/solarpaces/power_tower.cfm.

[58] J. C. Lagarias, J. A. Reeds, M. H. Wright, and P. E. Wright. Converge properties of the Nelder-Mead simplex method in low dimensions. *SIAM Journal on Optimization*, 9:112–147, 1998.

[59] W. Landman. Sensitivity analysis of a curved heliostat profile. In *Proceedings of Annual Student Symposium 2012 in CRSES*, 2012.

[60] J. Larmuth and P. Gauché. The effects of heliostat component cost on heliostat size. In *Proceedings of the 2nd Annual STERG SolarPACES Symposium*, 2014.

[61] J. Larmuth, K. J. Malan, and P. Gauché. Design and cost review of 2 m2 heliostat prototypes. Technical report, STERG, Stellenbosch University, 2014. http://concentrating.sun.ac.za/wp-content/uploads/2014/02/52.pdf.

[62] F. W. Lipps. Four different views of the Heliostat Flux Density Integral. *Solar Energy*, 18:555–560, 1976.

[63] F. W. Lipps and L. L. Vant-Hull. A cellwise method for the optimization of large central receiver systems. *Solar Energy*, 20:505–516, 1978.

[64] F. W. Lipps and M. D. Walzel. An analytic evaluation of the flux density due to sunlight reflected from a flat mirror having polygonal boundary. *Solar Energy*, 21:113–126, 1978.

[65] F.W. Lipps. Theory of Cellwise Optimization for Solar Central Receiver Systems. Technical Report SAND-85-8177, Houston Univ., TX (USA). Energy Lab., 1981.

[66] M. Locatelli and U. Raber. Packing equal circles in a square: a deterministic global optimization approach. *Discrete Applied Mathematics*, 122:139–166, 2002.

[67] T. R. Mancini. Catalog of solar heliostats. Technical Report III–1/00, SolarPaces, 2000. www.fika.org/jb/resources/Heliostat

[68] K. Miettinen. *Nonlinear multiobjective optimization*. Springer Science & Business Media, 2012.

[69] D. R. Mills. Advances in solar thermal electricity technology. *Solar Energy*, 76:19–31, 2004.

[70] M. Mitchell. *An introduction to genetic algorithms*. Massachusetts Institute of Technology press, 1996.

[71] N. Mladenovič, F. Plastria, and D. Vrosevič. Reformulation descent applied to circle packing problems. *Computers & Operations Research*, 32:2419–2434, 2005.

[72] A. Mokri, M. A. Ali, and M. Emziane. Solar energy in the United Arab Emirates: A review. *Renewable and Sustainable Energy Reviews*, 28:340–375, 2013.

[73] J. A. Nelder and Mead R. A simplex method for function minimization. *The Computer Journal*, 7:308–313, 1965.

[74] C. J. Noone, A. Ghobeity, A. H. Slocum, G. Tzamtzis, and A. Mitsos. Site selection for hillside central receiver solar thermal plants. *Solar Energy*, 85:839–848, 2011.

[75] C. J. Noone, M. Torrilhon, and A. Mitsos. Heliostat field optimization: A new computationally efficient model and biomimetic layout. *Solar Energy*, 86:792–803, 2012.

[76] R. Osuna, V. Fernández, S. Romero, M. Romero, and M. Sánchez. PS10: a 11.0-MWe Solar Tower Power Plant with Satured Steam Receiver. In *Proceedings of SolarPaces 2004*, 2004.

[77] U. A. Ozturk and B. A. Norman. Heuristic methods for wind energy conversion system positioning. *Electric Power Systems Research*, 70(3):179–185, 2004.

[78] A. Pfahl, M. Buselmeier, and M. Zaschke. Wind loads on heliostats and photovoltaic trackers of various aspect ratios. *Solar Energy*, 85:2185–2201, 2011.

[79] C. L. Pitman and L. L. Vant-Hull. Performance of optimized Solar Central Receiver Systems as a function of receiver thermal loss per unit area. *Solar Energy*, 37:457–468, 1986.

[80] R. Pitz-Paal, N. B. Botero, and A. Steinfeld. Heliostat field layout optimization for high-temperature solar thermochemical processing. *Solar Energy*, 85:334–343, 2011.

[81] J. Poland and K. S. Stadler. Stochastic optimal planning of solar thermal power. In *Proceedings of 2014 IEEE Conference on Control Applications (CCA) Part of 2014 IEEE Multi-conference on Systems and Control*, October 2014.

[82] M. Quero, M. Pfänder, C. Gertig, and R. Osuna Gonzalez-Aguilar. Method for distributing heliostats in tower plant (Patent US20130092156 A1), 2013.

[83] A. Ramos and F. Ramos. Strategies in Tower Solar Power Plant optimization. *Solar Energy*, 86:2536–2548, 2012.

[84] A. Ramos and F. Ramos. Heliostat blocking and shadowing efficiency in the video-game era. arXiv:1402.1690v1, 2014.

[85] V. S. Reddy, S. C. Kaushik, K. R. Ranjan, and S. k. Tyagi. State-of-the-art of solar thermal power plants- A review. *Renewable and Sustainable Energy Reviews*, 27:258–273, 2013.

[86] S. Relloso and E. García. Tower technology cost reduction approach after gemasolar experience. *Energy Procedia*, 69:1660–1666, 2015. SolarPaces 2014.

[87] M. G. C. Resende and C. C. Ribeiro. *Search Methodologies: Introductory Tutorials in Optimization and Decision Support Techniques. Chapter 11: GRASP: Greedy Randomized Adaptive Search Procedures.* Springer Science+Business Media New York, 2003.

[88] P. Richter, M. Frank, and E. Abrahám. Multi-objective optimization of solar tower power plants. In *Proceedings of European Conference on Mathematics for Industry (ECMI)*, 2014.

[89] M. Romero, R. Buck, and J. E. Pacheco. An update on Solar Central Receiver Systems, Projects and Technologies. *Journal of Solar Energy Engineering*, 124:(11 Pages), 2002.

[90] A. Rovira, M. J. Montes, M. Valdes, and J. M. Martínez-Val. Energy management in solar thermal power plants with double thermal storage system and subdivided solar field. *Applied Energy*, 88:4055–4066, 2011.

[91] M. Sánchez and M. Romero. Methodology for generation of heliostat field layout in central receiver systems based on yearly normalized energy surfaces. *Solar Energy*, 80(7):861–874, 2006.

[92] A. Sánchez-González and D. Santana. Solar flux distribution on central receivers: A projection method from analytic function. *Renewable Energy*, 74:576–587, 2014.

[93] J. Sanz-Bermejo, V. Gallardo-Natividad, J. Gonzalez-Aguilar, and M. Romero. Comparative system performance analysis of direct steam generation central receiver solar thermal power plants in megawatt range. *Journal of Solar Energy Engineering*, 136:(9 Pages), 2014.

[94] G. Sassi. Some notes on shadow and blockage effects. *Solar Energy*, 31(3):331–333, 1983.

[95] M. Schmitz, P. Schwarzbözl, R. Buck, and R. Pitz-Paal. Assesment of the potencial improvement due to multiple apertures in central receiver systems with secondary concentrators. *Solar Energy*, 80:111–120, 2006.

[96] P. Schramek and D. R. Mills. Multi-tower solar array. *Solar Energy*, 75(3):249–260, 2003.

[97] P. Schramek and D. R. Mills. Heliostats for maximum ground coverage. *Energy*, 29:701–713, 2004.

[98] P. Schramek, D. R. Mills, W. Stein, and P. Le Lièvre. Design of the Heliostat Field of the CSIRO Solar Tower. *Journal of Solar Energy Engineering*, 131(024505):(6 Pages), 2009.

[99] A. Segal and M. Epstein. Comparative performances of tower-top and tower-reflector central solar receivers. *Solar Energy*, 65:207–226, 1999.

[100] A. Segal and E. Teufel. Optimum layout of heliostat field when the tower-top receiver is provided with secondary concentrators. Technical report, Weizmann Institute of Science (SFERA), 2012. http://sfera.sollab.eu/downloads/JRA/WP13/R13.3b_SFERA_WP13T2_Opt_HelioField_Secondary_TopReceiver.pdf.

[101] E. J. Sheu, A. A. Mitsos, A. Eter, E. M. A. Mokheimer, M. A. Habib, and A. Al-Qutub. A Review of Hybrid Solar-Fossil Fuel Power Generation Systems

and Performance Metrics. *Journal of Solar Energy Engineering*, 134(041006):(17 Pages), 2012.

[102] F. M. F. Siala and M. E. Elayeb. Mathematical formulation of a graphical method for a no blocking heliostat field layout. *Renewable Energy*, 23:77–92, 2001.

[103] J. Spelling, D. Favrat, A. Martin, and G. Augsburger. Thermoeconomic optimization of a combined-cycle solar tower power plant. *Energy*, 41:113–120, 2012.

[104] W. B. Stine and R. W. Harrigan. *Power From The Sun*. John Wiley and Sons, 2001.

[105] J. W. Strachan and R. M. Houser. Testing and evaluation of large-area heliostats for solar thermal applications. Technical Report SAND92-1381, Sandia National Labs., 1993.

[106] F. Ueckerdt, L. Hirth, G. Luderer, and O. Edenhofer. System LCOE: What are the costs of variable renewables? *Energy*, 63:61–75, 2013.

[107] Stellenbosch University. Helio100. http://helio100.sun.ac.za/.

[108] L. L. Vant-Hull and A. F. Hildebrandt. Solar Thermal Power System based on optical transmission. *Solar Energy*, 18:31–39, 1976.

[109] V. V. Vazirani. *Approximation algorithms*. Springer Science & Business Media, 2013.

[110] M. D. Walzel, F. W. Lipps, and L. L. Vant-Hull. A solar flux density calculation for a solar tower concentrator using a two-dimensional hermite function expassion. *Solar Energy*, 19:239–253, 1977.

[111] X. Wei, Z. Lu, Z. Wang, W. Yu, H. Zhang, and Z. Yao. A new method for the design of the heliostat field layout for solar tower power plant. *Renewable Energy*, 35(9):1970–1975, 2010.

[112] X. Wei, Z. Lu, W. Yu, and Z. Wang. A new code for the design and analysis of the heliostat field layout for power tower system. *Solar Energy*, 84(4):685–690, 2010.

[113] I-A. Yeo and J-J. Yee. A proposal for a site location planning model of environmentally friendly urban energy supply plants using an environment and energy geographical information system (e-gis) database (db) and an artificial neural network (ann). *Applied Energy*, 119:99–117, 2014.

[114] P-y. Yin and T-Y. Wang. A grasp-vns algorithm for optimal wind-turbine placement in wind farms. *Renewable Energy*, 48:489–498, 2012.

[115] C. Zang, Z. Wang, H. Liu, and Y. Ruan. Experimental wind load model for heliostats. *Applied Energy*, 93:444–448, 2012.

[116] H. Zhang, I. Juchi, D. Favrat, and X. Pelet. Multi-objective thermoeconomic optimisation of the design of heliostat field of solar tower power plants. In *Proceedings of the Engineering for sustainable Energy in developing countries*, 2007.